UNIVERSITY OF COPENHAGEN
FACULTY OF SCIENCE

The Effect of Tumor Extracellular Matrix on T Cell Activity

Maria Tangen Søgaard
MSc Thesis
Submission date: May 20th, 2021

Supervisors:
Daniel H. Madsen, external supervisor and PI, National Center for Cancer Immune Therapy
Signe Z. Ingvarsen, external co-supervisor, National Center for Cancer Immune Therapy
Ala Trusina, internal supervisor, Niels Bohr Institute

Abstract

Cancer immunotherapy has revolutionized the treatment of cancer patients, but only a limited number of patients respond to this type of therapy. This suggests that yet unknown immunosuppressive mechanisms exist in the tumor microenvironment which limit treatment efficacy. Though changes in composition and properties of the tumor extracellular matrix are well-documented, little is known about the role of the extracellular matrix in modulation of the immune response. We therefore set out to identify immunoregulatory proteins in the tumor extracellular matrix.

We isolated fibroblasts from breast tumors or healthy breast tissue of transgenic mice expressing GFP in the fibroblasts. To mimic normal and tumor extracellular matrix, we generated cell-derived matrices from normal and cancer-associated fibroblasts, respectively. The matrices were decellularized and primary murine T cells were cultured on the matrices. The activity of T cells cultured on cancer-associated compared to normal fibroblast matrices was subsequently evaluated by analysis of their proliferation and activity marker expression. Further, a panel of selected matrix proteins overexpressed in tumor extracellular matrix were screened for their effect on T cell cytotoxicity using an xCELLigence Real-Time Cell Analyzer.

Though the normal and cancer-associated cell-derived matrices were structurally similar, expression profiles of extracellular matrix-related genes were markedly different in normal and cancer-associated fibroblasts. Flow cytometry on T cells cultured on cancer-associated cell-derived matrices revealed an increase in the number of PD-1-expressing cells and indicated a trend towards decreased proliferation and $CD8^+$ T cell differentiation. RT-qPCR and bulk RNAseq suggested a small down-regulation of T cell activity markers and upregulation of regulatory T cell markers in T cells cultured on cancer-associated cell-derived matrices. In the screening of selected matrix proteins, no clearly immunosuppressive proteins were identified. However, incubation of T cells with the extracellular matrix protein periostin increased their cytolysis of tumor cells in the xCELLigence assay.

Collectively, the results of this thesis point towards an immunomodulatory role of the extracellular matrix in cancer and warrant further investigation of the subject. Blocking immune inhibitory components of the tumor extracellular matrix or administration of stimulating ECM proteins could serve as a novel type of cancer immunotherapy.

Preface

In this Master's thesis, I investigated the contributions of extracellular matrix in general (part I) and specific extracellular matrix proteins (part II) to modulation of antitumor immune responses in cancer.

The research was conducted in collaboration with and carried out at the National Center for Cancer Immune Therapy at Herlev Hospital. In that regard, I acknowledge Daniel H. Madsen and Signe Z. Ingvarsen for their supervision, valuable discussions and comments on the thesis. I would also like to thank the members of the TSMI group for their practical and academic contributions. Especially thank you to Astrid Z. Johansen, Marie-Louise Thorseth and Anne Mette Hvid Larsen for stepping in as *de facto* laboratory co-supervisors during Signe's medical leave. Further, I would like to thank Arianna Draghi and Chris Chamberlain in the Marco Donia group for providing patient-derived samples for the second part of the thesis.

Finally, I acknowledge Ala Trusina for her supervision and moral support as well as Alexander V. Nielsen for introducing me to the analysis of single cell RNA sequencing data in Python.

University of Copenhagen
May 2021

Maria Tangen Søgaard

Contents

Chapter 1

Introduction

Cancer is a heterogeneous set of diseases characterized among other things by uncontrolled growth of transformed cells[1]. Cancers can be broadly classified as either solid or liquid. While liquid cancers refer to transformed cells circulating in the blood, solid cancers develop in organs and result in formation of tumors. These tumors consist not only of the transformed cells themselves, but also of stromal cells, immune cells, blood vessels, extracellular matrix, secreted factors etc., collectively referred to as the tumor microenvironment (TME). The interaction of the tumor cells with the TME is a major determinant of patient outcome[2–4]. This chapter introduces some of these tumor-TME interactions with emphasis on the modulation of antitumor immune responses.

Activation and suppression of antitumoral immune responses

Cells of the immune system and their functions

The immune system consists of a combination of physical barriers, cells and proteins that protect our bodies from invading pathogens[5]. Though the exact function of the various immune cells is highly context-dependent, a simplified introduction to the function of the most important cell types is given below.

All immune cells derive from the same hematopoietic stem cell that differentiates into either a myeloid or lymphoid lineage[6]. Immune cells of myeloid origin are generally associated with innate immunity, which is a part of the immune system that uses non-specific defense mechanisms to eliminate invading pathogens. Myeloid cells include granulocytes (eosinophils, basophils, neutrophils and mast cells), macrophages and dendritic cells (DCs) (fig. 1.1). Eosinophils, basophils and mast cells are mainly involved in parasitic infections and allergic reactions and kill pathogens by release of cytotoxic cellular contents[7,8]. Neutrophils are important effector cells in bacterial and fungal infections and kill these by release of granule-containing neutrophil extracellular traps or by phagocytosis[9]. Macrophages can have both pro- and anti-inflammatory functions depending on how they are activated. Pro- and anti-inflammatory macrophages are commonly referred to as either M1 or M2 macrophages, respectively[10]. Among other things, macrophages can phagocytose pathogens, present antigens from the engulfed pathogen on their cell surface and secrete immune-modulating cytokines[11]. Similarly, the main function of DCs is to present antigen and co-activating signals to lymphocytes[12]. Activation of innate immune cells relies heavily on recognition of pathogen-associated molecular patterns by pattern recognition receptors on the immune cell surface[13].

In contrast, the adaptive arm of the immune system - which eliminates pathogens based on their expression of pathogen-specific antigens - is highly dependent on presentation of antigens by antigen-presenting cells (APCs)[12]. Effector functions of adaptive immunity are generally attributed to cells of lymphoid origin (fig. 1.1). The two main types of lymphocytes are T cells and B cells. B cells secrete

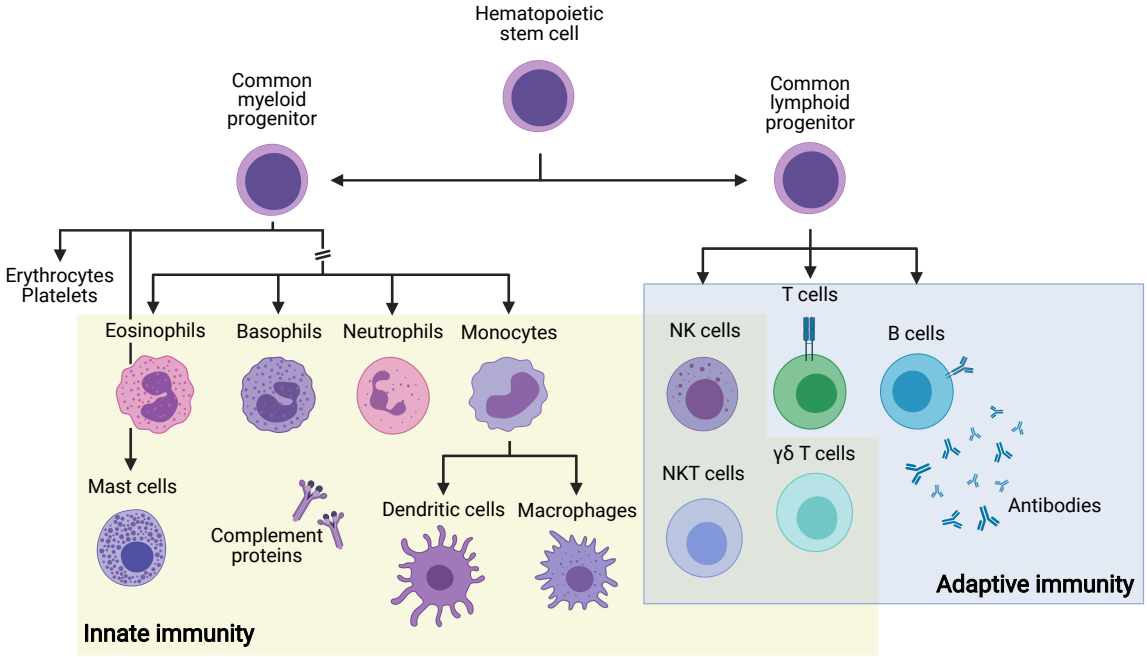

Figure 1.1: The most important cells of the immune system and their origin. All immune cells derive from the same hematopoietic stem cell. Innate cells are mainly of myeloid origin and include dendritic cells, mast cells, granulocytes and macrophages as well as complement proteins. Adaptive cells are mainly of lymphoid origin and include B and T cells. Antibodies are also important for adaptive immunity. Natural killer (NK) cells, natural killer T (NKT) cells and $\gamma\delta$ T cells exhibit both innate and adaptive characteristics. Figure adapted from [19] and [20].

cytokines, present antigens and differentiate into antibody-secreting plasma cells upon B cell receptor activation[14]. T cells either kill cells that have been infected by a pathogen or orchestrate immune responses via cytokine secretion[15]. These two functions of T cells are mediated by $CD8^+$ cytotoxic T lymphocytes (CTLs) and $CD4^+$ helper T cells (Th cells), respectively. Natural killer (NK) cells, though being lymphocytes, have roles in both innate and adaptive immunity[16], as do natural killer T cells[17] and $\gamma\delta$ T cells[18].

The theory of cancer immunoediting

The immune system plays a central role in the development of cancer[21]. In order to mount an antitumor immune response, T cells need to be presented with antigen. The higher the expression of tumor-associated or -specific antigens on the cancer cell surface, the more immunogenic the tumor. Since many cancer cells have mutations in their DNA replication and repair machinery genes, they tend to have higher mutation rates than healthy cells. These mutations gradually change the proteins produced by the cell, resulting in production of new and foreign antigens that can activate killing by T cells[22].

A compelling theory which has received massive attention since it was first formulated is that of cancer immunoediting. This theory divides cancer development into three phases each characterized by different types of interactions between cancer and immune cells (fig. 1.2)[23,24]. In the elimination phase of the cancer immunoediting theory, tumor-associated antigens released into circulation activate an antitumorigenic immune response which causes destruction of the cancer cells. Successful elimination of these cells will then revert the tissue back to its healthy state. However, selective pressure on the genetically unstable cancer cells can cause weakly immunogenic cells to enter the equilibrium phase in which the tumor is maintained in a dormant state by opposing pro- and antitumorigenic immune cell subsets. A tumor may remain in this phase for extended periods of time. Further progression to

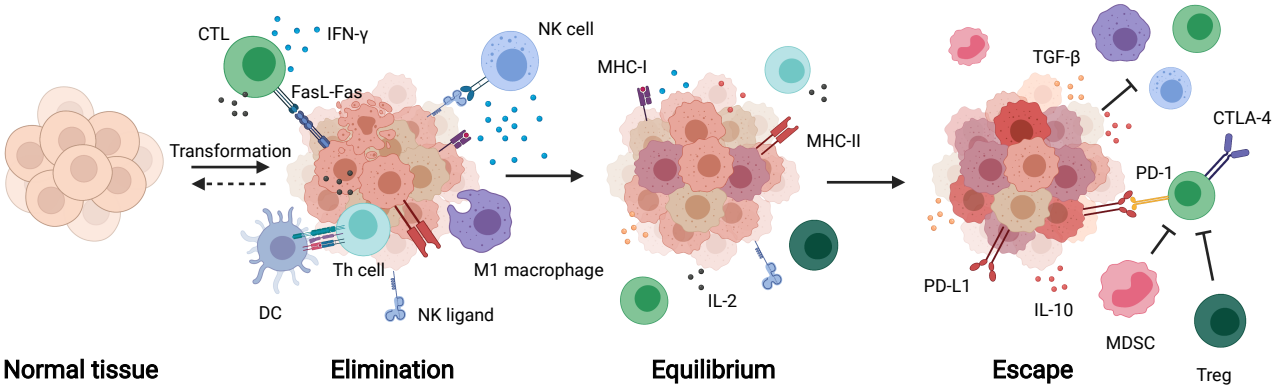

Figure 1.2: The concept of cancer immunoediting. When normal tissue is transformed to cancerous cells, an immune reponse is elicited against these cells to eliminate them. Successful elimination of the cancer cells will then restore tissue function. However, if the cancer cells avoid detection by the immune cells they may enter the equilibrium phase and likely progress to full immune escape. See body for details. Figure adapted from [24]. CTL = cytotoxic T lymphocyte, DC = dendritic cell, Th = T helper cell, NK = natural killer, MDSC = myeloid-derived suppressor cell, Treg = regulatory T cell.

the escape phase occurs by e.g. loss of tumor-associated antigens, secretion of anti-apoptotic factors or increased immunosuppression, ultimately allowing the tumor to grow and metastasize.

Activation of antitumor immune responses

Although several immune cells can exert cytotoxic antitumor effects, T cells are considered the most important in mediating antitumor immunity. Activation of antitumor T cell responses requires that APCs present tumor-associated antigens to T cells on protein complexes known as major histocompatibility complexes (MHC) (fig. 1.3)[25]. Binding of the T cell receptor to antigen presented on MHC class I results in activation and expansion of tumor-specific $CD8^+$ CTLs. In addition to binding of the T cell receptor to an MHC-I/peptide complex, an additional co-stimulatory signal is required to induce an efficient CTL response and prevent T cell unresponsiveness[26]. T cells express a variety of different co-stimulatory molecules on their surface including CD28, CD137 and ICOS[26]. In the ideal world, activated CTLs then migrate to tumor sites, infiltrate the tumor and kill the tumor cells by secretion of cytotoxic molecules called granzymes or by binding of apoptosis-inducing Fas ligand to tumor cell surface Fas[25,27].

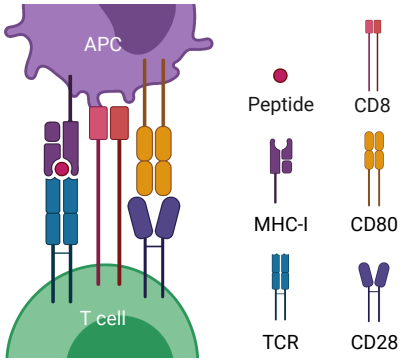

Figure 1.3: Antigen presentation to $CD8^+$ T cells. $CD8^+$ T cell activation involves binding of the T cell receptor (TCR) to peptide loaded onto MHC class I as well as binding of a co-stimulatory receptor to its cognate ligand on antigen-presenting cells (APCs).

Concomitant uptake of tumor antigens by APCs and presentation on MHC class II activates $CD4^+$ T cells. The balance of cytokines produced by tumor cells and other infiltrating immune cells determine differentiation of the $CD4^+$ cells into various Th cell subsets with distinct cytokine-secreting signatures[28]. The most important subset for antitumoral responses is the Th1 subset. Among other things, Th1 cells license CTL activation by DCs via CD40-CD40L interaction[29]. They also secrete IL-2 which induces T cell proliferation[30,31] as well as IFN-γ which upregulates expression of MHC class I and II on APCs[32,33] and induces a small subset of cytotoxic $CD4^+$ T lymphocytes[34–36].

IFN-γ is also a potent inducer of proinflammatory M1 macrophages which are characterized by their secretion of inflammatory cytokines and lymphocyte-trafficking chemokines[10]. Such macrophages

are able to lyse tumor cells, present antigen to and stimulate proliferation of T and NK cells as well as reciprocally induce Th1 cells to further augment the immune response[10,37].

Thus, collectively CTLs[38,39], Th1 cells[35,40,41], and M1 macrophages[10,37] along with NK cells[42–44] and other inflammatory immune cells[35,45] mediate antitumor immunity and cancer cell destruction leading, in principle, to tumor remission.

Evasion of antitumor immune responses

Established tumors also exploit several mechanisms that enable evasion of these antitumoral immune responses. While some evasion mechanisms such as downregulation of MHC class I/II or immune checkpoint expression can be constitutively active in the tumor others are induced by the antitumor immune response itself[46].

Immunogenicity and mutational burden

Continuous destruction of the highly immunogenic cancer cells by cytotoxic immune cells inevitably results in gradual selection for the less immunogenic cells. These cells avoid immune recognition by loss of tumor antigen or MHC molecule expression and consequently avoid the antitumor responses by the adaptive arm of the immune system[22]. They can also downregulate expression of or shed decoy NKG2D ligands to avoid destruction by NK cells[47]. Alternatively, if the tumor mutational burden is very high, chronic expression and presentation of tumor antigen can render the T cells exhausted and unable to perform effector functions[48].

Suppressive cells and cytokines

Cancer cells also secrete cytokines, chemokines and growth factors such as IL-10, M-CSF and CCL2 which recruit and induce tumor-associated macrophages (TAMs), myeloid-derived suppressor cells (MDSCs) and regulatory T cells (Tregs)[10,47]. TAMs are M2-like macrophages with well-known roles in induction of tumor growth, angiogenesis, invasion and metastasis[49,50]. Additionally, they are key players in skewing the tumor microenvironment towards a more immunosuppressive one by further recruiting and inducing Th2 cells, Tregs and MDSCs[10,37,51].

MDSCs are immature cells of myeloid origin that are unable to differentiate into DCs, macrophages or granulocytes[51]. Their immunosuppressive activities include secretion of arginase 1 and inducible nitric oxide synthase (iNOS), which deplete L-arginine in the extracellular space. Since arginine is required for cell cycle progression in T cells, arginase and iNOS activity inhibits T cell proliferation[47]. Further, secretion of reactive oxygen species (ROS) and nitric oxide (NO) inhibits MHC class II expression and induces T cell apoptosis. ROS and NO reactions with other molecules also form peroxynitrite which causes nitration/nitrosylation of key amino acids and proteins including the T cell receptor[51]. This alters the structure of the T cell receptor in a way that affects its interaction with MHC-I/peptide complexes, thus inhibiting T cell activation. MDSCs also induce Tregs and, in contrast to TAMs, appear to be able to suppress T cell activity in an antigen-specific manner[47,51].

$CD4^+$ T cells expressing the transcription factor FOXP3 are known as Tregs[52]. Though Tregs can be induced by tumor-, TAM- or MDSC-derived IL-10 or TGF-β, they require antigen stimulation for expansion and activation of their immunosuppressive capacities[52]. The antigen-specific Treg then inhibits the antitumor response by secretion of the immunosuppressive cytokines IL-10 and IL-35 as well as soluble and membrane-bound TGF-β[53]. Further, they metabolically disrupt conventional T cells by e.g. competitive IL-2 consumption[53,54]. Tregs also have high expression of immune checkpoints (see below) and can kill effector T and B cells by granzyme- or perforin-mediated cytolysis[53]. The immunosuppressive activities of Tregs not only affect antitumor activity by directly suppressing CTL effector mechanisms, they also do so indirectly by suppressing APC function and thus T cell activation[53].

Immune checkpoints

The amplitude and duration of a T cell response against a given antigen is a result of the balance between antigen presentation, co-stimulatory and co-inhibitory signals. Since antigen presentation by itself is not sufficient to induce a durable T cell response, the latter two are often referred to as immune checkpoints[55]. To this date, several dozen co-signaling molecules have been identified[26]. In addition to being either stimulatory or inhibitory, these can be further categorized on the basis of their structure. Accordingly, most co-signaling receptors belong to either the immunoglobulin superfamily (IgSF) or the tumor necrosis factor receptor superfamily (TNFRSF) of signaling molecules[26]. IgSF members contain an extracellular immunoglobulin-like domain which folds into the characteristic β-sandwich known as an Ig-fold[56]. Some of the most well-known co-stimulatory (e.g. CD28, ICOS) and -inhibitory (e.g. PD-1, CTLA-4) receptors all belong to the CD28 subfamily of the IgSF[26]. Other notable IgSF members include the inhibitory receptors TIM-3, TIGIT and LAG-3[26]. The TNFRSF members are characterized by one or more cysteine-rich domains in the extracellular region[57]. Many co-signaling molecules in the TNFRSF, including CD40 and CD137, are stimulatory[26,58].

In addition to their structural classification, co-signaling molecules can be classified according to their expression pattern[59]. Virtually all immune cells express immune checkpoint receptors (or their ligands)[59]. While many co-stimulatory receptors are constitutively expressed on the cell surface, inhibitory receptors tend to be upregulated upon immune cell activation[26]. T cell activation is typically achieved when the activating signal exceeds some threshold. In contrast, resolution of the immune response is automatically initiated upon T cell activation as inhibitory receptors are upregulated[59].

Inhibitory immune checkpoints that regulate T cell effector functions, such as PD-1/PD-L1, are often overexpressed in the TME[55]. Consequently, T cell activation by tumor-associated antigens is impeded or the T cells become exhausted[48]. Furthermore, many inhibitory immune checkpoint receptors, including CTLA-4, are constitutively expressed on Tregs[55]. CTLA-4 is a receptor for the T cell co-stimulatory ligands CD80 and CD86 expressed on APCs. Aside from competing against the T cell co-stimulatory molecule CD28, binding of CTLA-4 to CD80/CD86 sends inhibitory signals to the APC. Among other things, this downregulates CD80/CD86 expression and induces expression of indoleamine-2,3-dioxygenase (IDO), a tryptophan-degrading enzyme[53,55]. Conversion of tryptophan to kynurenine metabolites causes lymphocyte cell cycle arrest due to tryptophan deprivation and induces immunosuppression via kynurenine metabolite binding to the transcription factor aryl hydrocarbon receptor[60]. Interestingly, ligand binding to immune checkpoint receptors on Tregs does not inhibit the Treg but rather induces its proliferation[55].

Other mechanisms

Besides altering their immunogenicity, inducing suppressive cells and cytokines and upregulating inhibitory immune checkpoints, tumors utilize a number of additional immunosuppressive mechanisms. First, as tumors grow in size, their core typically becomes hypoxic because blood supply and angiogenesis is inadequate in comparison to oxygen consumption by the rapidly dividing cancer cells. Hypoxic conditions inhibit T cell proliferation[61], increases shedding of NKG2D ligands[62], recruits and induces TAMs[49,50] and Tregs[63] and tips the balance of glucose metabolism towards glycolysis rather than oxidative phosphorylation[61]. Due to the lactic acid production in the glycolytic pathway, this latter fact results in the generation of an acidic environment that further inhibits CTLs and the differentiation of monocytes to DCs[61]. Hypoxia also upregulates expression of CD73, a cell-surface ectoenzyme that participates in the conversion of ATP to adenosine[64]. Adenosine binding to its receptor A2aR, which is expressed on most leukocytes, has several immunosuppressive effects. These include inhibition of macrophage and neutrophil phagocytosis, inhibition of NF-κB activation and thus T- and B cell function as well as induction of Tregs[61,64].

In addition to modulating their energy metabolism, cancers also modulate their metabolism of

amino acids that are essential for T cell function. Upregulation of arginase and iNOS or IDO, tryptophan-2,3-dioxygenase (TDO) and tryptophan hydroxylases (TPHs) increases the degradation of L-arginine and tryptophan, respectively[46,61,65]. Depletion of these important amino acids is not only associated with an inhibition of T cell proliferation, but also induction of NK cell anergy, inhibition of monocyte differentiation to DCs as well as induction and proliferation of TAMs, Tregs and MDSCs[46,47,51,61].

Lastly, as will be described in the next section, there is increasing evidence that the extensive remodeling of and interactions with the extracellular matrix can modulate the homing and function of tumor-infiltrating immune cells.

Tumor extracellular matrix & fibroblasts

Composition and function of the ECM

The extracellular matrix (ECM) is the network of macromolecules that surrounds cells in tissues and organs either as sheet-like basement membrane that connects epithelial cells to underlying connective tissue or as a porous interstitial matrix between cells[66]. It makes up the majority of bone and cartilage but is present in larger or smaller amounts in all tissues and parts of the body[67,68]. The ECM not only serves as a scaffold for cells to attach to but also has important biophysical and -chemical roles in homeostasis and wound healing as well as disease. Ageing, wounding and the constant remodeling of the ECM by proteolytic activity and ECM secretion makes the ECM an ever-changing dynamic entity[69].

3 major classes of macromolecules make up the ECM, namely collagens, proteoglycans and glycoproteins (fig. 1.4a). Collagens confer structural and tensile strength to the ECM. They are homo- or heterotrimers of various collagen subunits that assemble to form fibrillar, sheet-like or cellular transmembrane structures[68]. The collagen subunit consists primarily of several repeating Gly-X-Y domains (where X and Y can be any amino acids but are often proline and 4-hydroxypoline) occasionally interrupted by other amino acids or non-collagen domains[70,71]. In total, 43 collagen subunits have been identified forming 28 different collagens[68,70,71].

Proteoglycans consist of a core protein to which several glycosaminoglycans (GAGs) and potentially other carbohydrates are attached. GAGs are polymers of sulfated and carbonated disaccharide subunits[68]. The negative charges on the sulfate and carbonate groups attract cations which are osmotically active. Consequently, they bind water to form hydrated gels that confer high compressive strength to the ECM[72]. Some types of GAGs also bind factors secreted into the ECM[68]. Proteoglycans are divided into families based on the protein domains (and to some extent the GAGs) they are made up of, the largest of which is the family of small leucine-rich repeat proteoglycans[68,70].

The last class, the ECM glycoproteins, is the largest and most diverse group of ECM proteins. Their unifying feature is that they are proteins linked with smaller, branched oligosachharides (i.e. not GAGs) and, like proteoglycans and collagens, they often share some of the same domain structures e.g. fibronectin domain types I-III[68,70]. Some of the most well-studied ECM glycoproteins are elastins which give elasticity to the ECM[73], laminins which are a major constituent of the basement membrane[74] and fibronectins which bind cell-surface integrin receptors and guide cellular adhesion[75]. However, glycoproteins serve many other functions in the ECM including guiding assembly of the ECM, binding of growth- and other secreted factors and interaction with cells to induce migration, proliferation or angiogenesis[73,76,77]. Indeed, many glycoproteins or cleaved fragments thereof (matrikines) may consist of growth-factor-like or similar domains that directly bind cellular receptors[77,78]. Glycoproteins that mediate such non-structural functions are often abundant in developing or wounded tissues with more moderate expression later in life[68,76].

Collectively, collagens, proteoglycans and ECM glycoproteins make up what is known as the core

matrisome. Bioinformatic and proteomic analyses have identified almost 300 different proteins in the core matrisome across different tissues with further variation introduced by splice variants, post-translational modification and cross-linking[66,70,79,80]. Additional ECM-associated proteins include growth factors, chemokines, and other secreted factors that bind to the ECM; ECM-modifying enzymes such as crosslinking enzymes and proteases; as well as lectins, galectins, semaphorins and similar proteins affiliated with the ECM[70,79].

Fibroblasts in healthy and diseased tissues

The primary cell type responsible for production of the ECM is the fibroblast, though cancer cells also contribute to a minor portion of tumor ECM[79,81]. Fibroblasts constitute a very heterogeneous population of stromal cells and have traditionally been defined as cells of mesenchymal origin that reside in the ECM[82]. No universal or specific markers for fibroblasts exist, so they are typically identified by a combination of morphology and location as well as the lack of lineage markers for epithelial cells, endothelial cells and leukocytes[83]. Nevertheless, depending on the application, vimentin, α-smooth muscle actin (α-SMA), fibroblast-specific protein-1 (FSP-1), fibroblast-activation protein (FAP), platelet-derived growth factor (PDGF) receptors and other markers have been used to distinguish fibroblasts from other cells[84]. In line with their roles in ECM production and degradation, fibroblasts are also key players in wound healing and tissue repair as well as secretion of growth factors for e.g. stimulation of angiogenesis[85–87]. The literature further suggests a role of fibroblasts as cytokine- and chemokine-producing sentinel cells and inflammatory regulators involved in failure to resolve acute inflammation and development of chronic inflammation[88,89]. However, fibroblasts only perform these functions when they are in their activated state[90].

Cancer-associated fibroblasts (CAFs) are irreversibly activated fibroblasts found in the TME[90]. In many years it was thought that CAFs were generated by activation of normal resident fibroblasts, but it is becoming clear that CAFs can also be generated from a variety of other stromal cells such as bone marrow-derived mesenchymal stem cells[83,91]. Like normal tissue-resident fibroblasts, CAFs constitute a very heterogeneous population of stromal cells in the tumor and recent studies have identified at least three distinct subsets in both human and murine models of cancer: (i) ECM-depositing, α-SMA and TGF-β expressing myofibroblast CAFs (myCAFs), (ii) cytokine- and chemokine-secreting inflammatory CAFs (iCAFs) and (iii) MHC-II-expressing antigen-presenting CAFs (apCAFs)[92–95]. These subtypes correspond well with the functions generally attributed to CAFs such as ECM production, crosslinking and degradation by myCAFs[84,90] or secretion of pro-tumorigenic/immunosuppressive soluble factors by iCAFs[84,96]. CAFs have also been found to directly suppress immune cells by inhibition of NK cell cytotoxicity or by antigen-specific deletion of $CD8^+$ T cells[97–100]. Further, CAFs have been shown to upregulate expression of PD-L1 in cancer cells[101,102] as well as TIM-3, PD-1, CTLA-4 and LAG-3 in cytotoxic and regulatory T cells[95,103]. The diverse roles of distinct CAF subsets are further highlighted by studies of fibroblast depletion in mouse models of cancer. Depletion of FAP-expressing cells in mice bearing subcutaneous LL2 tumors delayed tumor growth by increasing IFN-γ- and TNF-α-mediated tumor necrosis[99]. In contrast, specific deletion of α-SMA^+ fibroblasts in a mouse model of spontaneous pancreatic cancer accelerated cancer progression, increased Treg infiltration and CTLA-4 expression and decreased CTL and Th cell infiltration[104]. Thus, though the role of CAFs appears largely protumorigenic, different CAF subsets may either promote or restrain cancer development and progression.

Roles of the ECM in cancer progression

In comparison with ECMs in healthy tissue, the tumor ECM is associated with changes in both structure, density, stiffness, composition and hydration[66,80]. Such tumor-specific ECM arises due to cross-talk between the cancer cells and CAFs and facilitates cancer progression and metastasis.

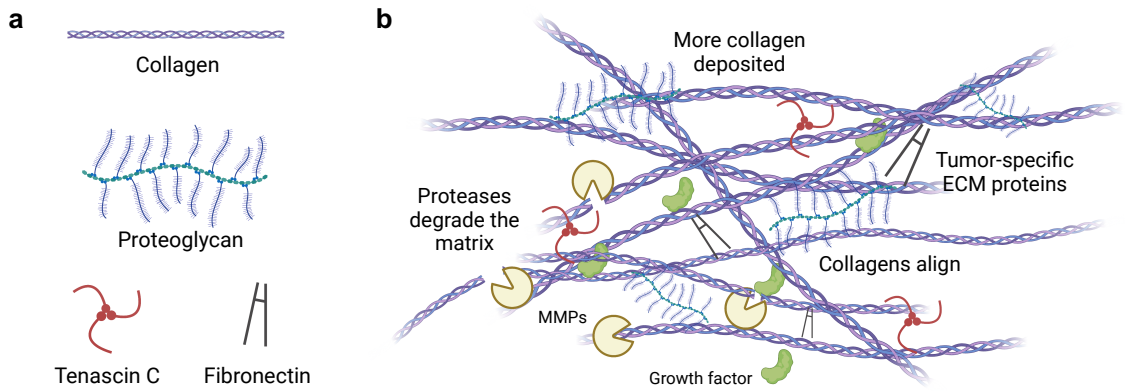

Figure 1.4: Tumor extracellular matrix (**a**) Both normal and tumor ECMs are made up of collagens, proteoglycans and glycoproteins such as tenascin and fibronectin. (**b**) The tumor-specific ECM is characterized by increased degradation of the ECM by proteases, increased deposition and alignment of structural ECM fibers and deposition of tumor-specific ECM proteins.

The TME is first of all characterized by increased activity of matrix-degrading enzymes and decreased activity of their inhibitors[66,80] (fig. 1.4b). Both cancer and stromal cells in the ECM are major sources of ECM-degrading enzymes called matrix metalloproteinases (MMPs)[79,81]. Degradation of the ECM not only allows deposition of a tumor-specific ECM, it also makes room for proliferating cancer cells to take up space and is crucial for their metastatic dissemination[105]. Additionally, local degradation of the matrix by MMPs is essential for breaching of basement membranes[106]. Proteolytic cleavage of the ECM also releases bound cytokines and growth factors such as TGF-β which can polarize immune cells towards a more suppressive phenotype[53,84,107]. Additionally, cleavage exposes cryptic binding sites in ECM molecules and generates biologically active proteolytic fragments, so-called matrikines[107]. Matrikines have historically been associated with antitumor activities[80,108,109]. However, Albrengues and colleagues found that dormant cancer cells could be awakened by cleaved fragments of laminin-111. More specifically, dormant cancer cells injected intravenously into syngeneic mice started to proliferate and form metastases only in hosts with chronically inflamed tissue. This was found to be due to cleavage of laminin-111 by neutrophil elastase and MMP-9[110]. Another study by O'Brien *et al.* found that collagen fragments efficiently recruited M2 macrophages in a Transwell chemotaxis assay[111].

Second, the tumor-specific ECM is associated with increased deposition and alignment of type I and other collagens as well as excessive crosslinking and post-translational modification of ECM fibers[80,100] (fig. 1.4b). Increases in collagen deposition and crosslinking leads to increased density and stiffness of the tumor ECM, which has been linked to poor survival in many cancers[112–116]. Activation of mechanosensitive integrins or the transcriptional regulators YAP and TAZ may explain such correlation. For example, increases in integrin signaling as a response to matrix stiffening has been shown to drive invasion of tumor cells[117] and accumulation of pro-tumorigenic CAFs[118]. In concert, YAP and TAZ regulate genes that control CAF activation as well as cancer cell proliferation, metabolism and stemness[119,120]. Further, a dense matrix impairs activation, proliferation and differentiation of T cells[121,122] and induces an immunosuppressive phenotype in macrophages[123–125]. Of note, collagens can directly inhibit immune function by binding to the inhibitory receptor LAIR-1 expressed on immune cells[126,127].

Moreover, the topography of the tumor ECM is also altered with collagen fibers being more aligned in the tumor ECM[128]. Such anisotropic collagen structures have been shown to guide the migration of cancer cells and thus increase their metastatic potential[129–131]. Though T cells are also guided by such aligned fibers, their migration is hindered in dense matrices[132].

Aside from increased deposition of structural ECM proteins, degradation of the normal healthy ECM also allows for deposition of an ECM with enhanced concentration of tumor-promoting ECM glycoproteins (fig. 1.4b). Indeed, ECM-related gene signatures with prognostic value frequently include a mix of both structural and non-structural proteins[81,133–138]. Besides influencing cancer cells themselves, several of these ECM glycoproteins have been proposed to directly influence antitumor immunity. For example, secreted protein acidic and cysteine-rich (SPARC) inhibits migration of neutrophils in the tumor[139] and together with osteopontin (OPN) recruits and promotes expansion of MDSCs[140]. OPN has also been shown to induce M2 polarization of TAMs and upregulate their expresison of PD-L1[141] and to suppress T cell activation and proliferation upon binding to CD44[142]. In addition, Collagen Triple Helix Repeat-Containing 1 (CTHRC1)[143], periostin (POSTN)[144] and versican (VCAN)[145] are associated with a high density of M2 macrophages in the TME. High VCAN expression also correlates with low T cell infiltration[146]. T cell infiltration is further inhibited by fibronectin-bound TNF-α[147] and tenascin C (TNC)[148], the latter of which also inhibits their proliferation[149] and activation[150–152]. Lastly, Transforming Growth Factor-β-Induced protein Ig-H3 (TGFBI) has been shown to inhibit T cell receptor signaling and modulate F4/80 macrophage activity via its interaction with integrin $\beta 3$[153]. Though matrix proteins are clearly implicated in the immunosuppressive roles of the TME, the literature on the subject is still sparse and most of the studies that exist have focused on the effect on myeloid cells. Thus, more studies are needed to establish the role of ECM proteins in immunosuppression.

Studying tumor ECM in vitro

Investigating the effects of tumor ECM constituents on cancer progression and antitumor immunity can be challenging. Many studies on extracellular matrix function have used either recombinant soluble proteins or pure matrices made from collagen, fibronectin or synthetic fibers[154]. While such studies have uncovered important information on cell-matrix interactions, they lack the biochemical and biomechanical complexity of a native ECM. For this purpose, *in vivo*-like materials such as the basement membrane extract Matrigel™ or decellularized native matrices can be used[154]. However, the Matrigel™ formulation shows high variability between batches, and decellularization of native matrices requires extensive processing to remove all immunogenic material.

Cell-derived matrices (CDMs) produced by fibroblasts cultured at high density presents an alternative to decellularized native matrices[155,156]. CDMs resemble the *in vivo* ECM well in terms of both composition and stiffness, but they can also be tuned by varying the culture conditions or genetically engineering the matrix-producing cells[157–160]. Further, unlike native matrices, CDMs are quite thin and are thus easily decellularized. Due to the thickness of the CDMs, they are also a popular choice for imaging applications[156]. Importantly, CAF-derived CDMs differ from CDMs produced by normal fibroblasts similarly to how the tumor ECM differs from normal ECM[161]. Collectively, these properties make CDMs a valuable tool for the *in vitro* study of tumor ECM.

Motivation & Aim of the project

Cancer is one of the leading causes of death worldwide amounting to approximately 10 million deaths in 2020[162]. Until recently, treatment options for cancer patients consisted primarily of chemotherapy, radiotherapy and surgery. However, over the last couple of decades, immunotherapeutic treatments – which aim to stimulate and increase destruction of the tumor by the patients' immune system – have become increasingly successful. A number of immunotherapeutic drugs and therapies – including various monoclonal antibodies and cytokines, adoptive cell therapies, immune checkpoint inhibitors, cancer vaccines and oncolytic viruses – have been approved for use in the clinic with several more in the pipeline[163,164]. Having said that, the response rates for patients treated with these drugs are still

very low, that is immunotherapy still fails to be effective in the majority of patients. A possible explanation for this is that the immunosuppressive character of the TME impedes the action anticipated of the drugs. Therefore, though a number of immunosuppressive pathways in the TME are already known[46,47,61], a lot of effort has gone into identifying additional immunosuppressive mechanisms locally in the tumor. As introduced above, such studies have primarily focused on secreted factors such as cytokines and cells infiltrating the tumor while little is known about the role of the ECM in immune suppression. This despite the fact that several ECM components have been shown to correlate with poor patient prognosis[81,112–116,133–138].

Our group has recently shown that the density of collagen – one of the major components of the ECM – can regulate both macrophage and T cell function[121,123]. Additionally, preliminary studies in our group suggest that T cells cultured on CAF CDMs are immunocompromised. The aim of this project was to identify and investigate additional components of the ECM that modulate T cell function. This was done by culturing T cells on cell-derived matrices produced by cancer-associated fibroblasts and subsequently evaluating the activity of the T cells in terms of proliferation and activity marker expression. Additionally, the effect of individual tumor matrix components on T cell cytotoxicity was investigated by xCELLigence assays. The identification of immunomodulatory ECM components would be a novel kind of immunomodulatory mechanism and thereby provide a new framework for improving the efficacy of cancer immunotherapy.

Chapter 2

Materials & Methods

Isolation of fibroblasts from MMTV-PyMT tumors or mammary gland tissue

Cancer-associated fibroblasts were isolated from primary tumor tissue of MMTV-PymT;*Col1a1*-GFP mice on an FVB;C57BL/6 background and normal fibroblasts from mammary gland tissue of littermate *Col1a1*-GFP mice. Tissue was excised from 10-12 week old female mice and frozen in FBS with 10% DMSO.

To isolate fibroblasts, the tissue was thawed at 37°C, washed briefly in RPMI 1640 medium, then cut into small pieces and incubated in digestion buffer (RPMI 1640 + 1% P/S with 2.1 mg/mL Collagenase type I + 75 µg/mL DNase I + 5 mM $CaCl_2$) for 2 hours at 37°C and 300 rpm. The solution was homogenized by pipetting, then passed through a 70 µm cell strainer to obtain a single cell suspension. The tissue digest was then resuspended in fibroblast growth medium (DMEM + 10% FBS + 1% P/S) and seeded in culture flasks for 2 days to let the cells rest before further isolation.

Isolation by raw culture Tissue digests that had been seeded in culture flasks were given fresh growth medium the day after thawing. Cells were kept in culture for 10 days at 37°C, 5% CO_2 before assessing fibroblast purity in the samples.

Isolation by differential adhesion Tissue digests that had rested for 2 days were harvested by trypsinization and resuspended in warm fibroblast growth medium. 2.5×10^5 cells/well were plated in 6-well tissue culture plates, then incubated for 15, 20, 40 or 60 min at 37°C, 5% CO_2. When the incubation time was up, the medium was carefully aspirated and transferred to a new well. Remaining cells were gently washed x1 in growth medium before adding fresh growth medium. Fibroblast purity in the aspirated and non-aspirated samples was assessed the next day.

Isolation by magnetically activated cell sorting (MACS) Tissue digests that had rested for 2 days were harvested by trypsinization and resuspended in cold fibroblast growth medium. CAFs were isolated using the mouse Tumor-Associated Fibroblast Isolation Kit (Miltenyi) or by depletion of $EpCAM^+$ cells using murine EpCAM/CD326 MicroBeads (Miltenyi) following the manufacturer's instructions but using an LD column in exchange for an LS column for the EpCAM bead isolation. Both the isolated fraction and the fraction to be discarded were resuspended in warm fibroblast growth medium and cultured at 37°C, 5% CO_2. Fibroblast purity in the samples was assessed the day after.

Fibroblast purity in samples taken before and after isolation was evaluated by fluorescence microscopy on a ZOE Fluorescent Cell Imager (BioRad) and by flow cytometry.

Optimized fibroblast isolation by MACS depletion of EpCAM$^+$ cells

Single cell suspensions of tumor/normal tissue digest were obtained by enzymatic digestion as described above. The single cell suspensions were depleted of EpCAM$^+$ cells using murine EpCAM/CD326 MicroBeads (Miltenyi) following the manufacturer's instructions with minor changes: incubation with the beads was decreased to 10 min, an LD column was interchanged for the LS column and the column was washed for a total of 3 times before eluting the magnetically labeled cells. The unlabeled cells were then cultured at 37°C, 5% CO_2 for about a week before proceeding, first in thawing medium (DMEM + 10% FBS + 2% P/S) but changing to growth medium (DMEM + 10% FBS + 1% P/S) after 2-3 days. Sample purity was evaluated by flow cytometry before and after isolation as well as upon seeding for generation of CDMs.

Evaluation of fibroblast purity by flow cytometry

Single cell suspensions containing GFP-expressing fibroblasts were spun down at 300g for 5 min and up to 10^6 cells were resuspended in 100 µL FACS buffer (PBS + 0.5% BSA [Sigma-Aldrich] + 5 mM EDTA [Sigma-Aldrich]). They were then stained for 30 min at 4°C with 1 µL each of Near-IR LIVE/DEAD™ cell stain kit (Invitrogen) and Brilliant Violet 421™ (BV421) anti-mouse CD326 (Ep-CAM) antibody (BioLegend). After staining, cells were washed twice in 1 mL FACS buffer, resuspended in FACS buffer and run on a BD FACSCanto™ II Cell Analyzer (BD Biosciences). Data were analyzed using FlowJo v. 10.

Generation of cell-derived matrices

Generation of CDMs was based on the protocols described in [155] and [156]. Briefly, wells of a 24-well plate were coated with 0.2% gelatin solution overnight, then crosslinked with 1% glutaraldehyde in PBS for 30 min. at RT. After crosslinking, the wells were washed 3x with PBS, blocked with fibroblast growth medium for 30-60 min. at RT, then washed again 3x with PBS. The gelatin-coated wells were then incubated in fibroblast growth medium for 1-4 days at 4°C.

Fibroblasts expanded *in vitro* for 1-2 passages were used for CDM production. We plated 1×10^5 normal or cancer-associated fibroblasts pr. well in the cross-linked gelatin-coated wells and cultured them for 3 days until very confluent (cells should be confluent on day 2). Matrix deposition was then stimulated by adding freshly prepared growth medium containing 50 µg/mL L-ascorbic acid sodium salt (Sigma-Aldrich A4034). The fibroblasts used here were very sensitive to the first stimulation, so medium was changed quickly but gently one well at a time for the first stimulation. Fibroblast cultures were replenished with new freshly prepared ascorbic acid medium every other day (Mon-Wed-Fri).

After 10 days of ascorbic acid treatment, the matrices were denuded of cells by incubation in warm extraction buffer (PBS + 0.5% Triton X-100 + 20 mM NH_4OH) for 3-5 min while observing cell lysis under the microscope. Next, the matrices were washed 2x in PBS and incubated with 10 µg/mL DNAse I (Worthington Biochem) in PBS for 30 min at 37°C to remove residual DNA. After one last wash, the matrices were either used immediately or stored overnight at 4°C in PBS + 1% P/S + 0.25 µg/mL Fungizone.

Decellularized matrices were imaged using a Leica DMi1 fitted with an S80 condenser and 10x-40x PH1 objectives. Fiber alignment in the matrices was quantified using the Directionality plugin in Fiji (v. 2.1.0)[165].

Fibroblast RNA isolation

Fibroblasts were seeded in 24-well plates and ascorbic acid stimulation begun as described for generation of CDMs. Cells were stimulated with ascorbic acid-containing medium for a total of 3 days, replenishing with freshly prepared medium on day 2. On day 3, cells were washed in PBS and total

RNA was isolated using the RNeasy Kit (Qiagen) according to manufacturer's instructions with β-mercaptoethanol added to the lysis buffer. RNA quantity and quality was determined using the 2100 Bioanalyzer (Agilent). Samples with total RNA RIN values > 9.7 were used for bulk RNA sequencing.

Isolation of T cells

To isolate murine splenic T cells, spleens taken from C57BL/6 mice were mashed and passed through a 70 µm cell strainer, then washed 1x in R10 medium before lysing red blood cells in RBC Lysis Solution (Qiagen) for 1 min while shaking. Cells were then washed in R10 medium before labeling with murine CD3ϵ MicroBead Kit (Miltenyi) for positive selection of CD3+ cells on a MACS column. For MACS isolation, manufacturer's instructions were followed except the incubation with CD3ϵ-Biotin and Anti-Biotin MicroBeads were increased to 20 and 25 min, respectively. The isolated cells were then resuspended in T cell medium (RPMI 1640 + 10% FBS + 1% P/S + 50 µM β-mercaptoethanol + 0.1 mM non-essential amino acids + 1 mM sodium pyruvate + 20 mM HEPES) and activated with Dynabeads™ Mouse T-activator CD3/CD28 (Gibco) and 50 U/mL IL-2.

T cell RNA isolation

Murine splenic T cells stimulated with Dynabeads™ Mouse T-activator CD3/CD28 and 50 U/mL IL-2 were seeded on CDMs at 10^6 cells/well and cultured in T cell medium at 37°C, 5% CO_2. After three days, T cells were harvested from the CDMs and stored at 4°C. The CDMs were then degraded by adding 1 mL 3 mg/mL collagenase type I (Worthington Biochem) pr. well and incubating for about 30 min at 37°C. After incubation, 1 mL R10 medium was added and samples were homogenized by pipetting. The degraded CDMs were transferred to the T cells previously aspirated. Samples were then washed x1 in PBS before isolating total RNA using the RNeasy Kit (Qiagen) according to manufacturer's instructions with β-mercaptoethanol added to the lysis buffer. RNA quantity and quality was determined using the 2100 Bioanalyzer (Agilent). Samples with total RNA RIN values > 7.3 were either kept separate or pooled by combining equal amounts of each replicate and used for RT-qPCR or bulk RNA sequencing.

T cell proliferation assay and flow cytometry

Murine splenic T cells isolated using CD3ϵ magnetic beads (Miltenyi) were stained with CellTrace Violet Cell Proliferation Kit (Invitrogen) according to manufacturer's instructions then resuspended in T cell medium and activated with Dynabeads™ Mouse T-activator CD3/CD28 (Gibco) and 50 U/mL IL-2. T cells were then seeded on CAF or NF CDMs at 10^6 cells/well and cultured for 4 days at 37°C, 5% CO_2. After 4 days, T cells were harvested from the CDMs by aspirating the medium and stored at 4°C while degrading CDMs with 3 mg/mL collagenase I as described above. Degraded CDMs were then transferred to the tubes with T cells followed by washing x1 in FACS buffer (PBS + 0.5% BSA [Sigma-Aldrich] + 5 mM EDTA [Sigma-Aldrich]). T cells were then resuspended in 50 µL FACS buffer and stained for 20 min at 4°C with 0.5 µL each of the following antibodies: FITC anti-mouse CD3, Pe/Cy7 anti-mouse CD4, APC anti-mouse CD8, PerCP/Cy5.5 anti-mouse CD25, PE anti-mouse CD267 (PD-1) and 1 µL Zombie Aqua Fixable Viability Kit (all from BioLegend). Samples were then washed x2 in FACS buffer, resuspended in FACS buffer and run on a BD FACSCanto™ II Cell Analyzer (BD Biosciences). Data was analyzed using the Proliferation Modeling plugin in FlowJo v. 10. Fluorescence minus one (FMO) controls and a negative control for Cell Trace Violet (no stimulation) were included in all experiments.

RT-qPCR

Total RNA was isolated from murine splenic T cells cultured on normal or CAF CDMs as described above. cDNA was generated from 100 ng total RNA using the iScript™ cDNA Synthesis Kit (Bio-Rad) following manufacturer's instructions.

A qPCR master mix was prepared by combining 5 µL Brilliant III Ultra-Fast SYBR® Green QPCR Master Mix (Agilent Technologies), 0.2 µL each of forward and reverse primers (Tag Copenhagen) pre-diluted to 10 µM, 0.45 µL UltraPure DEPC-treated water (Invitrogen) and 0.15 µL 1:500 ROX (Agilent Technologies). 6 µL of this master mix was loaded into the wells of a MicroAmp® Fast 96-well Reaction plate (Applied Biosystems) followed by 4 µL cDNA diluted 1:5. All samples were loaded in triplicates and 'no template'- and 'no reverse transcriptase' controls were always included. The plate was sealed with optical caps, spun down quickly then placed in an AriaMx Real-Time PCR System (Agilent Technologies). RT-qPCR was performed with 3 min activation at 95 °C, then for 40 cycles of 5 sec denaturation at 95°C and 20 sec annealing at 60°C followed by a melting curve analysis at 65°C-95°C in 0.5°C increments, 5 sec pr step.

Data was analyzed by the ΔΔCt method[166] using the average Ct value of the housekeeping genes (*Actb, Tubb5*) as an internal reference for normalization. This is equivalent to the Vandesompele method[167,168] when assuming 100% primer efficiency (see appendix A). Potential contamination of the samples with fibroblast RNA was ruled out by including a control for *Col1a1* expression. Primer information can be found in table B.1 in the appendix.

Bulk RNA sequencing

Total RNA (100 ng) isolated from ascorbic acid-stimulated fibroblasts or murine splenic T cells cultured on NF or CAF CDMs was prepared for sequencing using polydT-mediated cDNA synthesis (Illumina) in accordance with the manufacturer's instructions. Libraries were made with a NEBNext RNA Library Preparation Kit for Illumina. Library quality was assessed using Fragment Analyzer (AATI) followed by library quantification using the Illumina Library Quantification Kit. Sequencing was done on a NovaSeq 6000 platform (Illumina) with a minimum sequencing depth of 30 million reads per sample. Sequenced reads were aligned to the mus musculus mm10 using STAR[169]. Low-quality reads with MAPQ scores < 30 as well as unmapped and secondary alignments were removed using SAMtools. The gene expression count matrix was generated using featureCounts and annotated using GENCODE. The gene expression count matrix was further filtered to retain only those genes that were expressed in all samples and with an average read count > 10 across the samples.

The analysis of differential expression was performed using DESeq2 package[170] (v. 1.30.1) in R on variance-stabilized data (vst function). Principal component analysis was also performed using DESeq2. To generate volcano plots, data was shrunk using a heavy-tailed Cauchy prior distribution for effect sizes (apeglm package v. 1.12.0)[171] and plotted using the EnhancedVolcano package in R (v. 1.8.0). Heatmaps were generated from z-score-DESeq normalized counts using R (pheatmap package v. 1.0.12) on selected genes of interest.

Definition of extracellular matrix proteins

MatrisomeDB is a searchable database containing proteomic data from mass-spectrometric studies on ECM composition in various normal and cancererous tissues[172]. A list of ECM genes of interest was generated from the MatrisomeDB database (downloaded Sep. 26, 2020) by selecting core matrisome proteins (collagens, ECM glycoproteins, and proteoglycans) detected in all species and all tissues/tumor types and filtering for unique genes. This list contained a total of 261 core ECM genes.

Determining significantly upregulated ECM genes in LUAD fibroblasts

To determine differentially expressed genes in tumor vs. normal fibroblasts, we analyzed a single cell RNA sequencing dataset from patients with human lung adenocarcinoma (LUAD) which we accessed from the NCBI Gene Expression Omnibus database (accession code: GSE131907). The downloaded data set had already been subjected to quality control, normalization and filtering as described by Kim et al.[173] Briefly, quality control was performed with respect to mitochondrial genes ($\leq 20\%$), unique molecular identifiers (UMIs) and gene count (100-150,000 and 200-10,000) and normalized to $\log_2(\text{TPM}+1)$ before filtering out low-expression genes and centering the expression.

The downloaded scRNAseq dataset was further filtered to (i) only contain samples from the primary tumor and normal lung tissue (sample origin = tLung or nLung) (ii) only contain data from fibroblasts (Celltype.refined = Fibroblasts) and (iii) only contain the genes retrieved from the MatrisomeDB database as described above. This subset of the data set contained expression data on 253 ECM genes from 3239 cells (fibroblasts) in 11 patients.

Differential expression was determined by a Wilcoxon rank-sum test using tl.rank_genes_groups from the ScanPy package for Python and retaining only genes with an adjusted p-value < 0.05 and $\log_2(\text{FC}) \geq 1$. This list of genes differentially upregulated in tumor fibroblasts was then further filtered by discarding genes that were primarily expressed by another cell type in the dataset. The final list contained 38 ECM genes that were significantly upregulated in tumor fibroblasts compared to normal lung fibroblasts (see table B.3 in the appendix).

xCELLigence T cell cytotoxicity assays

A subset of the ECM genes significantly upregulated by tumor fibroblasts were ordered as recombinant human proteins (rhProteins) (details in table B.2 in the appendix) and screened for any immunomodulatory effect using an xCELLigence® Real-Time Cell Analysis (RTCA) instrument (Agilent). Prior to assessing the effect of rhProteins, optimal number of tumor cells and tumor-infiltrating lymphocytes (TILs) cells was determined by titration.

Baseline impedance was measured by adding 150 µL R10 medium to a 96-well E-plate (Agilent) after which 30,000 human patient-derived melanoma cells were seeded in a volume of 50 µL/well. Tumor cell proliferation was then measured for about 25-30 hours. Meanwhile, autologous rapidly expanded TILs (REP TILs) were thawed in pulmozyme buffer (RPMI 1640 + 1% P/S + 2.5% Pulmozyme® + 2.5 mmol/L $MgCl_2$) and rested overnight in RPMI 1640 + 10% heat-inactivated human serum + 1% P/S + 5 µg/mL rhProtein (if using).

The next day, TILs were harvested and washed then resuspended in R10 medium with rhProtein. 100 µL medium was then aspirated from the E-plate and 100 µL TILs were added for a final effector:target (E:T) cell ratio of 3:1 or 1:1 and rhProtein concentration of 5 µg/mL. Additionally, a negative control with fresh R10 medium without TILs or rhProtein was included as well as a control without rhProtein, a control containing 0.5% Triton X-100 and a control with TILs and 0.2 µM dexamethasone, which is a potent inhibitor of T cell cytotoxicity. T cell killing of tumor cells was then measured in the xCELLigence RTCA for 3 days.

The average normalized cell index for replicate wells was converted to % cytolysis as described in [174] for wells containing TILs or to tumor cell growth relative to the control for wells without TILs.

Statistical analysis

Data is presented as means ± SEM from independent experiments with at least 3 technical replicates pr condition unless otherwise noted. Statistical significance of flow data was assessed by a paired two-tailed Student's t-test. Statistical significance of RT-qPCR data was assessed by a two-tailed Student's t-test on $\Delta\Delta$Ct values. Differential gene expression was determined by a Wilcoxon rank-sum test for the scRNAseq data and a Wald test for the bulk RNAseq data. In both cases, p-values

were adjusted for multiple testing using the Benjamini-Hochberg method. Statistical significance of relative cytolysis in the xCELLigence RTCA screening assay was assessed by a one-tailed Student's t-test. Significance of differences between relative cytolysis for other xCELLigence assays was assessed by a one-way ANOVA and post-hoc Tukey HSD test where applicable. Where adherence to normality is an assumption of the statistical test, normality was assessed with the Shapiro-Wilk test. If normality was rejected, significance was assessed using log-transformed data after re-testing for normality. All statistical analyses except on bulk RNAseq were performed using SciPy v. 1.5.2 in Python v. 3.8.5. A p-value < 0.05 was rendered statistically significant. $^{*}p < 0.05$ $^{**}p < 0.01$ $^{***}p < 0.005$ $^{****}p < 0.001$

Chapter 3

Part I: Effect of tumor-associated cell-derived matrices on T cell activity

In this first part of the thesis, the effect of tumor extracellular matrix on T cell activity is investigated by culturing T cells on cell-derived matrices (CDMs). We first explore various methods for isolation of normal fibroblasts and cancer-associated fibroblasts from murine tissue. We next investigate the structure and potential composition of cell-derived matrices produced by these fibroblasts by analyzing matrix fiber orientation and fibroblast gene expression profiles, respectively. Lastly, the proliferation and activity of T cells cultured on these matrices is evaluated by flow cytometric and gene expression analyses.

Results

Methods for CAF isolation

In order to generate the CDMs for T cell culture, a relatively pure population of fibroblasts is needed. A common method used to isolate cells expressing a specific (surface) marker is by FACS sorting. However, FACS imposes a considerable amount of stress on the cells being sorted and consequently, the viability of the cells is often low after sorting. With limited cell survival, FACS sorting can therefore be challenging when the cell type of interest makes up only a small fraction of the starting material. Since fibroblasts make up a relatively small fraction of the cells in our mouse tumor model, we set out to find a more gentle method for isolation of fibroblasts from healthy and cancerous mammary gland tissue.

A number of methods were investigated for isolation of CAFs from primary tumors of female MMTV-PyMT;*Col1a1*-GFP mice (fig. 3.1a). These mice spontaneously develop breast tumors because of their overexpression of the polyoma middle T (PymT) oncogene under control of the mammary mouse tumor virus (MMTV) promoter. Additionally, the mice express GFP under the *Col1a1* promoter thereby labeling the *Col1a1*-expressing fibroblasts.

First, since fibroblasts are known to proliferate rapidly *in vitro*, we investigated whether fibroblasts in tumor single cell suspensions could outgrow the cancer cells by culturing them in fibroblast growth medium (fig. 3.1a, top). Second, since fibroblasts adhere strongly to plastic surfaces, we investigated whether potential differences in fibroblast and tumor cell adhesion could be exploited for fibroblast isolation using a differential adhesion protocol (fig. 3.1a, middle). Briefly, this was done by seeding the single cell suspensions in tissue culture plates and waiting 15, 20, 40 or 60 min, then aspirating the medium along with cells that had not yet attached to the plastic surface. Finally, we investigated whether fibroblasts could be efficiently isolated by magnetically activated cell sorting (MACS) (fig. 3.1a, bottom), using either a tumor-associated fibroblast isolation kit or by negative selection of tumor

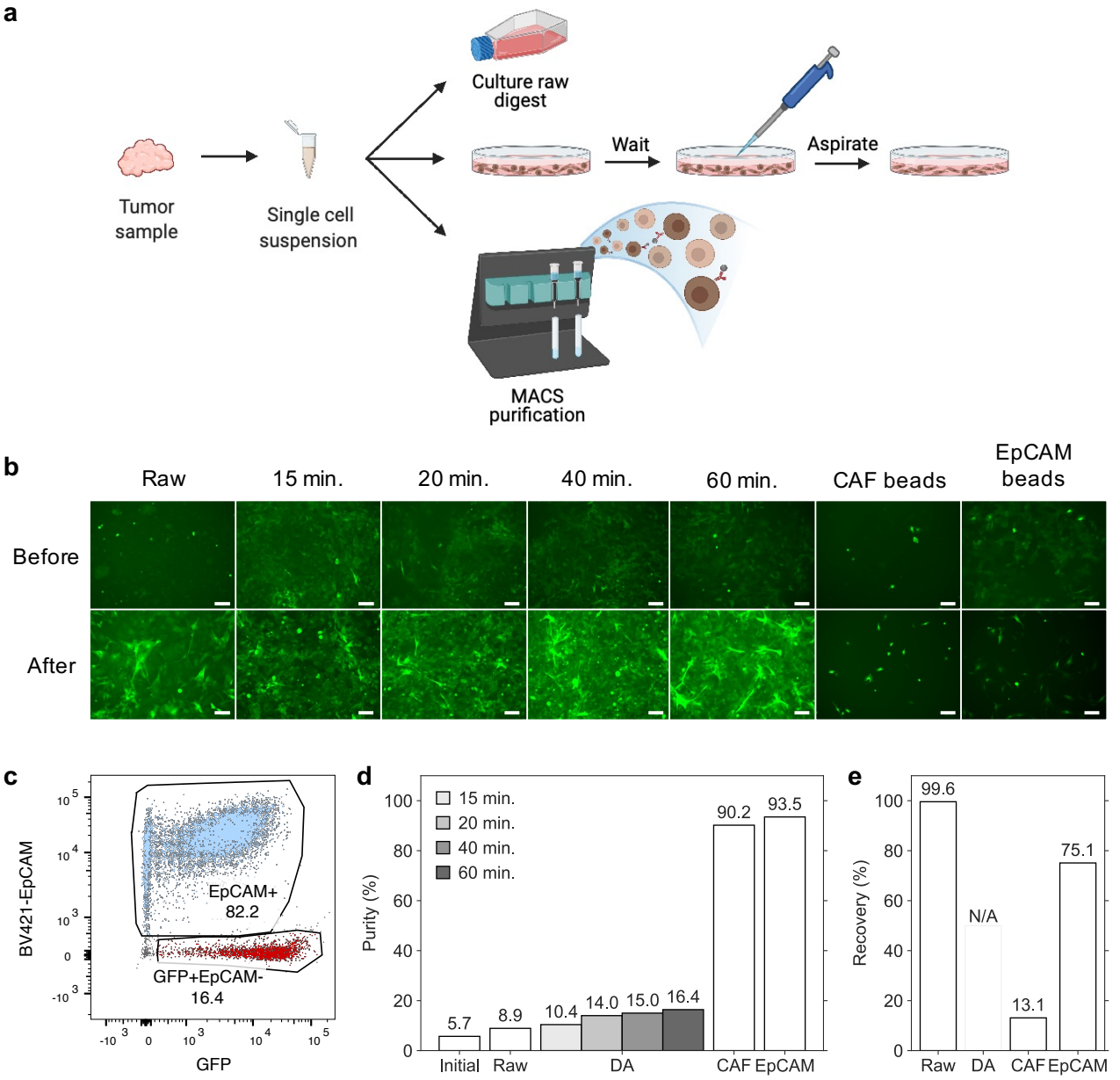

Figure 3.1: Different methods for isolation of fibroblasts yield different purities. Tumors from MMTV-PyMT;*col1a1*-GFP mice were excised at 10-12 weeks and frozen. (**a**) 3 different methods for isolation of fibroblasts were explored. They all started with obtaining single cell suspensions of the tumor sample, then either seeding the tumor digest for culture as is (top), using a differential adhesion (DA) method that takes advantage of different cells' tendency to physically adhere to plastic surfaces at different rates (middle) or by magnetically activated cell sorting (MACS, bottom) using either a cancer-associated fibroblast (CAF) magnetic bead kit or EpCAM magnetic beads. (**b**) Representative micrographs showing the density of fibroblasts (GFP, green) and tumor cells (autofluorescent) in the single cell suspensions before and after isolation with the indicated method. Raw = culture of the raw tumor digest. 15, 20, 40, 60 min. is the time incubated before aspirating the medium in the DA method. CAF and EpCAM beads = MACS isolation. Scale bars = 100 µm. (**c**) Gating of fibroblasts (GFP+EpCAM-) and tumor cells (EpCAM+) for flow cytometric analysis. Flow cytometry was used to quantify (**d**) the purity and (**e**) recovery of fibroblasts in the isolated fractions. Initial = fibroblast percentage in the tumor digest before isolation. There are no error bars on the bars as each of the methods were only tested once.

cells using magnetic EpCAM beads.

Before isolation, the main cell type in the tumor single cell suspensions is a slightly (auto)fluorescent cell type with irregular squamous-like morphology (fig. 3.1b), a description corresponding well with

that of epithelial cancer cells. In contrast, fibroblasts, defined here as GFP-expressing spindle- or stellate shaped cells, make up only a small portion of the tumor single cell suspensions. Other cells in the tumor microenvironment such as leukocytes cannot be seen under the fluorescent microscope.

Culturing the raw tumor digest in fibroblast growth medium for a week appears to increase the number of GFP^+ fibroblasts relative to autofluorescent tumor cells, but many tumor cells are still present in the sample (fig. 3.1b: raw). The trend is the same for the samples subjected to the differential adhesion protocol. Though the isolated fractions appear to be enriched in fibroblasts - and increasingly so with increasing incubation time - they still contain a large number of tumor cells (fig. 3.1b: 15 min, 20 min, 40 min, 60 min.). Increasing the incubation time beyond 60 min. was not relevant as most cells had attached to the plastic at that time such that barely any cells were aspirated with the medium (not shown). In contrast to the first two methods, the samples that were either positively selected using CAF beads or negatively selected using EpCAM magnetic beads mainly contain fluorescent cells i.e. fibroblasts (fig. 3.1b). Thus, it appears that these two methods are more efficient at removing tumor cells from the cell suspensions.

These observations are confirmed by flow cytometric analysis of the samples (fig. 3.1c-e). Fig. 3.1c shows the gating of the cells in the 60 min. differential adhesion sample into GFP^+EpCAM^- fibroblasts and $EpCAM^+$ cancer cells. This sample contains a significant portion ($\sim 80\,\%$) of $EpCAM^+$ cells that are either GFP^- or GFP^{lo}. The relatively large population of $GFP^{lo}EpCAM^+$ cells suggests that *Col1a1*, and thus GFP, is in fact expressed at low levels in the cancer cells. Additionally, the existence of a small population of GFP^-EpCAM^- cells shows that aside from cancer cells and fibroblasts, other cells are also present in the isolated samples. This is representative of all samples subjected to culture or a differential adhesion protocol, while MACS separated samples contained neither of the $EpCAM^+$ populations. However, while the tumor digest culture or differential adhesion methods did result in 1.5-3-fold enrichment of fibroblasts in the samples, the fibroblast purity was still $< 20\,\%$ (fig. 3.1d). In stark contrast, MACS isolation removed enough tumor cells from the samples to result in fibroblast purities of $90.2\,\%$ and $93.5\,\%$ using CAF or EpCAM beads, respectively (fig. 3.1d).

Besides purity, another important aspect for isolation of a specific cell type is the recovery of that cell type i.e. the fraction of the cells in the original sample that is captured during isolation. Especially when the cell type of interest is rare, as is the case for CAFs in these tumors, a high recovery is ideal. As expected, when the raw tumor digest was cultured all fibroblasts were retained in the sample (fig. 3.1e). Using EpCAM beads to negatively select for cancer cells, 75.1% of fibroblasts were recovered in the isolated fraction while only 13.1% of fibroblasts were recovered when using the CAF isolation kit.

Of the methods investigated for isolation of CAFs, MACS depletion of $EpCAM^+$ cells seemed most promising. We therefore further modified the protocol to optimize fibroblast yield.

Efficient fibroblast isolation from normal and MMTV-PyMT tumor tissue

Although the initial MACS protocol yielded a pure CAF population with high recovery, the absolute yield from a single tissue sample was still quite low. We hypothesized that isolating the fibroblasts immediately after obtaining single cell suspensions instead of resting them for a couple of days first might increase the number of fibroblasts obtained and thus reduce subsequent time needed for expansion. Additionally, we wanted to ensure that this method could also yield pure fibroblast populations from normal tissue samples. Thus, the above protocol for MACS depletion of $EpCAM^+$ tumor cells was then tested on normal mammary gland tissue and optimized to balance the yield of both normal fibroblasts (NFs) and CAFs.

When isolating cells by negative selection, the unlabeled fraction contains the cells of interest, while the labeled cells are discarded. After MACS separation of single cell suspensions of normal mammary gland tissue, the isolated and discarded fractions contain both GFP^+ fibroblasts as well as other cell types that are not fluorescent (fig. 3.2a, top left). However, after 4 days in culture, almost all the non-fluorescent cells in the isolated fraction have died, while they are still alive in the

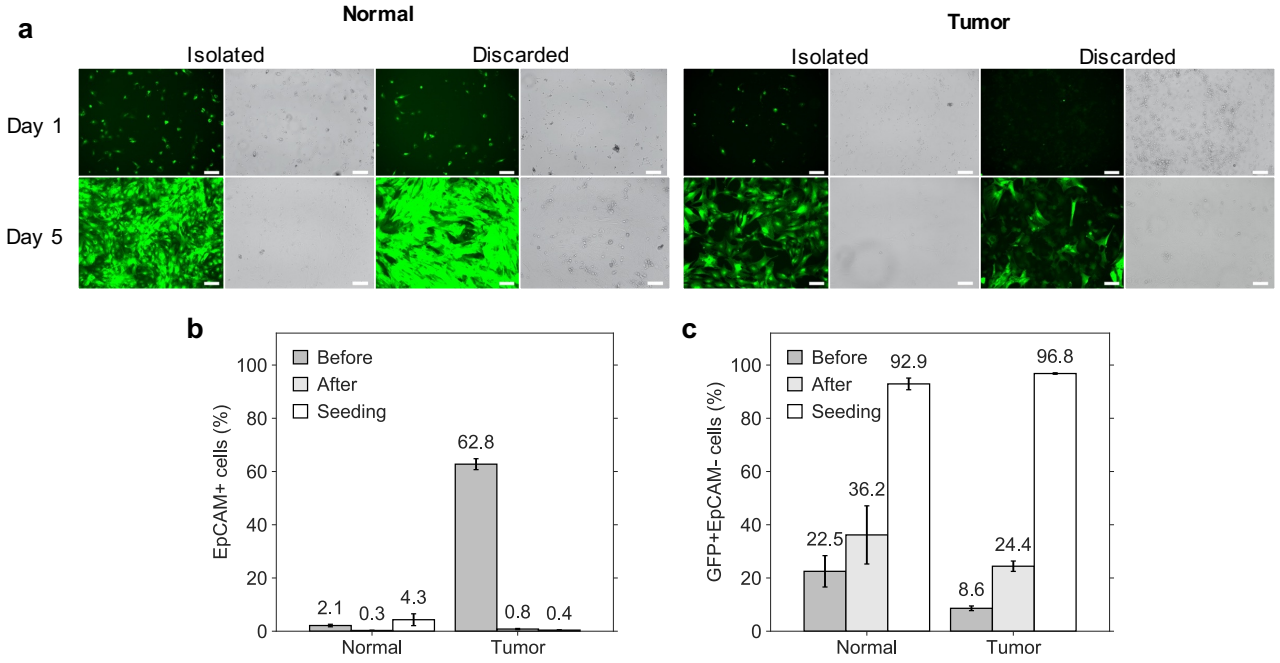

Figure 3.2: Fibroblast isolation by MACS depletion of EpCAM$^+$ generates samples with high purity. Tumors from MMTV-PyMT;*col1a1*-GFP mice or mammary gland tissue from healthy *Col1a1*-GFP littermates was excised at 10-12 weeks and frozen. Fibroblasts were isolated from thawed samples by MACS depletion of EpCAM$^+$ cells. (**a**) Representative fluorescent and brightfield micrographs of isolated and discarded samples from normal (left) and tumor tissue (right) taken on day 1 and day 5 after thawing and subsequent isolation. Scale bars = 100 µm. Percent (**b**) EpCAM$^+$ cells and **(c)** GFP$^+$EpCAM$^-$ fibroblasts of live single cells in the isolated fractions before MACS depletion (dark grey), after MACS depletion (light grey) and upon seeding for CDM generation after ~ 7 days in culture (white). EpCAM$^+$ cells and GFP$^+$EpCAM$^-$ cells were gated as in fig. 3.1c. Data are given as means ± SEM of 5 independent experiments using tissue from 3 different tumor-bearing mice and 2 different healthy mice.

discarded fraction. Therefore, the normal tissue sample must contain at least two different types of non-fluorescent cells: one type that is EpCAM$^+$ and survives during subsequent culture and another that does not. Likewise, the isolated tumor fraction contains a mixture of GFP$^+$ fibroblasts and non-fluorescent cells immediately after isolation, but upon 4 days of *in vitro* culture it appears to contain a pure fibroblast population (fig. 3.2a, top right). Conversely, the discarded tumor fraction primarily contains autofluorescent tumor cells as well as a small amount of fibroblasts. While some tumor cells do die after 4 days in culture, many of them remain viable and proliferate with the non-recovered fibroblasts. Overall, these micrographs indicate that fibroblasts can be efficiently isolated from both normal and tumor tissues by depletion of EpCAM$^+$ cells and subsequent *in vitro* culture.

We sought to further assess cell composition in the isolated samples by flow cytometric analysis before and after isolation as well as on the day of plating for CDM generation (fig. 3.2b-c). The initial MACS depletion with EpCAM beads efficiently removes EpCAM$^+$ cells from both normal and tumor single cell suspensions such that they make up $< 1\,\%$ of live cells after isolation (fig. 3.2b). This is a striking reduction for the tumor samples, which initially contain $> 60\%$ EpCAM$^+$ cells on average. After about a week of *in vitro* culture, the fraction of EpCAM$^+$ cells is reduced to $< 0.5\,\%$ for the tumor samples, while it has increased to $\sim 4\,\%$ for the normal samples. Thus, though there is a small fraction of EpCAM$^+$ (epithelial) cells among the normal mammary gland fibroblasts in the isolated samples, there is essentially no EpCAM$^+$ tumor cell contamination among the CAFs.

If the only goal of the isolation had been removal of the cancer cells, the fibroblasts could in principle have been seeded for CDM generation immediately after EpCAM$^+$ cell depletion. However, ideally the isolated samples should contain only fibroblasts, and MACS depletion of EpCAM$^+$ cells only increased the average fibroblast purity in the normal and tumor samples from 22.5% to 36.2%

and from 8.6% to 24.4%, respectively (fig. 3.2c). That is, after depletion of EpCAM$^+$ cells the samples still contain $> 60\,\%$ of non-fibroblast cells. Additional increases in fibroblast purity are obtained by culturing the isolated fractions *in vitro*. After 7 days in culture, most non-fluorescent/non-fibroblastic cells in the isolated fractions have died, resulting on average in a fibroblast purity of $92.9\,\%$ and $96.8\,\%$ in normal and tumor samples, respectively. In conclusion, pure populations of both NFs and CAFs can be isolated from our mouse model by MACS depletion of EpCAM$^+$ cells and subsequent *in vitro* culture for a short period of time.

Cell-derived matrices from NFs and CAFs are architecturally similar

After having efficiently isolated NFs and CAFs, CDMs were generated from each type by culturing them at high density in culture medium supplemented with ascorbic acid[155,156]. Generating CDMs from these fibroblasts was a major challenge, as cells often died within 24 hours of the first addition of ascorbic acid. Whether or not the cells would survive ascorbic acid treatment could usually be determined within minutes after ascorbic acid addition, since granules or vacuoles quickly formed in the cytoplasm of the cells that would die (fig. C.1 in appendix). If the cells did survive initial ascorbic acid stimulation, the matrices were denuded of cells after 10 days of ascorbic acid treatment to expose the collagen- and fibronectin-rich matrices (fig. 3.3a)[156].

In general, decellularized matrices from both NFs and CAFs appear highly isotropic with minimal alignment of CDM fibers (fig. 3.3b-e). To quantify the degree of fiber alignment, an orientation analysis was performed. A distribution of orientations in an image can be obtained by applying

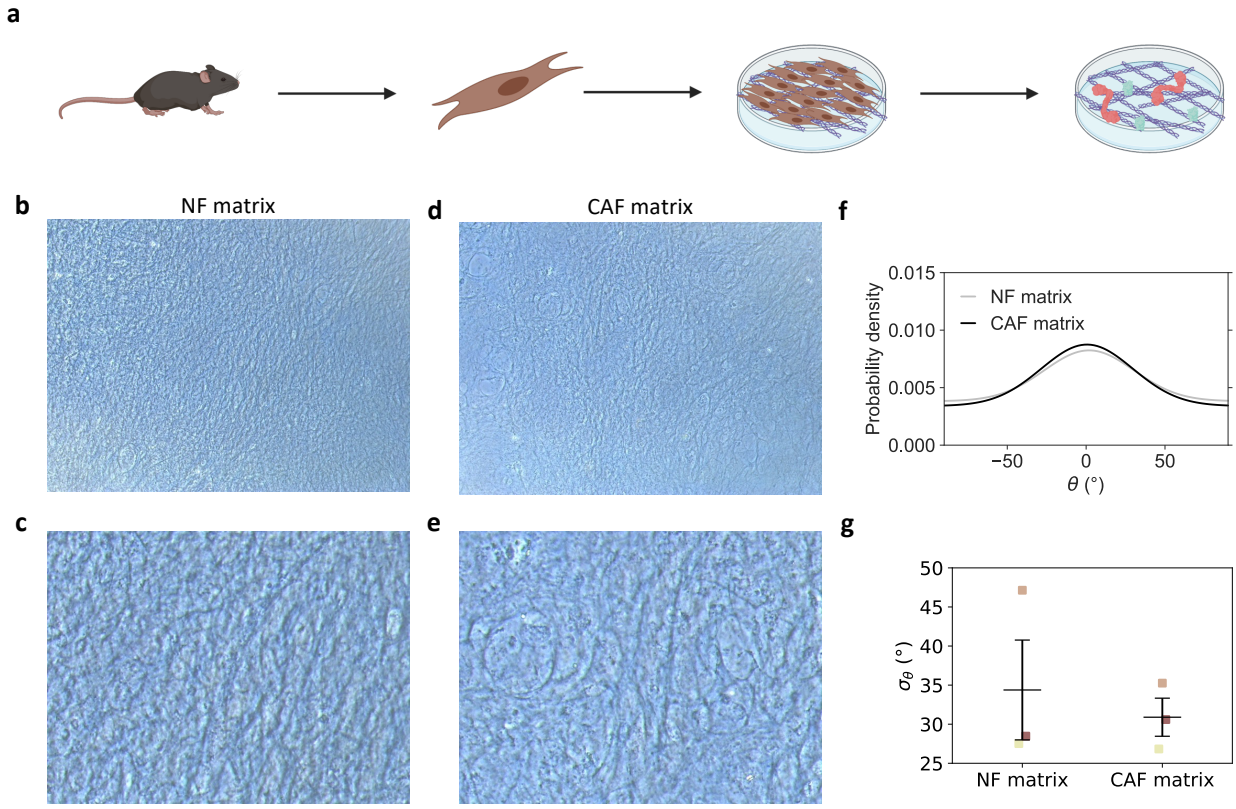

Figure 3.3: Cell-derived matrices from normal- and cancer-associated fibroblasts are structurally similar. (**a**) To generate CDMs, NFs and CAFs isolated from murine tissue were cultured at high density with ascorbic acid. Matrices were decellularized after 10 days when they were sufficiently thick. Representative phase contrast images of (**b, c**) NF and (**d, e**) CAF matrices at (b, d) low and (c, e) high magnification. (**f**) Average distribution of fiber orientation angle, θ, in NF and CAF matrices from three independent experiments. (**g**) Standard deviation, σ_θ, of orientation angle distributions for NF and CAF matrices from three independent experiments (different colors) as well as mean ± SEM.

a Fourier transform on the image and measuring the power at each angle in the resulting power spectrum. To this end, the Directionality plugin in Fiji[165] was used to derive the distribution of fiber orientations in NF and CAF matrices. The dispersion of these distributions was then used as a measure of the degree of fiber alignment in the matrices. On average, distributions of orientation angle, θ, are comparable between images of NF and CAF matrices (fig. 3.3f). Although there is a trend towards smaller dispersion, σ_θ, for CAF than NF matrices, indicating that fibers are more aligned in CDMs produced by CAFs, the difference is not significant (fig. 3.3g). Thus, there are no clear architectural differences between NF and CAF matrices.

CAFs and NFs express different ECM molecules

Although there seemed to be no structural differences between CAF- and NF-derived matrices, they might still differ in composition. To investigate whether CAFs and NFs differed in their expression of ECM proteins, we sequenced RNA from CAFs and NFs that had been stimulated with ascorbic acid for 3 days.

A principal component analysis (PCA) performed on the gene expression profiles shows that CAFs

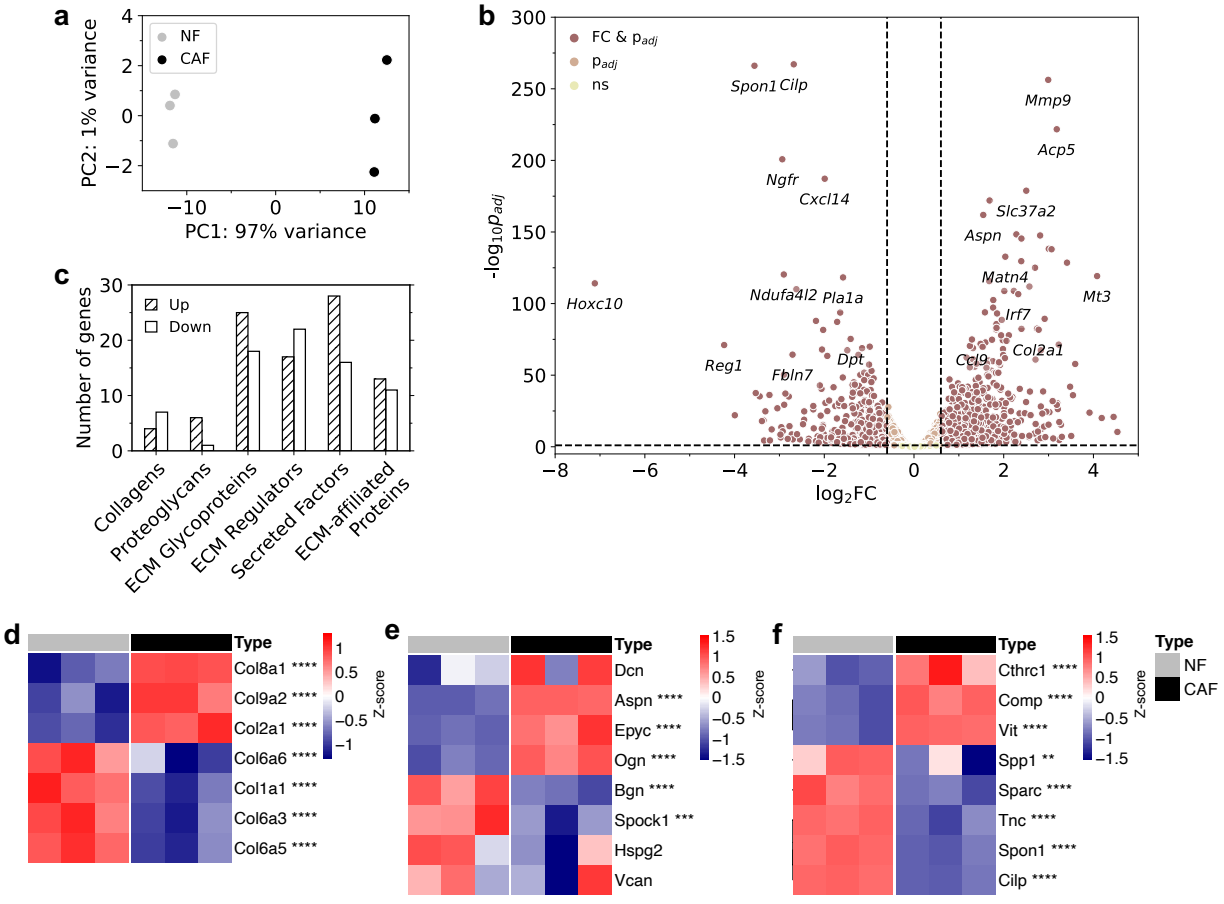

Figure 3.4: CAF and NF expression of ECM proteins is markedly different. Confluent CAFs and NFs were cultured in 50 µg/mL ascorbic-acid culture medium for 3 days followed by isolation and sequencing of RNA. (**a**) Principal component analysis (PCA) plot of CAFs and NFs. (**b**) Volcano plot of differentially expressed genes in CAFs relative to NFs. A subset of the most up- and downregulated genes are labeled with gene name. p_{adj} = adjusted p-value, FC = fold-change, ns = non-significant. (**c**) Number of significantly up- and downregulated ECM genes in CAFs relative to NFs plotted according to type of ECM gene. (**d-f**) Heatmaps showing z-score normalized gene expression level for a selected panel of (d) collagens, (e) proteoglycans and (f) ECM glycoproteins in CAFs and NFs. Asterisks indicate significantly regulated genes. 3 samples pr. cell type were sequenced.

and NFs can be easily separated based on the first principal component, which explains 97% of the variance (fig. 3.4a). Such clear separation of the two types of fibroblasts in the PCA plot indicates that their gene expression profiles are very different and suggests that many genes are differentially expressed. Indeed, a differential gene expression analysis identified 1255 differentially expressed genes (adjusted p-value < 0.05, abs($\log_2$ FC) > 0.6) out of 14617 genes analyzed in total. Of these, 827 genes were upregulated and 428 genes were downregulated in CAFs. A few genes with abs($\log_2$ FC) < 0.6 were also significantly up- or downregulated as depicted in the volcano plot in fig. 3.4b. Fig. 3.4b further shows that several of the most significantly up- and downregulated genes are ECM-related genes including *Spon1, Cilp, Mmp9* and *Aspn*.

In total, 168 of the differentially expressed genes are either core ECM or ECM-associated proteins. Especially ECM glycoproteins, ECM regulators and secreted factors are differentially expressed with over 40 up- or downregulated genes in each category (fig. 3.4c). Only few collagens and proteoglycans are differentially expressed between the two types of fibroblasts (fig. 3.4c), but heatmaps showing the the z-score normalized expression levels of selected genes still show a clear differential gene expression pattern (fig. 3.4d-e). As an example, subunits of collagen II, VIII, and IX are upregulated in CAFs while subunits of collagen I and VI are downregulated in CAFs (fig. 3.4d). Among the proteoglycans, *Aspn, Epyc* and *Ogn* are significantly upregulated while *Bgn* and *Spock1* are downregulated in CAFs (fig. 3.4e). The difference in gene expression is also striking for several ECM glycoproteins including for example CAF upregulation of *Cthrc1, Comp* and *Vit* and downregulation of *Sparc, Tnc, Spon1* and *Cilp* (fig. 3.4f). Thus, at the gene expression level it appears that NFs and CAFs could produce ECMs with different compositions and thus properties.

T cells cultured on CAF CDMs show signs of exhaustion

To assess the effect of CAF extracellular matrix on T cell activity, murine splenic T cells were cultured on NF- and CAF-derived CDMs for 4 days followed by evaluation of their phenotypic differences by flow cytometry. We first investigated expression of the co-inhibitory molecule PD-1. Though the majority of the T cells do not express PD-1, T cells cultured on CAF matrices do contain a larger fraction of PD-1-expressing T cells than those cultured on NF matrices (fig. 3.5a-b, fig. C.2a). However, the mean fluorescence intensity, i.e. the average level of PD-1 expression, did not differ (fig. C.2b).

PD-1 upregulation is a major characteristic of T cell exhaustion along with increased apoptosis and decreased proliferation[48]. We therefore further investigated whether viability and proliferation was affected in T cells cultured on CAF-derived CDMs compared to NF CDMs. In general, T cells cultured on either type of CDM are characterized by very high viability (fig. 3.5c-d, fig. C.2c). Culturing T cells on CAF CDMs does not reduce viability in any detectable way (fig. 3.5d).

Proliferation of T cells was assessed by a dye dilution assay. Prior to T cell stimulation, cells were labeled intracellularly with a membrane-permeable, amine-binding dye. For each subsequent cell division, the dye is divided evenly across daughter cells thus halving dye intensity in the cells. Because cell division is synchronized in the artificially stimulated cells, histograms of dye intensity contain distinct peaks for each division undergone by the cells. Both T cells cultured on NF and CAF CDMs proliferate readily with no noticable difference in Cell Trace Violet (CTV) intensity between the two (fig. 3.5e). There is, however, a non-significant trend towards fewer of the T cells starting to proliferate when seeded on CAF CDMs (fig. 3.5f, fig. C.2d). That is, the probability that a T cell will start dividing is likely smaller when seeded on CAF compared to NF CDMs. Further, culturing T cells on CAF matrices is associated with a tendency towards higher $CD4^+/CD8^+$ ratio i.e. fewer $CD8^+$ relative to $CD4^+$ T cells (fig. 3.5g).

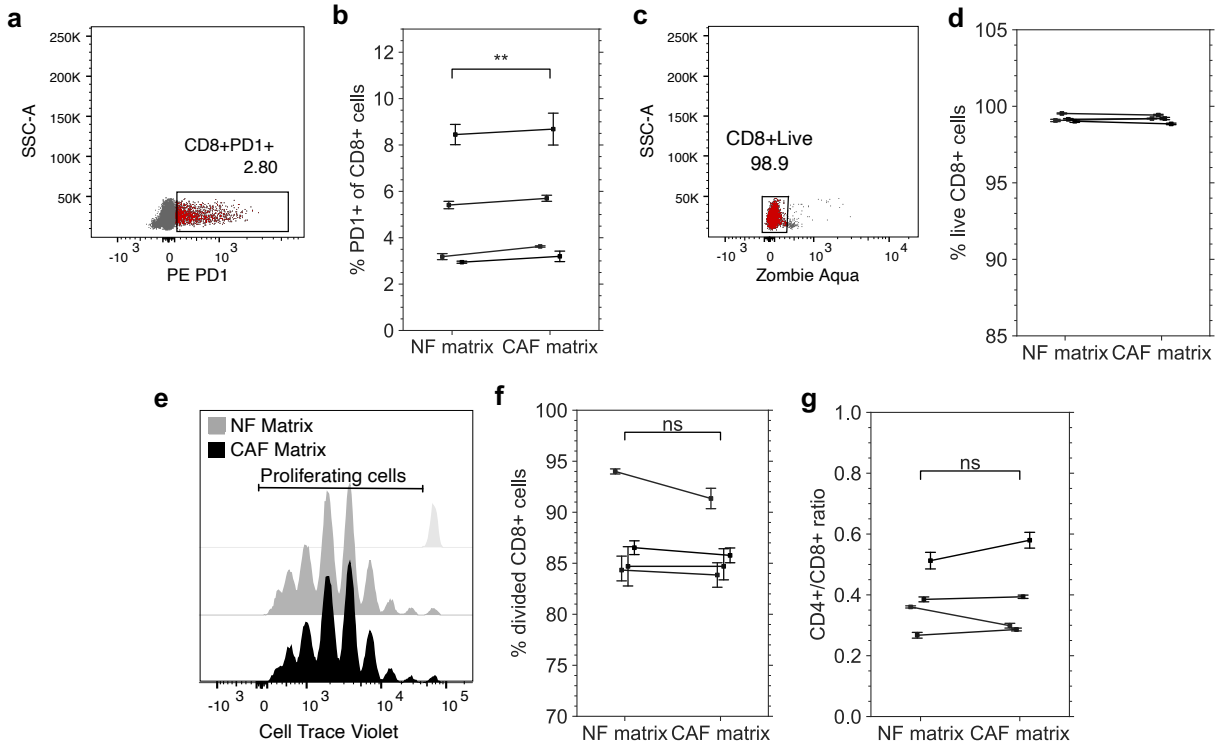

Figure 3.5: T cells cultured on CAF CDMs upregulate PD-1. Murine splenic $CD3^+$ T cells were labeled with Cell Trace Violet (CTV), stimulated with IL-2 and CD3/CD28 Dynabeads™ and cultured on NF- and CAF-derived CDMs. After 4 days, cells were harvested and stained for viability, CD3, CD4, CD8 and PD-1. (**a**) Example dotplot of PD-1 expression in live $CD8^+$ T cells cultured on CAF matrices. (**b**) Fraction of PD-1 expressing live $CD8^+$ T cells. (**c**) Example dotplot showing gating of $CD8^+$ cells negative for Zombie Aqua™ stain after culture on CAF CDMs. (**d**) Viability of $CD8^+$ T cells as determined from Zombie Aqua™ staining. (**e**) Representative example of CTV intensity in $CD8^+$ T cells cultured on NF and CAF CDMs. Unstimulated CTV-labeled cells were used as control (light grey, top). (**f**) Proliferation of $CD8^+$ T cells was quantified as the percentage of cells in the original culture that divided at least once (as defined in FlowJo). (**g**) $CD4^+/CD8^+$ ratio in live T cells. Figures **b, d** and **f,g** show mean ± SEM of at least 4 technical replicates from 4 independent experiments. Corresponding figures for $CD3^+$ and $CD4^+$ cells can be found in fig. C.2 in the appendix.

T cells cultured on CAF CDMs have altered gene expression profiles

Phenotypic evaluation of T cells cultured on CAF CDMs showed higher PD-1 expression as well as a tendency towards decreased proliferation and a decrease in the ratio of $CD8^+$ to $CD4^+$ T cells. To evaluate whether changes in T cell activity could also be observed on the gene expression level, we isolated total RNA from T cells cultured on NF and CAF CDMs for 3 days and used it for RT-qPCR and RNA sequencing.

RT-qPCR

Based on RNA sequencing results from a pilot study, we opted to quantify the expression level of the inflammatory cytokine IFN-γ and co-stimulatory molecule CD137 in the T cells using RT-qPCR. We first performed RT-qPCR on replicates from one experiment. As shown in fig. 3.6a, for this experiment IFN-γ (*Ifng*) appears to be upregulated in T cells cultured on CAF CDMs relative to T cells cultured on NF CDMs, whereas there is no difference in CD137 (*Tnfrsf9*) expression. This is opposite to what we expected from the pilot study. We therefore pooled RNA from each of several experiments and performed RT-qPCR on the pooled samples (fig. 3.6b). Doing so, we find that CD137 expression is downregulated in T cells cultured on CAF CDMs as well as a tendency towards downregulation of IFN-γ expression.

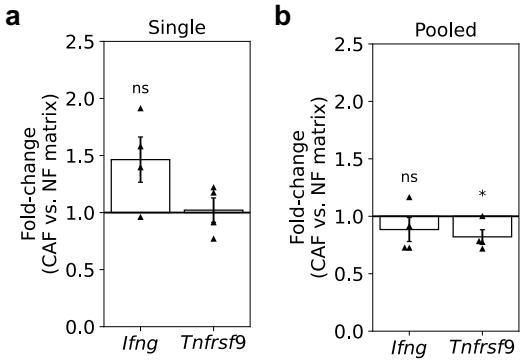

Figure 3.6: T cells cultured on CAF CDMs downregulate expression of CD137. RNA was isolated from murine splenic CD3$^+$ T cells cultured on CAF or NF CDMs for 3 days. (**a**) RT-qPCR performed on cell culture replicates from one experiment. Data shows mean ± SEM of 4 technical replicates from one experiment. (**b**) RT-qPCR performed on RNA pooled from all cell culture replicates in an experiment. Data shows mean ± SEM of pooled RNA from each of 4 independent experiments.

RNAseq on replicates from a single experiment

We further probed the differences in gene expression between T cells cultured on CAF and NF CDMs by sequencing the isolated RNA. As in the previous section, we first focused on replicates from a single experiment. Principal component analysis performed on the gene expression profiles separates the sequenced samples according to the type of matrix the T cells were cultured on (fig. 3.7a). However, while samples from T cells cultured on CAF CDMs cluster closely together, samples from T cells cultured on NF CDMs are more spread out in the PCA plot. This indicates great variation in the gene expression pattern of T cells cultured on NF CDMs.

Because samples could be separated according to culture conditions in the PCA plot, we performed a differential gene expression analysis to identify up- and downregulated genes in the T cells cultured on CAF CDMs. As shown in the volcano plot in fig. 3.7b, only three genes are differentially expressed (adjusted p-value < 0.1, abs($\log_2$ FC) > 0.6). Of these, expression of the gene for the muscle protein nebulin is upregulated in T cells cultured on CAF CDMs, while the transcriptional regulators Early Growth Response Protein 1 (EGR1) and -2 (EGR2) are downregulated.

The relative expression of a panel of T cell activation, T cell exhaustion and Treg cell markers are shown in the heatmaps in fig. 3.7c-e. The great variation in color for replicates of the same treatment indicate large differences in their gene expression levels, as could also be inferred from the PCA plot. Although none of the displayed genes are differentially expressed, certain trends are still evident. Of note, T cells cultured on CAF CDMs appear to downregulate the early activation marker CD69, the co-stimulatory molecule CD137 as well as the cytotoxic granzyme B molecules (*Gzmb*) (fig. 3.7c). Of the co-inhibitory molecules, T cells cultured on CAF CDMs appear to downregulate LAG-3 and, consistent with the flow analysis, upregulate PD-1 (*Pdcd1*) (fig. 3.7d). Lastly, there is also a trend towards upregulation of the transcription factor FOXP3, a marker for Tregs, in T cells cultured on CAF CDMs. Taken together these results indicate that the activity and function of T cells cultured on CAF CDMs is altered compared to T cells cultured on NF CDMs.

RNAseq on pooled samples

In order to establish whether the trends in gene expression observed for T cells from a single experiment were representative, we also sequenced pooled RNA from each of several experiments.

Principal component analysis clustered the sequenced samples according to experiment and not matrix type (fig. 3.8a), and we could therefore not perform differential expression analysis to compare the effect of NF vs. CAF matrices. Nevertheless, we still generated heatmaps for the same activation,

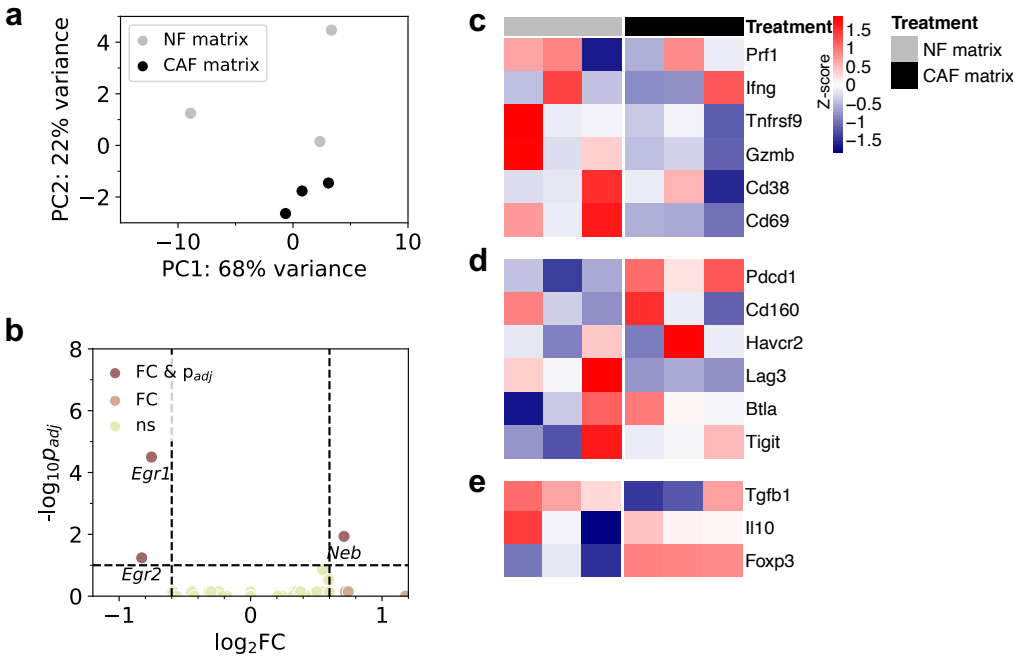

Figure 3.7: T cells cultured on CAF CDMs have altered gene expression profiles. Murine splenic CD3$^+$ T cells stimulated with IL-2 and CD3/CD28 Dynabeads™ were cultured for 3 days on CAF or NF CDMs followed by RNA isolation and sequencing. (**a**) Principal component analysis (PCA) plot of T cells cultured on NF and CAF CDMs. (**b**) Volcano plot showing differentially expressed genes in T cells cultured on CAF CDMs relative to NF CDMs. p_{adj} = adjusted p-value, FC = fold-change, ns = non-significant. (**c-d**) Heatmaps showing z-score-normalized gene expression levels for a panel of selected genes associated with (c) T cell activity, (d) T cell exhaustion and (e) regulatory T cells. 3 samples per condition from one experiment were sequenced.

exhaustion and Treg cell markers as in fig. 3.7 (fig. 3.8b-d). For most of the genes, the relative gene expression level is more similar within the same experiment than it is for the same culture conditions. This necessitates pairwise comparison within each experiment to assess the effect of CDM type on T cell gene expression. The heatmaps are therefore clustered column-wise according to experiment to ease intra-experiment comparison. For most of the experiments, there is a trend towards downregulation of CD137 and IFN-γ in T cells cultured on CAF compared to NF CDMs (fig. 3.8b), a trend which is consistent with RT-qPCR results. Differences in the within-experiment level of exhaustion marker expression are too small compared to differences in the across-experiment expression levels to be distinguished visually (fig. 3.8c). As for Treg cell markers, FOXP3 appears to be upregulated in T cells cultured on CAF CDMs for most of the experiments as well (fig. 3.8d).

While overall fewer trends are observed for the pooled RNA samples compared to replicates from a single experiment (fig. 3.7), the heatmaps for the pooled RNA samples still show a global tendency towards decreased effector T cell activity. However, large variation in the gene expression data both for individual and pooled samples remained a great challenge of data analysis.

Discussion

Methods for isolation of fibroblasts

Cell-derived matrices are *in vitro* native-like ECM's that can be generated by culturing fibroblasts at high density for prolonged periods. In order to generate CAF and NF CDMs, fibroblasts were isolated from primary tumors of MMTV-PyMT;*Col1a1*-GFP mice or mammary gland tissue from healthy *Col1a1*-GFP littermates, respectively. A number of methods were investigated for isolation

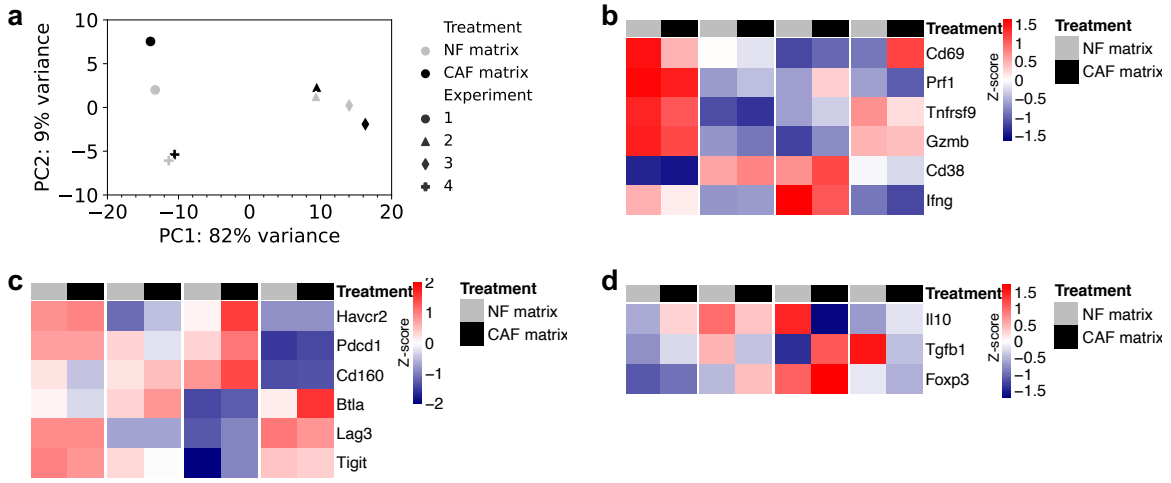

Figure 3.8: Gene expression profiles of T cells cultured on CAF CDMs vary between experiments. Murine splenic CD3$^+$ T cells stimulated with IL-2 and CD3/CD28 Dynabeads™ were cultured for 3 days on CAF or NF CDMs followed by RNA isolation, pooling and sequencing. (**a**) Principal component analysis (PCA) plot of pooled samples from T cells cultured on NF or CAF CDMs. (**b-d**) Heatmaps of z-score normalized gene expression levels obtained for pooled RNA for a panel of genes associated with (b) T cell activity, (c) T cell exhaustion and (d) regulatory T cells. Heatmaps are clustered column-wise according to experiment. RNA was pooled from 3-4 samples per condition for each of 4 independent experiments.

of fibroblasts.

Though fibroblasts are known for their rapid proliferation, CAFs from MMTV-PyMT tumors could not outgrow tumor cells during *in vitro* culture of raw tumor digests. This is likely due to the fact that many tumor cells can also be cultured in DMEM, a culture medium which is well suited for most adherent cells[175]. However, as cancer cells are quire robust, they willingly proliferate even under suboptimal conditions. Thus, the failure to obtain pure fibroblast populations with this method can be explained by the fact that culture conditions did not favor fibroblasts over cancer cells. A differential adhesion protocol was also investigated for isolation of CAFs. The motivation to use this method was initiated by a mishap in the laboratory where pure fibroblast populations were obtained after accidentally dropping a cell culture plate on the floor. However, though the controlled differential adhesion protocol did enrich the samples in fibroblasts, pure fibroblast populations could not be obtained with this method either.

Of the methods investigated, only MACS isolation by depletion of EpCAM$^+$ cells or using the CAF isolation kit yielded pure fibroblast populations. However, very few fibroblasts were recovered when using the CAF isolation kit compared to the EpCAM beads. There are two obvious explanations for this difference, both of which likely influence the outcome. First, the CAF kit procedure includes both a negative and a positive selection step, while the EpCAM procedure includes only a negative selection step. The additional step in the CAF procedure increases the probability that fibroblasts will be lost during labeling and washing steps thus ultimately decreasing the recovery. Moreover, there might be differences in the degree to which cells can be recovered depending on whether they are labeled with the magnetic beads (positive selection) or not (negative selection). Second, a positive selection requires that the antibodies used to label the fibroblasts are actually present. In the CAF isolation kit, magnetic beads for positive selection are conjugated to monoclonal anti-CD90.2 antibody. As fibroblasts constitute a heterogeneous cell population[94,95], it is possible that fibroblasts in the MMTV-PyMT tumors are lost during positive selection because they do not express CD90.2 and are therefore not labeled.

The low recovery of cells when using the CAF beads would require culturing for extended periods of time in order to obtain enough cells for CDM generation. This would not be ideal as culture of

primary cells *in vitro* results in gradual loss of their *in vivo* properties. Therefore, the longer the CAFs would be kept in culture, the less likely it would be that CDMs generated from them would differ from CDMs generated by NFs kept in culture for the same amount of time. Thus, the CAF isolation kit was not ideal for the purposes of this project. In contrast, MACS isolation of fibroblasts using EpCAM beads efficiently removed contaminating $EpCAM^+$ cells from the single cell suspensions with an acceptable recovery rate. Very pure fibroblast populations ($> 93\,\%$) could then be obtained while expanding the cultures in fibroblast growth medium for 1-2 passages.

Sensitivity of fibroblasts to ascorbate

The isolated fibroblasts were used to generate CDMs by culturing them at high density and supplementing with ascorbic acid. However, maintaining the fibroblasts, and especially the CAFs, alive upon the first stimulation with ascorbic acid remained a significant challenge. Often, cell death occurred within 24 hours of ascorbic acid addition, but formation of vacuoles or granules were seen already within minutes after stimulation. Several factors that might possibly explain such cytotoxic effects of ascorbic acid treatment were investigated, including fibroblast seeding density and confluence as well as ascorbic acid concentration (not shown)[176]. However, no definitive conclusions could be drawn from these investigations. Nevertheless, it seemed that the viability of the fibroblasts was maximized if exposure to air was minimized when the culture medium was changed.

Pharmacological doses of ascorbate have been shown to selectively kill cancer cells by induction of autophagy-associated cell death[177,178]. In these and other studies, the cytotoxic effects of ascorbate were mediated by reduction of O_2 to H_2O_2. Selective killing of cancer cells compared to healthy cells was attributed to lower expression of antioxidant enzymes such as catalase in the tumors[176,178]. Such autophagy-associated cell death is characterized by extensive cytoplasmic vacuolization[179]. The fibroblasts isolated in this study also formed vacuoles upon addition of ascorbic acid-containing culture medium. Thus, it is very likely that they responded to ascorbic acid treatment in a similar manner as has been reported for cancer cells.

Interestingly, treatment with catalase has been observed to abrogate ascorbate-induced cytotoxicity in cancer cells[176–178]. Thus, addition of catalase or another antioxidant enzyme to the ascorbic acid-containing culture medium might ameliorate the cytotoxic effects of ascorbate on the fibroblasts. This was, however, not investigated as cell survival could be greatly improved by minimizing the time that the fibroblasts were without medium, and thus exposed to air, during medium exchange.

Differences between CDMs generated by CAFs and NFs

Alignment of ECM fibers

It is a generally accepted hallmark of the tumor ECM that its fibers are more aligned than ECM fibers in healthy tissue[80,128,155]. The CDMs generated by NFs and CAFs in this study appeared isotropic and very similar in their architecture, both by visual inspection and when quantifying the orientation of matrix fibers. Nevertheless, there was a tendency towards CAF matrices exhibiting slightly more aligned fibers than NF matrices.

The CDMs were imaged using a simple phase contrast microscope. It is, however, more common to use second harmonic imaging or immunofluorescence microscopy to image ECM components[155,180,181]. One explanation for the lack of difference between the two types of matrices might therefore be that not all fiber types can be observed under a phase contrast microscope. Rather more sophisticated imaging modalities may be needed in order to correctly visualize and subsequently quantify the fibers.

Nevertheless, Park et al. also isolated fibroblasts from MMTV-PyMT mice and used them to generate CDMs[180]. Immunofluorescence imaging of the fibronectin-stained matrices revealed isotropic matrices with minimal differences between CAF and NF matrices. In the same paper, CDMs generated

by human vulval-, cervical- and oral tumor-derived fibroblasts were highly aligned. Further, Kaukonen et al. generated CDMs using fibroblasts from a patient with head and neck squamous cell carcinoma[156]. Again, though not quantified, these human CDMs appeared highly aligned and anisotropic with minimal differences between CDMs generated by normal and tumor-associated fibroblasts. Thus, the degree of fiber alignment in the CDMs appears to not only depend on the activation state of the fibroblasts but also to be very species- and tissue-dependent.

Expression of ECM molecules

The CAFs and NFs used to generate the CDMs exhibited substantial differences in their gene expression profiles with almost 10% of the total number of detected genes being differentially expressed. Several of the most differentially expressed genes were core ECM- or ECM-associated proteins. The murine matrisome consists of approximately 300 core ECM proteins and 850 ECM-associated proteins[172,182]. We found 168 ($\sim 15\,\%$) of these to be differentially expressed in CAFs compared to NFs. This suggests that CDMs produced by CAFs and NFs differ in composition. However, direct analysis of the protein composition in the CDMs is required to establish whether the observed differences in fibroblast gene expression translate to differences in CDM composition.

The core matrisome is made up of collagens, proteoglycans and ECM glycoproteins[182]. Collagens mainly confer structural and biomechanical properties to the ECM[68]. Proteoglycans and ECM glycoproteins, on the other hand, contain several binding domains for integrins and other cellular receptors suggesting an important role of these proteins in regulating cellular function[70]. A large number of the differentially expressed ECM genes identified in this study were ECM glycoprotein genes. Surprisingly, the ECM glycoproteins osteopontin, SPARC and tenascin C – which have previously been reported to be upregulated in tumor ECM tissue[183–185] and implicated in inhibition of antitumor immunity[139–142,148,149] – were downregulated in CAFs compared NFs. However, it has been shown that CAFs and cancer cells contribute differently to ECM production[79,81]. Therefore, although a particular protein may be specific for tumor ECM, fibroblasts may not necessarily be the source of the protein. Further, the same reports show that the composition of the tumor ECM depends on both tissue and tumor type. Caution should therefore be exercised in defining particular genes as specific for tumor ECM across cancer types or models.

We mainly considered core ECM proteins in our analysis of differential gene expression in CAFs vs. NFs. However, ECM-associated proteins may also alter the structure and composition of the CDMs and interact with cells seeded on the matrices. For example, during CDM production, fibroblast-derived ECM-remodeling enzymes such as MMPs and cross-linking enzymes may alter ECM fiber integrity and stiffness, respectively. Surprisingly, all lysyl oxidases and lysyl hydroxylases, which catalyze key reactions in the formation of collagen crosslinks, were significantly downregulated in CAFs compared to NFs (although $\mathrm{abs}(\log_2 \mathrm{FC}) < 0.6$, not shown) indicating that CAF CDMs could be less stiff than NF CDMs.

Further, the ECM has been reported to function as a reservoir for soluble factors. Consequently, cleaved protein fragments as well as fibroblast-derived matrix-bound cytokines and growth factors might modulate the function of cells subsequently cultured on the CDMs. Alternatively, binding of secreted factors to the matrix may prevent signaling molecules from interacting with cellular receptors. It is for example well-known that latent transforming growth factor β (TGF-β) complexes bind to ECM proteins such as decorin, collagen and fibronectin via latent TGF-β binding proteins[186,187]. The inactive ECM-bound TGF-β can then be converted to its active form by plasmin- or MMP-mediated cleavage *in vivo* or by physicochemical interactions *in vitro*[187]. However, such matrix-bound secreted factors are likely removed during decellularization of the matrices and would therefore play a negligible role in modulation of T cell responses.

Collectively, the observed differences in CAF and NF expression of ECM-related proteins may result in production of CDMs with differing compositions, properties and functions.

Effect of CAF CDMs on T cell activity

Differential regulation of T cell activity

Cell-derived matrices recapitulate many properties of native ECM[157,159]. They have previously been used to study cancer cell proliferation, migration and metastasis[156,188,189] as well as CAF contribution to tumor progression[98,180,190]. In this regard, it has been shown that CDMs generated by CAFs are sufficient to induce a CAF-like phenotype in normal fibroblasts cultured on the decellularized CDMs, a phenotypic switch not observed when fibroblasts were cultured on NF CDMs[190]. It has also been shown that culturing MDA-MB-231 breast cancer cells or HeLa cells on NF CDMs impedes cancer cell growth by inducing epigenetic changes in the cells that regulate expression of YAP and TAZ[188]. Our study provides a new dimension to the regulatory properties of CAF CDMs in that T cell activity is also differentially affected when cultured on CAF vs. NF CDMs.

The activity of T cells cultured on CAF CDMs appeared to be altered when compared to T cells cultured on NF CDMs. Flow cytometric analysis detected a significant upregulation of the co-inhibitory molecule PD-1 by T cells cultured on CAF CDMs, a trend that could also be inferred on the gene expression level. At the gene expression level we also identified a global trend towards downregulation of the co-stimulatory CD137 molecule and the pro-inflammatory cytokine IFN-γ. Downregulation of CD137 and IFN-γ by T cells cultured on CAF CDMs was previously indicated by a pilot study performed in our group (unpublished). In this thesis, we further found that T cells cultured on CAF CDMs tended to upregulate expression of the Treg transcription factor FOXP3. These observations point towards an inhibitory effect of CAF CDMs on T cell activity.

Interestingly, we also found the transcription factors EGR1 and -2 to be downregulated in T cells cultured on CAF CDMs. Others have shown that EGR1 binding to the promoter region of T-bet, a transcriptional regulator of Th1 cell differentiation, and concomitant T cell receptor signaling induces T-bet transcription and downstream IFN-γ production in *in vitro* cultured T cells[191]. Yet other studies have shown that EGR1 is critical for expression of the co-stimulatory molecule CD40L[192,193] as wells as the critical cytokine IL-2[194,195] and the β chain of the IL-2 receptor, IL-2Rβ[196]. Both EGR1, -2 and -3 have also been implicated in the upregulation of FasL expression by T cells[197,198]. Thus, differential expression of EGR1 and -2 in T cells cultured on NF vs. CAF CDMs could possibly explain their differing activities. Nevertheless, there are also several indications of T cell inhibitory roles of EGR2 and -3[199,200]. The functional consequence of EGR1 and -2 downregulation in T cells cultured on CAF CDMs and potential connections to decreased IFN-γ secretion should be studied further.

Unresponsive and exhausted T cells are characterized by lower viability and proliferation than their activated counterparts[48]. We observed a slight trend towards decreased proliferation - but not viability - of T cells cultured on CAF CDMs suggesting that activation of these T cells is impaired. It has previously been shown in our group that culturing T cells in dense 3D collagen matrices also restricts T cell proliferation without affecting viability[121]. As CAFs increase deposition of collagen in the tumor ECM[67], CAF-derived CDMs may also have high collagen content and modulate T cell proliferation via a mechanism similar to that of high-density 3D collagen gels.

Our previous study along with other related studies suggest a role for substrate rigidity in regulating T cell activation[121,122,201]. CAFs are known to increase deposition and crosslinking of stromal collagens[67], thus leading to increased stiffness of tumor ECM. In this study, we also observed considerable differences in the expression of ECM-related genes by the CAFs and NFs used to generate CDMs. Several ECM glycoproteins and proteoglycans have previously been associated with inhibition of T cell responses[100,142,146–153]. The observed effects of CAF CDMs on T cells could therefore either be due to an effect of specific ECM proteins on T cell activity or it could be due to differences in the physical properties of NF and CAF CDMs. As neither the composition nor the stiffness or thickness of the produced CDMs were investigated, the origin of altered T cell activity when cultured on CAF CDMs cannot be inferred.

Variation and reproducibility of CDM production

This study provides evidence that CAF and NF CDMs differentially affect T cell activity, but fails to provide an unambiguous picture of the effect. Although certain trends of differential T cell regulation were observed, the differences were small, inconsistent and non-significant. Results were also characterized by high variation both between samples in the same experiment and between independent experiments.

One important source of this variation could be a lack of reproducibility in CDM production, since CDMs with different properties would affect T cells differently. CDM properties are known to be highly dependent on fibroblast type, seeding density and other experimental conditions[155,156]. In this study, one of the major challenges associated with CDM production was maintaining the fibroblasts alive upon stimulation with ascorbic acid. Whether the fibroblasts survived initial ascorbic acid treatment seemed, to some extent, random in nature. Thus, although the same number of cells were plated for CDM generation, the response of the fibroblasts to ascorbic acid stimulation could ultimately result in a different number of CDM-producing cells between samples and hence CDMs of varying thickness or density. In addition, decellularization of matrices was performed one at a time and only inspected visually. Variation in CDM structure and integrity could therefore also arise due to too extensive CDM extraction, and thus degradation, in some samples[156].

Batch variation in CDM production could also arise due to differences between the fibroblasts used to generate each batch of CDMs. Different fibroblast proteomes could give rise to CDMs of varying compositions and stiffnesses, while slight variations in fibroblast activation state or viability could potentially result in different rates of CDM production. As CDM production was observed for a fixed number of days, this latter factor could result in CDMs of varying thicknesses. T cells cultured on the CDMs would then feel the underlying plastic surface vs. the matrix fibers to different degrees and respond accordingly.

Large variation between CDM samples and batches could explain the inconsistent results but only to some extent the small effect sizes. Another reason for the small effect sizes could be that T cells were stimulated with both artificial CD3/CD28 beads and IL-2, which induces strong activation in T cells[202]. As T cell activity is a result of the balance between activating and inhibitory signals[59], T cell inhibition of strongly activated cells may be hard to achieve. Commensurate with this line of thinking, it has been shown that inhibition of T cell Kv1.3 voltage-gated potassium channels by Kv1.3 blockers increased with decreasing CD3/CD28 bead:lymphocyte ratio, that is T cell stimulation strength[203]. Similarly, milder T cell stimulation might cause CAF CDM inhibitory effects to be stronger relative to activation and consequently reveal larger differences between T cells cultured on NF and CAF CDMs.

Chapter 4

Part II: Effect of tumor matricellular proteins on T cell cytotoxicity

In part I of this thesis, the effect of tumor extracellular matrix on T cell activity was assessed by culturing murine splenic T cells on CDMs produced by CAFs and subsequently evaluating the proliferation and gene expression profiles of the T cells. Since the CDMs were produced by primary CAFs, they are *in vitro* equivalents to whole tumor ECMs. A complementary approach to investigating the effect of tumor extracellular matrix on T cell activity would be to study the effect of individual tumor ECM constituents on T cell activity. In part II of this thesis we pursue such an approach.

We first select a set of potentially immunosuppresive proteins through an analysis of ECM-related gene expression in fibroblasts from patients with lung adenocarcinoma. We next assess the ability of each protein to modulate T cell cytotoxicity in a T cell-mediated killing assay. Lastly, the immunomodulatory effect of one of these proteins is investigated further.

Results

Selection of potentially immunosuppressive ECM proteins

In order to be able to investigate the effect of individual tumor ECM constituents on T cell activity, a set of tumor ECM proteins of interest were selected. Based on the assumption that immunosuppressive molecules are upregulated in tumors, we first identified significantly upregulated genes in human lung adenocarcinoma (LUAD) fibroblasts compared to normal lung fibroblasts from the same patients using the dataset presented in [173] and defining ECM genes as those listed in the online MatrisomeDB database[172]. Of the 21934 genes expressed by either tumor or normal lung fibroblasts, 2759 genes are significantly upregulated in the tumor fibroblasts (Wilcoxon rank-sum, $p < 0.05$, $\log_2 \mathrm{FC} \geq 1$) of which 38 are core matrisome proteins (fig. 4.1a, table B.3). More than half of these upregulated ECM proteins are glycoproteins, however, collagens and a small number of proteoglycans are also upregulated in the LUAD fibroblasts (fig. 4.1b).

The upregulation of a gene can generally be attributed to 3 different scenarios. Either (i) more cells are expressing the gene, (ii) the cells that express the gene increase their level of expression or (iii) a combination of the two. From the distribution of expression level we can determine which of these reasons explain why a given gene is differentially expressed. Fig. 4.1c shows examples of the 3 scenarios among the genes upregulated in CAFs compared to NFs. In this dataset more CAFs than NFs express *TGFBI* and *VCAN*, while CAFs generally express a higher amount of *COL1A1* and *BGN* than NFs do. As for *POSTN*, barely any NFs express the gene while a fair number of CAFs express it. That is, *POSTN* is specifically expressed by CAFs. A similar pattern is seen for many of the other upregulated genes (not shown).

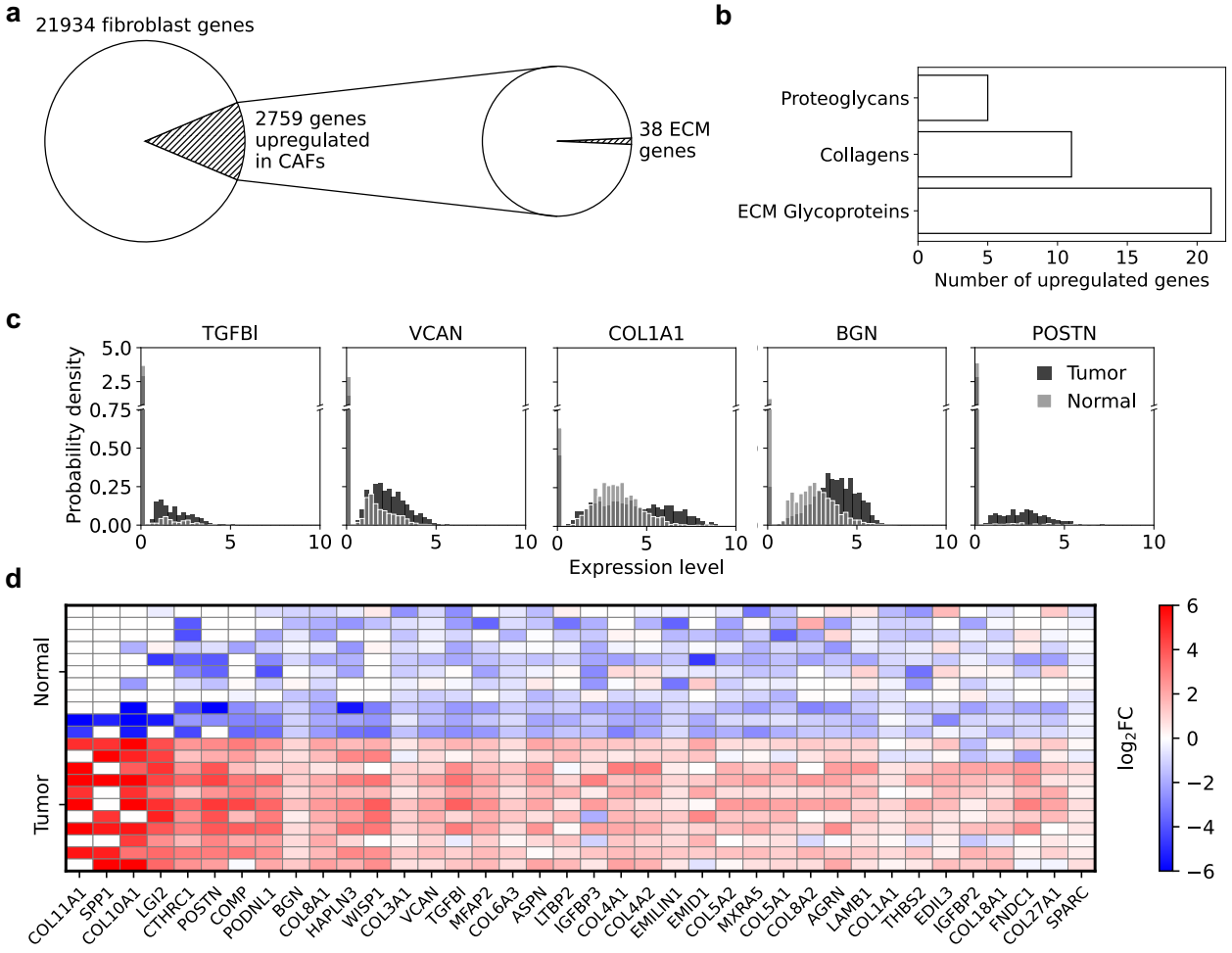

Figure 4.1: Identifying tumor ECM proteins of interest. scRNAseq data from patients with metastatic lung adenocarcinoma (LUAD) was obtained from NCBI GEO (accession code: GSE131907). The dataset was used for (**a**) differential expression analysis of NF vs CAF genes to determine significantly upregulated genes in CAFs ($\log_2 \mathrm{FC} \geq 1$, adjusted p-value < 0.05). These were subsequently filtered for core ECM genes only (table B.3). (**b**) The number of upregulated ECM proteins classified as proteoglycans, collagens and glycoproteins, respectively. (**c**) Representative examples of the expression level distributions observed for the upregulated ECM genes. Distributions are shown both for CAFs (tumor) and NFs (normal). (**d**) Heatmap of fold-change gene expression in CAFs and NFs from 11 patients with LUAD for all genes significantly upregulated in CAFs. For each patient, fold-change in NFs was calculated with respect to the average gene expression in CAFs and vice versa. White squares either correspond to a $\log_2 \mathrm{FC} = 0$ or lack of expression of the gene in a given patient.

The expression patterns of the upregulated genes not only vary between genes but also between patients, as can be inferred from the heatmap of fold-changes in fig. 4.1d. For example, 7 patients express OPN (*SPP1*) in CAFs, whereas only 1 of them express it in normal fibroblasts. In contrast, almost all patients express *CTHRC1* in both normal- and cancer-associated fibroblasts. However, the level of expression and thus fold-change of *CTHRC1* varies widely between patients, especially in the normal fibroblasts. For yet other genes, e.g. *IGFBP3*, some patients show a downregulation of that gene in their CAFs compared to NFs, despite the gene overall being upregulated in CAFs.

Because all these 38 genes are upregulated in CAFs compared to NFs, the secretion of each of their gene products into the ECM contributes to the altered composition and properties of tumor- compared to normal ECM. From the 38 ECM proteins, we selected 10 of them for analysis of potentially immunosuppressive activity. The selection was based on commercial availability of recombinant proteins and the degree of upregulation in CAFs compared to NFs (table 4.1).

Table 4.1: List of proteins selected for cytotoxicity assays and the type of ECM protein.

Gene	Recombinant protein name (alternative name)	ECM protein category
AGRN	Agrin	ECM glycoprotein
BGN	Biglycan	Proteoglycan
COMP	Cartilage oligomeric matrix protein (Thrombospondin-5)	ECM glycoprotein
IGFBP3	Insulin-like growth factor-binding protein-3	ECM glycoprotein
MATN3	Matrillin-3	ECM glycoprotein
POSTN	Periostin (Osteoblast-specific factor-2)	ECM glycoprotein
SPP1	Osteopontin (Secreted phosphoprotein 1, Bone sialoprotein-1)	ECM glycoprotein
TGFBI	Transforming growth factor-β-induced protein (βIg-H3)	ECM glycoprotein
VCAN	Versican	Proteoglycan
WISP1	WNT1-inducible-signaling pathway protein-1 (CCN4)	ECM glycoprotein

Principle and optimization of the xCELLigence RTCA killing assay

To investigate the potential immune modulatory effects of individual ECM components, a cellular assay to measure T cell-mediated killing of cancer cells was employed. For this purpose, we obtained primary patient-derived melanoma cells and autologous tumor-infiltrating lymphocytes (TILs). Since the TILs and tumor cells were isolated from the same patient, the TILs did not need to be artificially activated before use and already had tumor-specific T cell receptors.

The principle behind xCELLigence Real-Time Cell Analyzer (RTCA) killing assays is shown in fig. 4.2. To perform an xCELLigence RTCA killing assay, adherent tumor cells are first seeded in gold-coated cell culture plates and allowed to become confluent (fig. 4.2a). Non-adherent effector immune cells or other soluble components are subsequently added, and killing of the tumor cells is detected. The change in the degree of cell adhesion due to growth or killing of the target cells is measured indirectly as the impedance across the gold-coated electrodes. The impedance is converted to a cell index, which increases as the adherent cells proliferate (fig. 4.2b). When effector cells are added and kill the adherent cells, the cell index decreases accordingly as cells detach. The higher the ratio of effector to target cells, the more efficiently the target cells are killed and the faster the cell index decreases. The cell index can also be converted to % target cell cytolysis by calculating the change in cell index relative to the cell index of the negative control (fig. 4.2c).

For each new experiment, the number of target and effector cells to use has to be optimized according to the cell type used. Fig. 4.3a shows growth curves for the tumor cells used in this study seeded at different densities. As expected, the higher the seeding density, the larger the cell index (CI) is, but the shape of the growth curves is the same for all seeding densities. In general, the CI initially increases as the cells fall to the bottom of the wells, then plateaus for a while after which it starts to increase again as the cells proliferate. Because these tumor cells are primary cells, they grow relatively slowly compared to immortalized cell lines and therefore do not reach confluence (saturation in CI) at any of the seeding densities within the two days of the experiment. We therefore chose to use a seeding density of 30,000 cells/well in subsequent experiments - this is a relatively high seeding density but low enough that we do not risk cell death due to growth medium starvation during the 4 days a typical experiment lasts.

The effector:target (E:T) cell ratio also needs to be optimized according to the aim of the experiment. Fig. 4.3b shows the CI over time for an effector cell titration experiment using our tumor cells and TILs. Note that the CI has been normalized to the time of TIL addition as is customary for these types of experiments. For increasing E:T ratio, the normalized CI increases at slower and slower rates

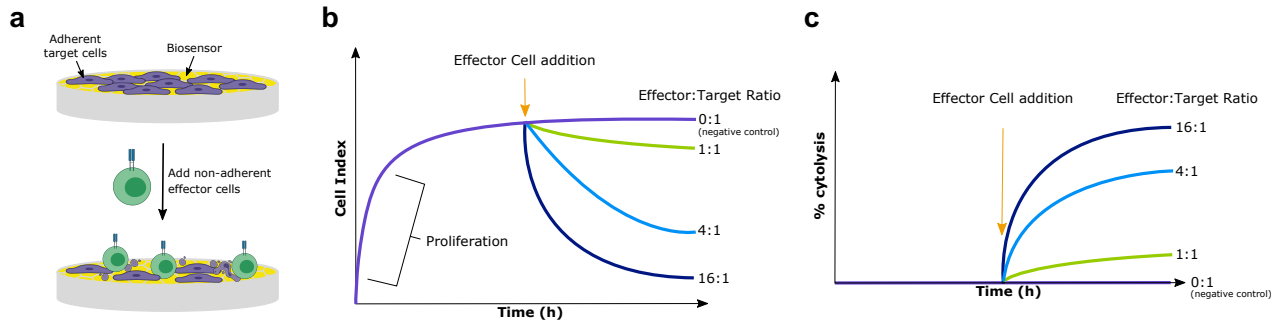

Figure 4.2: Principle of the xCELLigence RTCA killing assay. (**a**) The xCELLigence RTCA killing assay consists of two steps. 1) Seeding of adherent target cells on gold-coated cell culture plates and growth to confluence and 2) addition of non-adherent effector cells. The impedance across the gold-coated electrodes is used as a measure of cell adhesion and thus indirectly target cell growth or killing. (**b**) The impedance is converted to a cell index which changes as the adherent cells proliferate or die, respectively. The higher the ratio of effector to target cells, the more efficiently the target cells are killed. (**c**) % target cell cytolysis for curves shown in (b). Figures adapted from [204].

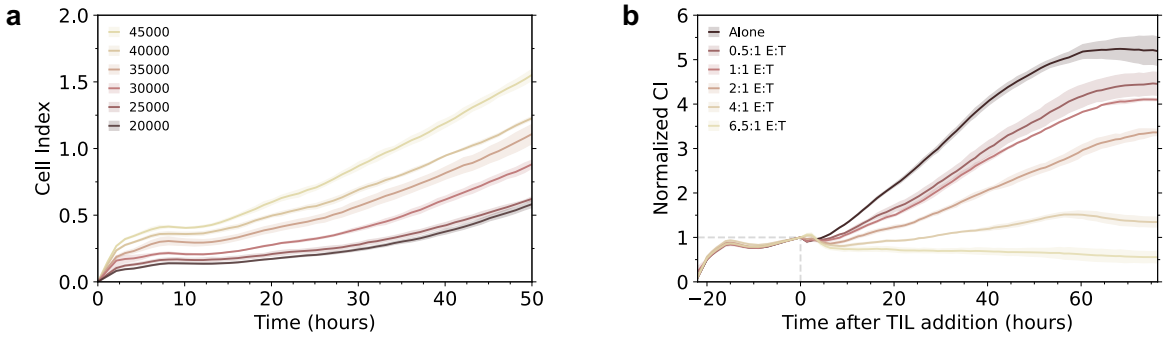

Figure 4.3: Titration of tumor cells and TILs for the xCELLigence RTCA killing assay. (**a**) Patient-derived melanoma cells were seeded in a range from 20,000-45,000 cells/well and incubated in an xCELLigence RTCA. Figure shows average cell index over time for 2-3 replicates pr. condition. (**b**) Patient-derived melanoma cells were seeded at 30,000 cells/well and incubated in an xCELLigence RTCA. After approximately 24 hours, autologours TILs were added at E:T ratios ranging from 0.5:1 to 6.5:1. Figure shows average cell index over time for 2 replicates pr. condition, normalized to the time of TIL addition as indicated by the dashed grey lines. Alone = tumor cells only, no TILs added. Shaded area corresponds to SEM.

- it even decreases for the high (6.5:1) E:T ratio. That is, the higher the E:T ratio, the more tumor cell growth is inhibited as is also depicted in fig. 4.2b. If we were to add T cell-inhibiting agents to the cells, the growth curve would change similarly to if we had reduced the E:T ratio. Conversely, adding T cell-stimulating or other cytotoxic agents to the cells would change the growth curve similarly to if we increased the E:T ratio. Since the aim of this study is to identify immune modulatory ECM components with no preference over immune suppression or -stimulation, we chose an intermediate (3:1) E:T ratio for subsequent screening experiments, which would allow observation of both T cell inhibition and stimulation.

Screening of recombinant proteins for effects on T cell cytotoxicity

To assess the potential immunomodulatory effect of the proteins listed in table 4.1, TILs were incubated with one of the recombinant proteins and killing of tumor cells by TILs was subsequently measured using the xCELLigence RTCA. Fig. 4.4a shows the normalized CI over time for cells incubated with and without the ECM glycoprotein periostin (POSTN). When there are only tumor cells in the culture, the CI increases nearly linearly over time as the cells proliferate and adhere to a still larger fraction of the well area. When TILs have been added to the tumor cell cultures, the CI remains approximately

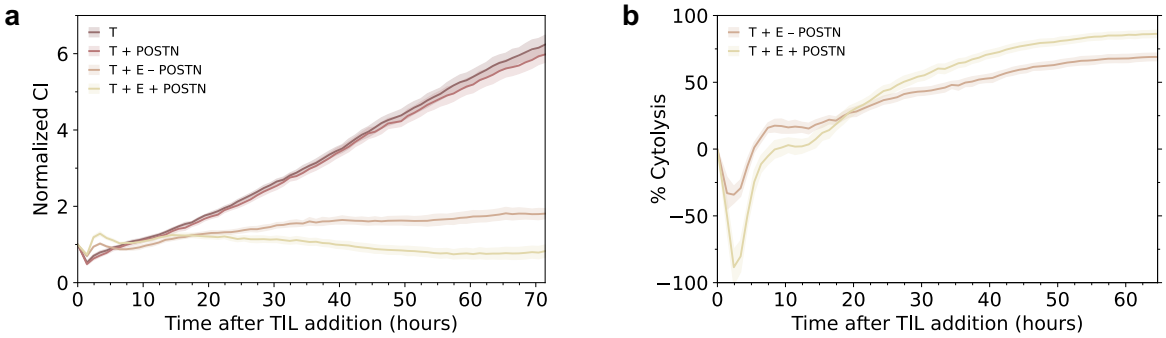

Figure 4.4: Effect of recombinant POSTN on TIL cytotoxicity. Patient-derived melanoma cells were seeded and incubated overnight in an xCELLigence RTCA. After 24 hours, recombinant periostin (POSTN) at 5 µg/mL and/or autologous REP TILs that had been pre-incubated for 24 hours with the protein were added to the tumor cells. (**a**) Example of normalized cell index (CI) traces and (**b**) the conversion to % cytolysis as shown for cells incubated with (+) and without (-) POSTN at E:T ratio 3:1. T = target/tumor cells, E = effector cells/TILs. Traces show the mean of 4 replicates and the shaded area corresponds to SEM.

constant for the duration of the experiment. This can be interpreted as T cells killing the tumor cells at approximately the same rate as the tumor cells proliferate thus resulting in no apparent change of tumor cell adhesion across the plate. Given that this premise is accepted, the relative change in CI between wells with and without TILs is the % tumor cell cytolysis by the T cells (fig. 4.4b).

If, in addition to TILs, POSTN is added to the tumor cell cultures, the CI slightly decreases over time indicating that POSTN increases tumor cell cytolysis (fig. 4.4a). In contrast, adding only POSTN and not TILs to the tumor cell cultures has no effect on the CI compared to cultures with tumor cells only. Thus, the decrease in CI observed when both TILs and POSTN are added to the tumor cells must be due to an effect of POSTN on the TILs. Presumably, POSTN therefore enhances the cytotoxicity of the TILs which can be easily seen in fig. 4.4b. At the endpoint of the experiment, TILs incubated with and without POSTN confer $\sim 85\,\%$ and $\sim 70\,\%$ cytolysis, respectively. That is, POSTN appears to increase the cytotoxicity of TILs by $\sim 20\,\%$.

The same experiment was repeated for the other proteins listed in table 4.1 (fig. C.3). The ratio of % cytolysis for TILs incubated with vs. without recombinant protein is shown in fig. 4.5a. Though for most of the proteins TIL cytotoxicity remains the same regardless of their addition to the cell culture, some of the proteins selected for screening appear to either enhance (POSTN, COMP) or diminish (VCAN, WISP1, MATN3) TIL cytotoxicity. However, when the recombinant proteins are added to tumor cell cultures without TILs, tumor cell growth is affected for the majority of the proteins (fig. 4.5b). In particular, tumor cells appear to grow faster when VCAN, WISP1 or MATN3 is added or slower when COMP is added. Thus, for these proteins changes in tumor cell cytolysis seem to be mediated by effects on the tumor cells rather than the TILs. POSTN, however, does not affect the proliferation of tumor cells. These effects become very clear when the % cytolysis is normalized with respect to the effect of the protein on tumor cell growth (fig. 4.5c). Here, most proteins result in a relative cytolysis of approximately 1 except for POSTN where the relative cytolysis is 1.17 ± 0.03 (mean ± SEM). Consequently, of the 10 proteins tested only POSTN significantly modulates tumor cell cytolysis by T cells.

Further probing the effect of POSTN

The E:T ratio used for screening of the recombinant ECM proteins was quite high and therefore resulted in almost 100% tumor cell cytolysis when POSTN was added to the tumor/TIL co-cultures (fig. 4.4). We hypothesized that the size of the effect of POSTN on TILs could be increased if the E:T ratio was decreased. Additionally, we wanted to verify that the effect was also present if POSTN

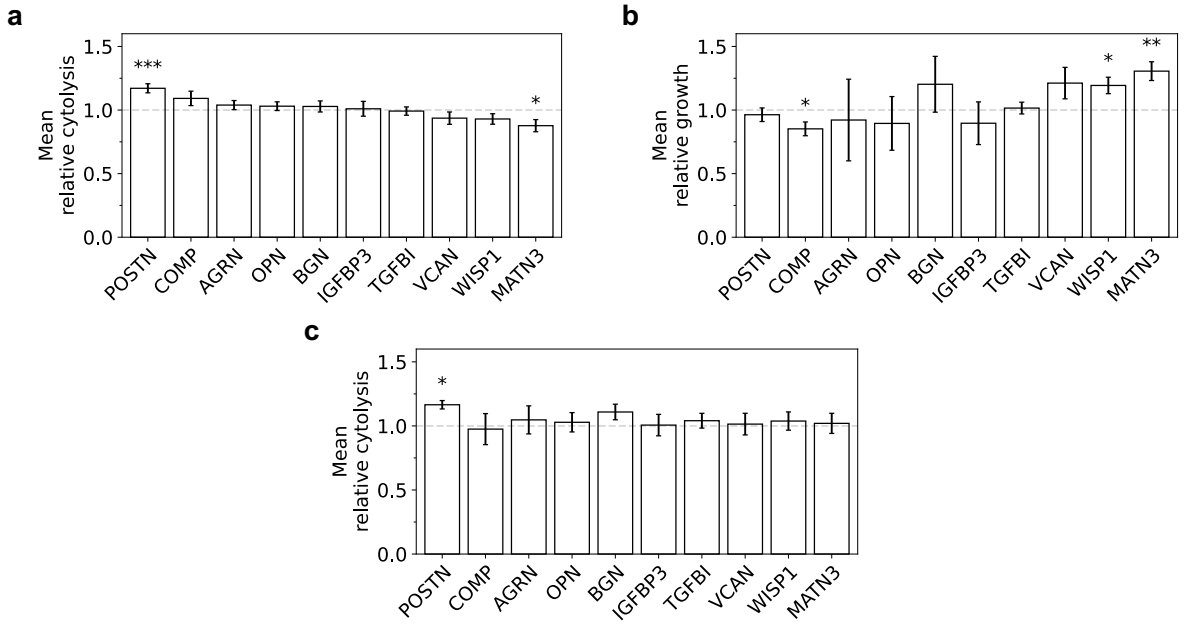

Figure 4.5: Screening recombinant ECM proteins for effects on TIL cytotoxicity. Patient-derived melanoma cells were seeded and incubated overnight in an xCELLigence RTCA. After 24 hours, recombinant ECM protein at 5 µg/mL and/or autologous REP TILs that had been pre-incubated for 24 hours with the protein were added to the tumor cells. The effect of selected recombinant ECM proteins on normalized CI was converted to (**a**) % cytolysis and (**b**) tumor cell growth relative to samples without ECM protein. (**c**) Effect of recombinant ECM proteins on % cytolysis relative to samples without ECM protein when correcting for the effect on tumor growth. Bars show mean ± SEM of 3-4 replicates each from 1-2 independent experiments at 65 hours after TIL addition to tumor cell cultures. Fig. C.3 shows examples of the normalized CI over time for all recombinant proteins except POSTN.

from another supplier was used.

The normalized CI over time for two different E:T ratios using POSTN from two different suppliers is shown in fig. 4.6a. Indeed, for TILs incubated with either of the recombinant POSTN preparations, the normalized CI values are lower than for TILs not incubated with POSTN. While the effect of the BioLegend preparation is not as high as that of the preparation from R&D Systems, both preparations increase TIL cytotoxicity significantly. Specifically, at a 1:1 E:T ratio the R&D Systems preparation resulted in a relative cytolysis of 1.80 ± 0.14 while the BioLegend preparation resulted in 1.53 ± 0.14 relative cytolysis (mean ± SEM) (fig. 4.6b).

We also wanted to investigate whether pre-incubation of the TILs with POSTN was sufficient to increase their cytotoxicity. Thus, we incubated TILs with POSTN both before and during co-culture with tumor cells as previously (full incubation), only during co-culture (post-incubation) or only before the co-culture (pre-incubation).

It appears that both pre- and post-incubation of TILs with POSTN affects the cytotoxicity of TILs (fig. 4.6c-d). Though full incubation yields the highest tumor cell cytolysis of these three conditions, both pre- and post-incubation increases the cytolysis of tumor cells relative to TILs not incubated with protein. After TIL addition, the normalized CIs for full- and post-incubated TILs seem to initially follow each other while that for pre-incubated TILs follows the one without POSTN (fig. 4.6c). However, around the 30-40 hour mark, the normalized CI for pre-incubated TILs plateaus compared to TILs without POSTN, resulting in separation of the two curves. At the same time, the normalized CIs for the full- and post-incubated TILs separate in a similar manner such that the slope of the full incubation curve decreases compared to the post-incubation curve. Thus, the full incubation curve adopts properties of both the pre- and post-incubation curves. From about 50 hours after TIL addition and onwards, there is clear separation between the normalized CIs for the three conditions

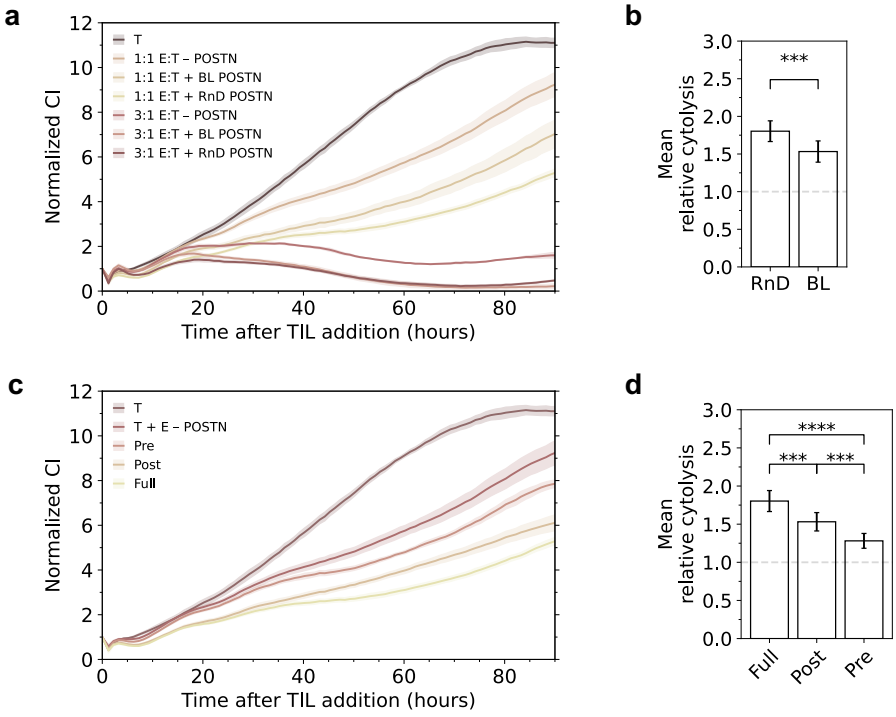

Figure 4.6: Further effects of POSTN on T cell cytotoxicity. Patient-derived melanoma cells were seeded and incubated overnight in an xCELLigence RTCA. After 24 hours, (**a**) recombinant POSTN at 5 µg/mL and autologous REP TILs that had been pre-incubated for 24 hours with POSTN were added to the tumor cells at either a 3:1 or 1:1 ratio. BL POSTN = periostin from BioLegend. RnD POSTN = periostin from R&D Systems. (**b**) % cytolysis relative to TILs not incubated with POSTN for the two different POSTN preparations at 1:1 E:T ratio. In (**c, d**) TILs were either pre-incubated with POSTN for 24 hours (pre), POSTN was added with the TILs (post) or both (full). (c) Examples of normalized cell index (CI) traces over time. (d) % cytolysis relative to TILs not incubated with POSTN. T = target/tumor cells. E = effector cells/TILs.

as well as that for TILs not incubated with POSTN.

At the 65-hour mark, the ratio of % cytolysis for TILs incubated with vs. without POSTN is 1.80 ± 0.14, 1.53 ± 0.12 and 1.28 ± 0.10 for full-, post- and pre-incubated TILs, respectively (mean $\pm$ SEM, fig. 4.6d). That is, while pre-incubation with POSTN does confer a 28% increase in cytotoxicity of TILs relative to TILs not incubated with POSTN, post-incubation results in a larger effect (53% increase) and full incubation maximizes the effect of POSTN on TILs (80% increase). Thus apparently, POSTN acts both before and during tumor/TIL co-culture to increase the cytotoxicity of TILs.

Discussion

Tumor ECM

We defined a tumor ECM gene signature by differential expression analysis of NF and CAF genes in patients with metastatic LUAD. Specifically, we focused on ECM genes whose expression is upregulated in CAFs compared to NFs. To that end, we found 38 ECM genes that were overexpressed in CAFs.

A tumor ECM should in principle not only be defined by those genes that are upregulated in the ECM-producing cells but also by downregulated genes. Our interest lied in identifying immunosuppressive ECM constituents which we would expect to be upregulated in metastatic tumors. Even so it is also possible that indirect immunosuppression could arise from a lack of stimulating signals as opposed to overactivation of inhibitory receptors. In this regard, a couple of studies have shown that the ECM proteins collagen, laminin and fibronectin can interact with T cells in a CD3-dependent

manner to induce proliferation[205–207]. Although these studies are relatively old and lack follow-up investigation, one can only speculate that other ECM proteins could play similar co-stimulatory roles. Reduced secretion of these proteins because of their downregulation in ECM-producing fibroblasts would then result in diminished T cell activation.

Nevertheless, Yuzhalin *et al.* showed that overexpressed ECM genes predict poor prognosis in a broad range of cancers[138]. Based on a meta-analysis of multiple datasets from several different types of adenocarcinoma, they identified a gene signature consisting of 9 overexpressed core matrisome genes. This ECM gene signature accurately predicted the long-term outcome for patients with each of the different cancers. Since (i) few instances of ECM-protein co-stimulation have been observed and (ii) overexpresseed ECM proteins can predict poor prognosis in many cancer types, overexpressed genes in the tumor matrisome arguably constitutes the most interesting subset of genes for investigation of immunosuppression.

The majority of genes in the 9-gene tumor ECM signature identified by Yuzhalin *et al.* coincide with upregulated tumor ECM genes found in this study (*COL11A1, COL10A1, SPP1, COL1A1, BGN, COMP, AGRN*)[138]. Further, another study showed that a gene signature comprised of 9 core and 20 ECM-associated genes could predict the overall survival of non-small cell lung cancer patients[136]. Here, 4 of the 9 differentially expressed core matrisome gene products were upregulated, namely *COL11A1, SPP1, COL10A1* and *CTHRC1*. Again, all these 4 genes were found to be among the most upregulated genes in tumor fibroblasts in our analysis. Thus, despite the fact that tumor ECM composition has been shown to be highly dependent on tissue type[79,81], several of the upregulated ECM proteins selected in this study are overexpressed in a variety of cancers and are predictors of poor prognosis. Therefore, any immunosuppressive functions of these proteins could likely represent a general immuno-evasive mechanism harnessed by cancer cells.

Screening for immunomodulatory effects of ECM proteins

Of the 38 proteins that were overexpressed in LUAD CAFs compared to normal fibroblasts, we selected 10 of them for screening of potential immunosuppressive effects. Specifically, we assessed their influence on T cell cytotoxicity and tumor growth using an xCELLigence RTCA.

ECM proteins affect tumor cell growth

Some of the proteins selected for screening appeared to accelerate the growth of tumor cells. These included VCAN, WISP1 and MATN3. Conversely, COMP seemed to inhibit tumor cell growth. As T cell cytotoxicity is only measured indirectly in the xCELLigence instrument, the apparent effect on TIL cytotoxicity when incubated with these proteins could also be a consequence of altered cancer cell proliferation/adhesion. We therefore did not investigate these proteins further. However, since more aggressive tumors would require a stronger immune response to be eradicated and vice versa, these proteins could still contribute to tumor escape or elimination, respectively.

Periostin increases TIL cytotoxicity

POSTN increased TIL cytotoxicity by up to 80% when incubated with TILs both before and during tumor/TIL co-culture. However, incubating the TILs with POSTN only before or during co-culture also increased the cytotoxicity of TILs. Further, the cell index over time for TILs that had been fully incubated with POSTN exhibited characteristics of both pre- and post-incubated TIL cell indices. Therefore, it appears that pre- and post-incubation of TILs with POSTN increases TIL cytotoxicity in distinct ways.

The mechanism behind the increase in tumor cell cytolysis when TILs were incubated with POSTN was not investigated. However, it may be due to a number of reasons such as induction of T cell proliferation or effector molecule expression/secretion. Increased expression of e.g. granzymes or FasL

would increase tumor cell cytolysis by increasing the cytotoxicity of the individual T cells. In contrast, increased proliferation would increase the number of TILs relative to tumor cells thereby increasing the overall system capacity to kill the tumor cells. There have been no reports on POSTN induction of proliferation in T cells, but POSTN has been shown to induce proliferation in cardiomyocytes[208], keratinocytes[209] and a number of cancers[210]. In this thesis, no effect of POSTN on cancer cell proliferation was observed. Alternatively, increased tumor cell cytolysis upon POSTN treatment may be due to increased expression of proteins associated with antigen presentation in tumor cells e.g. MHC or TAP proteins, or it may sensitize tumor cells to T-cell-mediated killing.

Besides, POSTN has also been found *in vivo* to recruit Wnt ligands in the cancer stem cell niche and thus increase Wnt signaling in the TME[211]. Several studies have shown that an increase in Wnt signaling in tumors is associated with a decrease in T cell infiltration[212,213] and blocking of CTL differentiation[214] thereby inhibiting antitumor immunity. This discrepancy between *in vitro* and *in vivo* findings needs to be investigated further before the role of POSTN in antitumor immunity can be definitively established.

ECM proteins with no effect on T cell cytotoxicity

The majority of the screened proteins (AGRN, OPN, BGN, IGFBP3 and TGFBI) neither affected tumor cell growth nor TIL cytotoxicity. However, the hypothesis that these proteins could have direct suppressive effects on T cell cytotoxicity cannot yet be fully rejected for a number of reasons. First, TILs were only incubated with recombinant protein for 24 hours prior to addition to tumor cell cultures and it may take longer before their potential effect on the T cells manifests itself phenotypically. Indeed, we saw that the difference in % cytolysis between TILs incubated with and without POSTN, respectively, increased over time. Hence, a longer pre-incubation of the TILs with the proteins might reveal a larger and thus measurable effect.

Second – and this applies to all the proteins investigated in this study – the proteins were only screened for effects on a single patient-derived tumor cell line and autologous TILs. Since cancers are known for their high levels of both intratumoral and interpatient heterogeneity[215,216], what has been observed here needs to be confirmed in cells derived from other patients. Further, the role of these proteins in modulation of immune responses in other cancers should be investigated.

Third, regulation of T cell function by these proteins might require additional protein or cellular components. Such indirect inhibitory effects are well-known in the case of the co-inhibitory molecule CTLA-4 which impairs activation of T cells via its interaction with DCs[53,55]. Indeed many ECM proteins have been shown to recruit and induce an immunosuppressive phenotype in myeloid cells[140,141,143–145,153]. Further, it could be that the proteins primarily exert their function on $CD4^+$ T cells. In this case, minimal immunoregulatory effects would be observed in this study as the TILs used had been enriched for $CD8^+$ T cells. ECM proteins may also have other regulatory functions. In this regard, POSTN has been shown *in vitro* to enhance collagen crosslinking by activation of the crosslinking enzyme lysyl oxidase[217]. As was described in the introduction, such increases in ECM stiffness are then able to modulate T cell and macrophage activation and polarization[121–125]. Other matricellular proteins may have analogous functions.

Furthermore, if these proteins were able to modulate T cell function, the effect sizes of individual proteins might be too small to observe by themselves but could add up significantly when combined. This is corroborated by the fact that most often single proteins rarely act as prognostic markers. Rather aberrant expression of a combination of proteins collectively predict patient prognosis in most cancers[216,218,219]. Moreover, a tumor tends to utilize not one but several different immunosuppressive mechanisms to facilitate immune escape[220]. This implies that the protein and cellular interactions along a single pathway are not strong enough to inhibit antitumor immunity. Instead, various mechanisms acting on different axes are required to suppress an immune response.

Lastly, ECM proteins are normally embedded in a non-soluble matrix of collagens and other

structural ECM proteins. The addition of recombinant soluble ECM components to the cell cultures might therefore not reflect how the proteins are presented to cells *in vivo*. Consequently, the biological function of the proteins might differ in the cell cultures compared to in the tumor microenvironment.

Chapter 5

Conclusions & Outlook

This study aimed to investigate the contribution of tumor extracellular matrix to modulation of the antitumor immune response in cancer. Our research showed that the extracellular matrix as a whole as well as individual extracellular matrix components are able to regulate both the activation and cytotoxicity of T cells.

In part I of the thesis we found that while NF and CAF expression of extracellular matrix constituents differed considerably, cell-derived matrices produced by NFs and CAFs were architecturally similar. T cells cultured on CAF matrices had slightly altered gene expression profiles compared to T cells cultured on NF matrices. In particular, expression of T cell activity markers and regulatory T cell markers appeared dysregulated in T cells cultured on CAF CDMs. However, large variations in gene expression levels warrant further investigation of these effects. In part II, we identified the extracellular matrix protein periostin as a modulator of T cell cytotoxicity. Surprisingly, incubation of T cells with recombinant periostin augmented cytolysis of tumor cells as measured using the xCELLigence Real-Time Cell Analysis assay. Several other ECM proteins appeared to influence the proliferation of tumor cells but had no effect on T cell-mediated killing.

Although several studies have investigated the relationship between specific extracellular matrix constituents and antitumor immunity before, this project is the first to study the effect of tumor extracellular matrix as a whole on T cell activity. Further, CDMs have previously been used as a tool for 3D culture of a variety of cells, but to date no one has used them for 3D culture of T cells. Part I of the thesis therefore presents a novel approach to studying the effects of extracellular matrix on immune cell subsets.

Our results indicated a suppressive effect of extracellular matrix on T cell activity, but further studies are needed before the inhibitory role of tumor extracellular matrix can be definitively established. We observed large variations in T cell response to culture on the CDMs and speculated that lack of reproducibility in CDM generation may partly account for this. We therefore suggest that future studies examine factors such as matrix integrity and thickness prior to cell culture on the CDMs to ensure consistent CDM production. Further, CDM stiffness, viscoelasticity and composition could be investigated by AFM, rheologic and proteomic methods, respectively, in order to further control for variation as well as indicate possible mechanisms of differential T cell regulation by NF and CAF CDMs. The large variation between samples was mainly observed for RNA sequencing data. Alternative approaches to studying T cell activity such as using enzyme-linked immunosorbent assays to study cytokine release and employing larger RT-qPCR panels could be utilized to give a clearer picture of the effect of CAF CDMs on T cell function. It would also be interesting to investigate the effect of CAF CDMs on other immune cell subsets such as macrophages which are able to modulate T cell function and hence antitumor immunity.

Periostin has previously been investigated for its role in TAM recruitment, metastatic niche formation and tumor progression and is suggested to have tumor-promoting roles. We here reported conflicting data indicating a T cell-stimulating antitumor function of periostin. The enhanced cytotoxicity of T cells after exposure to periostin may be used as a future therapeutic strategy to aid tumor elimination. However, further aspects of periostin-related increase in tumor cell cytolysis first need to be investigated before such an application can be realized.

First of all, our study only provided evidence that periostin increases tumor cell cytolysis by tumor-infiltrating lymphocytes from a single patient. Further studies would need to verify this effect of periostin more generally by investigating its effect on multiple other patient-derived cell lines.

Second, this study provided an indirect measurement of enhanced T cell-mediated killing of tumor cells when incubated with periostin. This finding should be confirmed by other more direct methods in order to delineate the mechanism behind the periostin-mediated effects. In this regard, we speculated that periostin may modulate T cell cytotoxicity by increasing their proliferation or effector molecule secretion. Alternatively, periostin may affect tumor cells by sensitizing the tumor cells to T cell-mediated killing or by increasing their presentation of tumor-associated antigens. Such hypotheses could be investigated by assessing e.g. tumor- and T cell gene expression by RNA sequencing as well as tumor cell surface expression of MHC molecules and effector molecule production in T cells by flow cytometry. Another interesting direction would be to identify which receptor(s) mediate the effect.

Lastly, the approach employed here to study T cell cytotoxicity involved addition of soluble ECM proteins to tumor/T cell co-cultures. This simple setup does not encompass the much more complex interactions in a tumor where T cell activity is also influenced by a myriad of other proteins and cell types, and where periostin could have opposing effects on different types of cells. Therefore, the influence of periostin on cancer cells and other immune cell subsets should be investigated further. Future studies would also need to validate our findings *in vivo* via for example injection of recombinant periostin into murine tumors and ultimately studies of periostin knockout or overexpression in CAFs.

Collectively, the findings of this thesis suggest that the tumor extracellular matrix plays a role in the modulation of antitumor immune responses and consequently tumor progression. While on one hand the tumor extracellular matrix seems to impede T cell function, specific components of the tumor ECM can enhance T cell cytotoxic capabilities. Our results therefore motivate investigation of tumor extracellular matrix-related therapies as a novel type of cancer immunotherapy.

Bibliography

1. Hanahan, D. & Weinberg, R. A. The hallmarks of cancer. *Cell* **100,** 57–70 (2000).
2. Hurst, D. R. & Welch, D. R. Metastasis suppressor genes: at the interface between the environment and tumor cell growth. *International Review of Cell and Molecular Biology* **286,** 107–180 (2011).
3. Albini, A., Mirisola, V. & Pfeffer, U. Metastasis signatures: genes regulating tumor–microenvironment interactions predict metastatic behavior. *Cancer and Metastasis Reviews* **27,** 75–83 (2008).
4. Ding, Q. *et al.* A nine-gene signature related to tumor microenvironment predicts overall survival with ovarian cancer. *Aging (Albany NY)* **12,** 4879 (2020).
5. Delves, P. J. & Roitt, I. M. The immune system. *New England Journal of Medicine* **343,** 37–49 (2000).
6. Rieger, M. A. & Schroeder, T. Hematopoiesis. *Cold Spring Harbor Perspectives in Biology* **4,** a008250 (2012).
7. Rothenberg, M. E. & Hogan, S. P. The eosinophil. *Annual Review of Immunology* **24,** 147–174 (2006).
8. Kawakami, T. & Galli, S. J. Regulation of mast-cell and basophil function and survival by IgE. *Nature Reviews Immunology* **2,** 773–786 (2002).
9. Mayadas, T. N., Cullere, X. & Lowell, C. A. The multifaceted functions of neutrophils. *Annual Review of Pathology: Mechanisms of Disease* **9,** 181–218 (2014).
10. Mantovani, A., Sozzani, S., Locati, M., Allavena, P. & Sica, A. Macrophage polarization: tumor-associated macrophages as a paradigm for polarized M2 mononuclear phagocytes. *Trends in Immunology* **23,** 549–555 (2002).
11. Fujiwara, N. & Kobayashi, K. Macrophages in inflammation. *Current Drug Targets-Inflammation & Allergy* **4,** 281–286 (2005).
12. Banchereau, J. & Steinman, R. M. Dendritic cells and the control of immunity. *Nature* **392,** 245–252 (1998).
13. Janeway Jr, C. A. & Medzhitov, R. Innate immune recognition. *Annual Review of Immunology* **20,** 197–216 (2002).
14. LeBien, T. W. & Tedder, T. F. B lymphocytes: how they develop and function. *Blood* **112,** 1570–1580 (2008).
15. Williams, M. A. & Bevan, M. J. Effector and memory CTL differentiation. *Annual Review of Immunology* **25,** 171–192 (2007).
16. Vivier, E. *et al.* Innate or adaptive immunity? The example of natural killer cells. *Science* **331,** 44–49 (2011).
17. Brennan, P. J., Brigl, M. & Brenner, M. B. Invariant natural killer T cells: an innate activation scheme linked to diverse effector functions. *Nature Reviews Immunology* **13,** 101–117 (2013).

18. Vantourout, P. & Hayday, A. Six-of-the-best: unique contributions of $\gamma\delta$ T cells to immunology. *Nature Reviews Immunology* **13,** 88–100 (2013).

19. Dranoff, G. Cytokines in cancer pathogenesis and cancer therapy. *Nature Reviews Cancer* **4,** 11–22 (2004).

20. Lee, M. K. *et al.* Interplay between clonal hematopoiesis of indeterminate potential and metabolism. *Trends in Endocrinology & Metabolism* **31,** 525–535 (2020).

21. Hanahan, D. & Weinberg, R. A. Hallmarks of cancer: the next generation. *Cell* **144,** 646–674 (2011).

22. Fares, C. M., Van Allen, E. M., Drake, C. G., Allison, J. P. & Hu-Lieskovan, S. Mechanisms of resistance to immune checkpoint blockade: why does checkpoint inhibitor immunotherapy not work for all patients? *American Society of Clinical Oncology Educational Book* **39,** 147–164 (2019).

23. Dunn, G. P., Bruce, A. T., Ikeda, H., Old, L. J. & Schreiber, R. D. Cancer immunoediting: from immunosurveillance to tumor escape. *Nature Immunology* **3,** 991–998 (2002).

24. Schreiber, R. D., Old, L. J. & Smyth, M. J. Cancer immunoediting: integrating immunity's roles in cancer suppression and promotion. *Science* **331,** 1565–1570 (2011).

25. Chen, D. S. & Mellman, I. Oncology meets immunology: the cancer-immunity cycle. *Immunity* **39,** 1–10 (2013).

26. Chen, L. & Flies, D. B. Molecular mechanisms of T cell co-stimulation and co-inhibition. *Nature Reviews Immunology* **13,** 227–242 (2013).

27. Martínez-Lostao, L., Anel, A. & Pardo, J. How do cytotoxic lymphocytes kill cancer cells? *Clinical Cancer Research* **21,** 5047–5056 (2015).

28. O'Shea, J. J. & Paul, W. E. Mechanisms underlying lineage commitment and plasticity of helper CD4+ T cells. *Science* **327,** 1098–1102 (2010).

29. Smith, C. M. *et al.* Cognate CD4+ T cell licensing of dendritic cells in CD8+ T cell immunity. *Nature Immunology* **5,** 1143–1148 (2004).

30. Mier, J. W. & Gallo, R. C. Purification and some characteristics of human T-cell growth factor from phytohemagglutinin-stimulated lymphocyte-conditioned media. *Proceedings of the National Academy of Sciences* **77,** 6134–6138 (1980).

31. Baker, P. E., Gillis, S., Ferm, M. M. & Smith, K. A. The effect of T cell growth factor on the generation of cytolytic T cells. *The Journal of Immunology* **121,** 2168–2173 (1978).

32. King, D. & Jones, P. Induction of Ia and H-2 antigens on a macrophage cell line by immune interferon. *The Journal of Immunology* **131,** 315–318 (1983).

33. Basham, T. & Merigan, T. C. Recombinant interferon-gamma increases HLA-DR synthesis and expression. *The Journal of Immunology* **130,** 1492–1494 (1983).

34. Appay, V. The physiological role of cytotoxic CD4+ T-cells: the holy grail? *Clinical and Experimental Immunology* **138,** 10 (2004).

35. Pardoll, D. M. & Topalian, S. L. The role of CD4+ T cell responses in antitumor immunity. *Current Opinion in Immunology* **10,** 588–594 (1998).

36. Van de Berg, P. J., van Leeuwen, E. M., Ten Berge, I. J. & van Lier, R. Cytotoxic human CD4+ T cells. *Current Opinion in Immunology* **20,** 339–343 (2008).

37. Biswas, S. K. & Mantovani, A. Macrophage plasticity and interaction with lymphocyte subsets: cancer as a paradigm. *Nature Immunology* **11,** 889–896 (2010).

38. Lupatov, A. Y. & Brondz, B. D. Formation of specific antitumor cytotoxic T-lymphocytes in monoculture. *Bulletin of Experimental Biology and Medicine* **113,** 184–186 (1992).

39. Echchakir, H. *et al.* Evidence for in situ expansion of diverse antitumor-specific cytotoxic T lymphocyte clones in a human large cell carcinoma of the lung. *International Immunology* **12,** 537–546 (2000).

40. Nishimura, T. *et al.* Distinct role of antigen-specific T helper type 1 (Th1) and Th2 cells in tumor eradication in vivo. *The Journal of Experimental Medicine* **190,** 617–628 (1999).

41. Hung, K. *et al.* The central role of CD4+ T cells in the antitumor immune response. *The Journal of Experimental Medicine* **188,** 2357–2368 (1998).

42. Van den Broek, M. F., Kägi, D., Zinkernagel, R. M. & Hengartner, H. Perforin dependence of natural killer cell-mediated tumor control in vivo. *European Journal of Immunology* **25,** 3514–3516 (1995).

43. Riccardi, C., Santoni, A., Barlozzari, T., Puccetti, P. & Herberman, R. In vivo natural reactivity of mice against tumor cells. *International Journal of Cancer* **25,** 475–486 (1980).

44. Smyth, M. J., Crowe, N. Y. & Godfrey, D. I. NK cells and NKT cells collaborate in host protection from methylcholanthrene-induced fibrosarcoma. *International Immunology* **13,** 459–463 (2001).

45. Carretero, R. *et al.* Eosinophils orchestrate cancer rejection by normalizing tumor vessels and enhancing infiltration of CD8+ T cells. *Nature Immunology* **16,** 609–617 (2015).

46. Munn, D. H. & Bronte, V. Immune suppressive mechanisms in the tumor microenvironment. *Current Opinion in Immunology* **39,** 1–6 (2016).

47. Lindau, D., Gielen, P., Kroesen, M., Wesseling, P. & Adema, G. J. The immunosuppressive tumour network: myeloid-derived suppressor cells, regulatory T cells and natural killer T cells. *Immunology* **138,** 105–115 (2013).

48. Wherry, E. J. T cell exhaustion. *Nature Immunology* **12,** 492–499 (2011).

49. Lewis, C. E. & Pollard, J. W. Distinct role of macrophages in different tumor microenvironments. *Cancer Research* **66,** 605–612 (2006).

50. Quail, D. F. & Joyce, J. A. Microenvironmental regulation of tumor progression and metastasis. *Nature Medicine* **19,** 1423–1437 (2013).

51. Gabrilovich, D. I. & Nagaraj, S. Myeloid-derived suppressor cells as regulators of the immune system. *Nature Reviews Immunology* **9,** 162–174 (2009).

52. Nishikawa, H. & Sakaguchi, S. Regulatory T cells in tumor immunity. *International Journal of Cancer* **127,** 759–767 (2010).

53. Vignali, D. A., Collison, L. W. & Workman, C. J. How regulatory T cells work. *Nature Reviews Immunology* **8,** 523–532 (2008).

54. Tanaka, A. & Sakaguchi, S. Regulatory T cells in cancer immunotherapy. *Cell Research* **27,** 109–118 (2017).

55. Pardoll, D. M. The blockade of immune checkpoints in cancer immunotherapy. *Nature Reviews Cancer* **12,** 252–264 (2012).

56. Bodelón, G., Palomino, C. & Fernández, L. Á. Immunoglobulin domains in Escherichia coli and other enterobacteria: from pathogenesis to applications in antibody technologies. *FEMS Microbiology Reviews* **37,** 204–250 (2013).

57. Vanamee, É. S. & Faustman, D. L. Structural principles of tumor necrosis factor superfamily signaling. *Science Signaling* **11** (2018).

58. Kumar, P., Bhattacharya, P. & Prabhakar, B. S. A comprehensive review on the role of co-signaling receptors and Treg homeostasis in autoimmunity and tumor immunity. *Journal of autoimmunity* **95,** 77–99 (2018).

59. Rumpret, M. *et al.* Functional categories of immune inhibitory receptors. *Nature Reviews Immunology,* 1–10 (2020).

60. Munn, D. H. & Mellor, A. L. Indoleamine 2, 3 dioxygenase and metabolic control of immune responses. *Trends in Immunology* **34,** 137–143 (2013).

61. Becker, J. C., Andersen, M. H., Schrama, D. & thor Straten, P. Immune-suppressive properties of the tumor microenvironment. *Cancer Immunology, Immunotherapy* **62,** 1137–1148 (2013).

62. Siemens, D. R. *et al.* Hypoxia increases tumor cell shedding of MHC class I chain-related molecule: role of nitric oxide. *Cancer Research* **68,** 4746–4753 (2008).

63. Clambey, E. T. *et al.* Hypoxia-inducible factor-1 alpha–dependent induction of FoxP3 drives regulatory T-cell abundance and function during inflammatory hypoxia of the mucosa. *Proceedings of the National Academy of Sciences* **109,** E2784–E2793 (2012).

64. Stagg, J. & Smyth, M. Extracellular adenosine triphosphate and adenosine in cancer. *Oncogene* **29,** 5346–5358 (2010).

65. Singh, R., Pervin, S., Karimi, A., Cederbaum, S. & Chaudhuri, G. Arginase activity in human breast cancer cell lines: Nω-hydroxy-L-arginine selectively inhibits cell proliferation and induces apoptosis in MDA-MB-468 cells. *Cancer Research* **60,** 3305–3312 (2000).

66. Gordon-Weeks, A. & Yuzhalin, A. E. Cancer Extracellular Matrix Proteins Regulate Tumour Immunity. *Cancers* **12,** 3331 (2020).

67. Nissen, N. I., Karsdal, M. & Willumsen, N. Collagens and Cancer associated fibroblasts in the reactive stroma and its relation to Cancer biology. *Journal of Experimental & Clinical Cancer Research* **38,** 1–12 (2019).

68. Theocharis, A. D., Skandalis, S. S., Gialeli, C. & Karamanos, N. K. Extracellular matrix structure. *Advanced Drug Delivery Reviews* **97,** 4–27 (2016).

69. Frantz, C., Stewart, K. M. & Weaver, V. M. The extracellular matrix at a glance. *Journal of Cell Science* **123,** 4195–4200 (2010).

70. Hynes, R. O. & Naba, A. Overview of the matrisome—an inventory of extracellular matrix constituents and functions. *Cold Spring Harbor Perspectives in Biology* **4,** a004903 (2012).

71. Kadler, K. E., Baldock, C., Bella, J. & Boot-Handford, R. P. Collagens at a glance. *Journal of Cell Science* **120,** 1955–1958 (2007).

72. Maroudas, A. Balance between swelling pressure and collagen tension in normal and degenerate cartilage. *Nature* **260,** 808–809 (1976).

73. Kielty, C. M., Sherratt, M. J. & Shuttleworth, C. A. Elastic fibres. *Journal of Cell Science* **115,** 2817–2828 (2002).

74. Domogatskaya, A., Rodin, S. & Tryggvason, K. Functional diversity of laminins. *Annual Review of Cell and Developmental Biology* **28,** 523–553 (2012).

75. Pankov, R. & Yamada, K. M. Fibronectin at a glance. *Journal of Cell Science* **115,** 3861–3863 (2002).

76. Bornstein, P. & Sage, E. H. Matricellular proteins: extracellular modulators of cell function. *Current Opinion in Cell Biology* **14,** 608–616 (2002).

77. Hynes, R. O. The extracellular matrix: not just pretty fibrils. *Science* **326,** 1216–1219 (2009).

78. Ricard-Blum, S. & Salza, R. Matricryptins and matrikines: biologically active fragments of the extracellular matrix. *Experimental Dermatology* **23,** 457–463 (2014).

79. Naba, A. *et al.* The matrisome: in silico definition and in vivo characterization by proteomics of normal and tumor extracellular matrices. *Molecular & Cellular Proteomics* **11,** M111–014647 (2012).

80. Cox, T. R. The matrix in cancer. *Nature Reviews Cancer,* 1–22 (2021).

81. Naba, A., Clauser, K. R., Lamar, J. M., Carr, S. A. & Hynes, R. O. Extracellular matrix signatures of human mammary carcinoma identify novel metastasis promoters. *eLife* **3,** e01308 (2014).

82. Chang, H. Y. *et al.* Diversity, topographic differentiation, and positional memory in human fibroblasts. *Proceedings of the National Academy of Sciences* **99,** 12877–12882 (2002).

83. Sahai, E. *et al.* A framework for advancing our understanding of cancer-associated fibroblasts. *Nature Reviews Cancer* **20,** 174–186 (2020).

84. Kalluri, R. & Zeisberg, M. Fibroblasts in cancer. *Nature Reviews Cancer* **6,** 392–401 (2006).

85. Presta, M. *et al.* Fibroblast growth factor/fibroblast growth factor receptor system in angiogenesis. *Cytokine & growth factor reviews* **16,** 159–178 (2005).

86. Montesano, R., Vassalli, J.-D., Baird, A., Guillemin, R. & Orci, L. Basic fibroblast growth factor induces angiogenesis in vitro. *Proceedings of the National Academy of Sciences* **83,** 7297–7301 (1986).

87. Sorrell, J. M. & Caplan, A. I. Fibroblasts—a diverse population at the center of it all. *International Review of Cell and Molecular Biology* **276,** 161–214 (2009).

88. Smith, R. S., Smith, T. J., Blieden, T. M. & Phipps, R. P. Fibroblasts as sentinel cells. Synthesis of chemokines and regulation of inflammation. *The American Journal of Pathology* **151,** 317 (1997).

89. Buckley, C. D. *et al.* Fibroblasts regulate the switch from acute resolving to chronic persistent inflammation. *Trends in Immunology* **22,** 199–204 (2001).

90. Kalluri, R. The biology and function of fibroblasts in cancer. *Nature Reviews Cancer* **16,** 582 (2016).

91. Sperb, N., Tsesmelis, M. & Wirth, T. Crosstalk between Tumor and Stromal Cells in Pancreatic Ductal Adenocarcinoma. *International Journal of Molecular Sciences* **21,** 5486 (2020).

92. Öhlund, D. *et al.* Distinct populations of inflammatory fibroblasts and myofibroblasts in pancreatic cancer. *Journal of Experimental Medicine* **214,** 579–596 (2017).

93. Elyada, E. *et al.* Cross-species single-cell analysis of pancreatic ductal adenocarcinoma reveals antigen-presenting cancer-associated fibroblasts. *Cancer Discovery* **9,** 1102–1123 (2019).

94. Sebastian, A. *et al.* Single-cell Transcriptomic Analysis of Tumor-Derived Fibroblasts and Normal Tissue-Resident Fibroblasts Reveals Fibroblast Heterogeneity in Breast Cancer. *Cancers* **12,** 1307 (2020).

95. Kieffer, Y. *et al.* Single-cell analysis reveals fibroblast clusters linked to immunotherapy resistance in cancer. *Cancer Discovery* **10,** 1330–1351 (2020).

96. Erez, N., Truitt, M., Olson, P. & Hanahan, D. Cancer-associated fibroblasts are activated in incipient neoplasia to orchestrate tumor-promoting inflammation in an NF-κB-dependent manner. *Cancer Cell* **17,** 135–147 (2010).

97. Lakins, M. A., Ghorani, E., Munir, H., Martins, C. P. & Shields, J. D. Cancer-associated fibroblasts induce antigen-specific deletion of CD8+ T Cells to protect tumour cells. *Nature Communications* **9,** 1–9 (2018).

98. Francescone, R. *et al.* Netrin G1 Promotes Pancreatic Tumorigenesis through Cancer-Associated Fibroblast–Driven Nutritional Support and Immunosuppression. *Cancer Discovery* **11,** 446–479 (2021).

99. Kraman, M. *et al.* Suppression of antitumor immunity by stromal cells expressing fibroblast activation protein–α. *Science* **330,** 827–830 (2010).

100. Baker, A. T., Abuwarwar, M. H., Poly, L., Wilkins, S. & Fletcher, A. L. Cancer-associated fibroblasts and T cells: from mechanisms to outcomes. *The Journal of Immunology* **206,** 310–320 (2021).

101. Inoue, C. *et al.* PD-L1 induction by cancer-associated fibroblast-derived factors in lung adenocarcinoma cells. *Cancers* **11,** 1257 (2019).

102. Li, Z. *et al.* Cancer-associated fibroblasts promote PD-L1 expression in mice cancer cells via secreting CXCL5. *International Journal of Cancer* **145,** 1946–1957 (2019).

103. Gorchs, L. *et al.* Human pancreatic carcinoma-associated fibroblasts promote expression of co-inhibitory markers on CD4+ and CD8+ T-cells. *Frontiers in Immunology* **10,** 847 (2019).

104. Özdemir, B. C. *et al.* Depletion of carcinoma-associated fibroblasts and fibrosis induces immunosuppression and accelerates pancreas cancer with reduced survival. *Cancer Cell* **25,** 719–734 (2014).

105. Friedl, P. & Wolf, K. Tumour-cell invasion and migration: diversity and escape mechanisms. *Nature Reviews Cancer* **3,** 362–374 (2003).

106. Rowe, R. G. & Weiss, S. J. Breaching the basement membrane: who, when and how? *Trends in Cell Biology* **18,** 560–574 (2008).

107. Mott, J. D. & Werb, Z. Regulation of matrix biology by matrix metalloproteinases. *Current Opinion in Cell Biology* **16,** 558–564 (2004).

108. Hope, C. *et al.* Immunoregulatory roles of versican proteolysis in the myeloma microenvironment. *Blood* **128,** 680–685 (2016).

109. Aszodi, A., Legate, K. R., Nakchbandi, I. & Fässler, R. What mouse mutants teach us about extracellular matrix function. *Annual Reviews in Cell Developmental Biololy* **22,** 591–621 (2006).

110. Albrengues, J. *et al.* Neutrophil extracellular traps produced during inflammation awaken dormant cancer cells in mice. *Science* **361** (2018).

111. O'Brien, J. *et al.* Alternatively activated macrophages and collagen remodeling characterize the postpartum involuting mammary gland across species. *The American Journal of Pathology* **176,** 1241–1255 (2010).

112. Boyd, N. F. *et al.* Mammographic density and the risk and detection of breast cancer. *New England Journal of Medicine* **356,** 227–236 (2007).

113. Martin, M. L. *et al.* Density of tumour stroma is correlated to outcome after adoptive transfer of CD4+ and CD8+ T cells in a murine mammary carcinoma model. *Breast Cancer Research and Treatment* **121,** 753–763 (2010).

114. Whatcott, C. J. *et al.* Desmoplasia in primary tumors and metastatic lesions of pancreatic cancer. *Clinical Cancer Research* **21,** 3561–3568 (2015).

115. Xia, Y. *et al.* YAP promotes ovarian cancer cell tumorigenesis and is indicative of a poor prognosis for ovarian cancer patients. *PLoS One* **9,** e91770 (2014).

116. Halvorsen, T. & Seim, E. Association between invasiveness, inflammatory reaction, desmoplasia and survival in colorectal cancer. *Journal of Clinical Pathology* **42,** 162–166 (1989).

117. Levental, K. R. *et al.* Matrix crosslinking forces tumor progression by enhancing integrin signaling. *Cell* **139,** 891–906 (2009).

118. Puig, M. *et al.* Matrix stiffening and β1 integrin drive subtype-specific fibroblast accumulation in lung cancer. *Molecular Cancer Research* **13,** 161–173 (2015).

119. Zanconato, F., Cordenonsi, M. & Piccolo, S. YAP and TAZ: a signalling hub of the tumour microenvironment. *Nature Reviews Cancer* **19,** 454–464 (2019).

120. Calvo, F. *et al.* Mechanotransduction and YAP-dependent matrix remodelling is required for the generation and maintenance of cancer-associated fibroblasts. *Nature Cell Biology* **15,** 637–646 (2013).

121. Kuczek, D. E. *et al.* Collagen density regulates the activity of tumor-infiltrating T cells. *Journal for Immunotherapy of Cancer* **7,** 1–15 (2019).

122. O'Connor, R. S. *et al.* Substrate rigidity regulates human T cell activation and proliferation. *The Journal of Immunology* **189,** 1330–1339 (2012).

123. Larsen, A. M. H. *et al.* Collagen density modulates the immunosuppressive functions of macrophages. *The Journal of Immunology* **205,** 1461–1472 (2020).

124. Stahl, M. *et al.* Lung collagens perpetuate pulmonary fibrosis via CD204 and M2 macrophage activation. *PLoS One* **8,** e81382 (2013).

125. Friedemann, M. *et al.* Instructing human macrophage polarization by stiffness and glycosaminoglycan functionalization in 3D collagen networks. *Advanced Healthcare Materials* **6,** 1600967 (2017).

126. Rygiel, T. P., Stolte, E. H., de Ruiter, T., van de Weijer, M. L. & Meyaard, L. Tumor-expressed collagens can modulate immune cell function through the inhibitory collagen receptor LAIR-1. *Molecular Immunology* **49,** 402–406 (2011).

127. Lebbink, R. J. *et al.* Collagens are functional, high affinity ligands for the inhibitory immune receptor LAIR-1. *The Journal of Experimental Medicine* **203,** 1419–1425 (2006).

128. Provenzano, P. P. *et al.* Collagen reorganization at the tumor-stromal interface facilitates local invasion. *BMC Medicine* **4,** 1–15 (2006).

129. Fraley, S. I. *et al.* Three-dimensional matrix fiber alignment modulates cell migration and MT1-MMP utility by spatially and temporally directing protrusions. *Scientific Reports* **5,** 1–13 (2015).

130. Provenzano, P. P., Inman, D. R., Eliceiri, K. W., Trier, S. M. & Keely, P. J. Contact guidance mediated three-dimensional cell migration is regulated by Rho/ROCK-dependent matrix reorganization. *Biophysical Journal* **95,** 5374–5384 (2008).

131. Ray, A., Slama, Z. M., Morford, R. K., Madden, S. A. & Provenzano, P. P. Enhanced directional migration of cancer stem cells in 3D aligned collagen matrices. *Biophysical Journal* **112,** 1023–1036 (2017).

132. Salmon, H. *et al.* Matrix architecture defines the preferential localization and migration of T cells into the stroma of human lung tumors. *The Journal of Clinical Investigation* **122,** 899–910 (2012).

133. Ricciardelli, C. *et al.* Elevated levels of versican but not decorin predict disease progression in early-stage prostate cancer. *Clinical Cancer Research* **4,** 963–971 (1998).

134. Ricciardelli, C. *et al.* Regulation of stromal versican expression by breast cancer cells and importance to relapse-free survival in patients with node-negative primary breast cancer. *Clinical Cancer Research* **8,** 1054–1060 (2002).

135. Torres, S. *et al.* Proteome profiling of cancer-associated fibroblasts identifies novel proinflammatory signatures and prognostic markers for colorectal cancer. *Clinical Cancer Research* **19,** 6006–6019 (2013).

136. Lim, S. B., Tan, S. J., Wan-Teck, L. & Lim, C. T. An extracellular matrix-related prognostic and predictive indicator for early-stage non-small cell lung cancer. *Nature Communications* **8,** 1–11 (2017).

137. Tian, C. *et al.* Proteomic analyses of ECM during pancreatic ductal adenocarcinoma progression reveal different contributions by tumor and stromal cells. *Proceedings of the National Academy of Sciences* **116,** 19609–19618 (2019).

138. Yuzhalin, A. E., Urbonas, T., Silva, M. A., Muschel, R. J. & Gordon-Weeks, A. N. A core matrisome gene signature predicts cancer outcome. *British Journal of Cancer* **118,** 435–440 (2018).

139. Alvarez, M. J. *et al.* Secreted protein acidic and rich in cysteine produced by human melanoma cells modulates polymorphonuclear leukocyte recruitment and antitumor cytotoxic capacity. *Cancer Research* **65,** 5123–5132 (2005).

140. Sangaletti, S., Chiodoni, C., Tripodo, C. & Colombo, M. P. Common extracellular matrix regulation of myeloid cell activity in the bone marrow and tumor microenvironments. *Cancer Immunology, Immunotherapy* **66,** 1059–1067 (2017).

141. Zhang, Y., Du, W., Chen, Z. & Xiang, C. Upregulation of PD-L1 by SPP1 mediates macrophage polarization and facilitates immune escape in lung adenocarcinoma. *Experimental Cell Research* **359,** 449–457 (2017).

142. Klement, J. D. *et al.* An osteopontin/CD44 immune checkpoint controls CD8+ T cell activation and tumor immune evasion. *The Journal of Clinical Investigation* **128,** 5549–5560 (2018).

143. Li, L.-Y. *et al.* CTHRC1 promotes M2-like macrophage recruitment and myometrial invasion in endometrial carcinoma by integrin-Akt signaling pathway. *Clinical & Experimental Metastasis* **36,** 351–363 (2019).

144. Zhou, W. *et al.* Periostin secreted by glioblastoma stem cells recruits M2 tumour-associated macrophages and promotes malignant growth. *Nature Cell Biology* **17,** 170–182 (2015).

145. Hartley, G., Regan, D., Guth, A. & Dow, S. Regulation of PD-L1 expression on murine tumor-associated monocytes and macrophages by locally produced TNF-α. *Cancer Immunology, Immunotherapy* **66,** 523–535 (2017).

146. Gorter, A. *et al.* Versican expression is associated with tumor-infiltrating CD8-positive T cells and infiltration depth in cervical cancer. *Modern Pathology* **23,** 1605–1615 (2010).

147. Franitza, S. *et al.* TNF-α associated with extracellular matrix fibronectin provides a stop signal for chemotactically migrating T cells. *The Journal of Immunology* **165,** 2738–2747 (2000).

148. Huang, J.-Y. *et al.* Extracellular matrix of glioblastoma inhibits polarization and transmigration of T cells: the role of tenascin-C in immune suppression. *The Journal of Immunology* **185,** 1450–1459 (2010).

149. Parekh, K. *et al.* Tenascin-C, over expressed in lung cancer down regulates effector functions of tumor infiltrating lymphocytes. *Lung Cancer* **47,** 17–29 (2005).

150. Hemesath, T. J., Marton, L. S. & Stefansson, K. Inhibition of T cell activation by the extracellular matrix protein tenascin. *The Journal of Immunology* **152,** 5199–5207 (1994).

151. Jachetti, E. *et al.* Tenascin-C protects cancer stem–like cells from immune surveillance by arresting T-cell activation. *Cancer Research* **75,** 2095–2108 (2015).

152. Mirzaei, R. *et al.* Brain tumor-initiating cells export tenascin-C associated with exosomes to suppress T cell activity. *OncoImmunology* **7,** e1478647 (2018).

153. Goehrig, D. *et al.* Stromal protein βig-h3 reprogrammes tumour microenvironment in pancreatic cancer. *Gut* **68,** 693–707 (2019).

154. Hussey, G. S., Dziki, J. L. & Badylak, S. F. Extracellular matrix-based materials for regenerative medicine. *Nature Reviews Materials* **3,** 159–173 (2018).

155. Franco-Barraza, J., Beacham, D. A., Amatangelo, M. D. & Cukierman, E. Preparation of extracellular matrices produced by cultured and primary fibroblasts. *Current Protocols in Cell Biology* **71,** 10–9 (2016).

156. Kaukonen, R., Jacquemet, G., Hamidi, H. & Ivaska, J. Cell-derived matrices for studying cell proliferation and directional migration in a complex 3D microenvironment. *Nature Protocols* **12,** 2376 (2017).

157. Ahlfors, J.-E. W. & Billiar, K. L. Biomechanical and biochemical characteristics of a human fibroblast-produced and remodeled matrix. *Biomaterials* **28,** 2183–2191 (2007).

158. Auger, F. A. *et al.* Multistep production of bioengineered skin substitutes: sequential modulation of culture conditions. *In Vitro Cellular & Developmental Biology-Animal* **36,** 96–103 (2000).

159. Cukierman, E., Pankov, R., Stevens, D. R. & Yamada, K. M. Taking cell-matrix adhesions to the third dimension. *Science* **294,** 1708–1712 (2001).

160. Fitzpatrick, L. E. & McDevitt, T. C. Cell-derived matrices for tissue engineering and regenerative medicine applications. *Biomaterials Ccience* **3,** 12–24 (2015).

161. Quiros, R. M. *et al.* Ovarian normal and tumor-associated fibroblasts retain in vivo stromal characteristics in a 3-D matrix-dependent manner. *Gynecologic Oncology* **110,** 99–109 (2008).

162. Sung, H. *et al.* Global cancer statistics 2020: GLOBOCAN estimates of incidence and mortality worldwide for 36 cancers in 185 countries. *CA: A Cancer Journal for Clinicians* (2021).

163. Braun, D. A. *et al.* Beyond conventional immune-checkpoint inhibition—novel immunotherapies for renal cell carcinoma. *Nature Reviews Clinical Oncology,* 1–16 (2021).

164. Sharma, P. *et al.* The Next Decade of Immune Checkpoint Therapy. *Cancer Discovery* **11,** 838–857 (2021).

165. Schindelin, J. *et al.* Fiji: an open-source platform for biological-image analysis. *Nature Methods* **9,** 676–682 (2012).

166. Livak, K. J. & Schmittgen, T. D. Analysis of relative gene expression data using real-time quantitative PCR and the $2^{-\Delta\Delta\mathrm{CT}}$ method. *Methods* **25,** 402–408 (2001).

167. Vandesompele, J. *et al.* Accurate normalization of real-time quantitative RT-PCR data by geometric averaging of multiple internal control genes. *Genome Biology* **3,** 1–12 (2002).

168. Hellemans, J., Mortier, G., De Paepe, A., Speleman, F. & Vandesompele, J. qBase relative quantification framework and software for management and automated analysis of real-time quantitative PCR data. *Genome Biology* **8,** 1–14 (2007).

169. Dobin, A. *et al.* STAR: ultrafast universal RNA-seq aligner. *Bioinformatics* **29,** 15–21 (2013).

170. Love, M. I., Huber, W. & Anders, S. Moderated estimation of fold change and dispersion for RNA-seq data with DESeq2. *Genome Biology* **15,** 1–21 (2014).

171. Zhu, A., Ibrahim, J. G. & Love, M. I. Heavy-tailed prior distributions for sequence count data: removing the noise and preserving large differences. *Bioinformatics* **35,** 2084–2092 (2019).

172. Shao, X., Taha, I. N., Clauser, K. R., Gao, Y. & Naba, A. MatrisomeDB: the ECM-protein knowledge database. *Nucleic Acids Research* **48,** D1136–D1144 (2020).

173. Kim, N. *et al.* Single-cell RNA sequencing demonstrates the molecular and cellular reprogramming of metastatic lung adenocarcinoma. *Nature Communications* **11,** 1–15 (2020).

174. Xi, B., Ye, P., Golubovskaya, V. & Abassi, Y. in *Immuno-Oncology* 35–50 (Springer, 2020).

175. Arora, M. Cell culture media: a review. *Mater Methods* **3,** 24 (2013).

176. Wu, Y.-K., Tu, Y.-K., Yu, J. & Cheng, N.-C. The influence of cell culture density on the cytotoxicity of adipose-derived stem cells induced by L-ascorbic acid-2-phosphate. *Scientific Reports* **10,** 1–11 (2020).

177. Du, J. *et al.* Mechanisms of ascorbate-induced cytotoxicity in pancreatic cancer. *Clinical Cancer Research* **16,** 509–520 (2010).

178. Doskey, C. M. *et al.* Tumor cells have decreased ability to metabolize H2O2: Implications for pharmacological ascorbate in cancer therapy. *Redox Biology* **10,** 274–284 (2016).

179. Kroemer, G. & Levine, B. Autophagic cell death: the story of a misnomer. *Nature Reviews Molecular Cell Biology* **9,** 1004–1010 (2008).

180. Park, D. *et al.* Extracellular matrix anisotropy is determined by TFAP2C-dependent regulation of cell collisions. *Nature Materials* **19,** 227–238 (2020).

181. Chen, X., Nadiarynkh, O., Plotnikov, S. & Campagnola, P. J. Second harmonic generation microscopy for quantitative analysis of collagen fibrillar structure. *Nature Protocols* **7,** 654–669 (2012).

182. Naba, A. *et al.* The extracellular matrix: Tools and insights for the "omics" era. *Matrix Biology* **49,** 10–24 (2016).

183. Orend, G. & Chiquet-Ehrismann, R. Tenascin-C induced signaling in cancer. *Cancer Letters* **244,** 143–163 (2006).

184. Porter, P. L., Sage, E. H., Lane, T. F., Funk, S. E. & Gown, A. M. Distribution of SPARC in normal and neoplastic human tissue. *Journal of Histochemistry & Cytochemistry* **43,** 791–800 (1995).

185. Coppola, D. *et al.* Correlation of osteopontin protein expression and pathological stage across a wide variety of tumor histologies. *Clinical Cancer Research* **10,** 184–190 (2004).

186. Taipale, J., Miyazono, K., Heldin, C.-H. & Keski-Oja, J. Latent transforming growth factor-beta 1 associates to fibroblast extracellular matrix via latent TGF-beta binding protein. *Journal of Cell Biology* **124,** 171–181 (1994).

187. Hyytiäinen, M., Penttinen, C. & Keski-Oja, J. Latent TGF-β binding proteins: extracellular matrix association and roles in TGF-β activation. *Critical Reviews in Clinical Laboratory Sciences* **41,** 233–264 (2004).

188. Kaukonen, R. *et al.* Normal stroma suppresses cancer cell proliferation via mechanosensitive regulation of JMJD1a-mediated transcription. *Nature Communications* **7,** 1–15 (2016).

189. Jacquemet, G. *et al.* Rac1 is deactivated at integrin activation sites through an IQGAP1–filamin-A–RacGAP1 pathway. *Journal of Cell Science* **126,** 4121–4135 (2013).

190. Amatangelo, M. D., Bassi, D. E., Klein-Szanto, A. J. & Cukierman, E. Stroma-derived three-dimensional matrices are necessary and sufficient to promote desmoplastic differentiation of normal fibroblasts. *The American Journal of Pathology* **167,** 475–488 (2005).

191. Shin, H.-J., Lee, J.-B., Park, S.-H., Chang, J. & Lee, C.-W. T-bet expression is regulated by EGR1-mediated signaling in activated T cells. *Clinical Immunology* **131,** 385–394 (2009).

192. Cron, R. Q. *et al.* Early growth response-1 is required for CD154 transcription. *The Journal of Immunology* **176,** 811–818 (2006).

193. Crist, S. A., Elzey, B. D., Ahmann, M. T. & Ratliff, T. L. Early growth response-1 (EGR-1) and nuclear factor of activated T cells (NFAT) cooperate to mediate CD40L expression in megakaryocytes and platelets. *Journal of Biological Chemistry* **288,** 33985–33996 (2013).

194. Skerka, C., Decker, E. L. & Zipfel, P. F. A regulatory element in the human interleukin 2 gene promoter is a binding site for the zinc finger proteins Sp1 and EGR-1. *Journal of Biological Chemistry* **270,** 22500–22506 (1995).

195. Collins, S., Wolfraim, L. A., Drake, C. G., Horton, M. R. & Powell, J. D. Cutting Edge: TCR-induced NAB2 enhances T cell function by coactivating IL-2 transcription. *The Journal of Immunology* **177,** 8301–8305 (2006).

196. Lin, J.-X. & Leonard, W. J. The immediate-early gene product Egr-1 regulates the human interleukin-2 receptor beta-chain promoter through noncanonical Egr and Sp1 binding sites. *Molecular and Cellular Biology* **17,** 3714–3722 (1997).

197. Mittelstadt, P. R. & Ashwell, J. D. Role of Egr-2 in up-regulation of Fas ligand in normal T cells and aberrant double-negative lpr and gld T cells. *Journal of Biological Chemistry* **274,** 3222–3227 (1999).

198. Dzialo-Hatton, R., Milbrandt, J., Hockett, R. D. & Weaver, C. T. Differential expression of Fas ligand in Th1 and Th2 cells is regulated by early growth response gene and NF-AT family members. *The Journal of Immunology* **166,** 4534–4542 (2001).

199. Zheng, Y. *et al.* Egr2-dependent gene expression profiling and ChIP-Seq reveal novel biologic targets in T cell anergy. *Molecular Immunology* **55,** 283–291 (2013).

200. Safford, M. *et al.* Egr-2 and Egr-3 are negative regulators of T cell activation. *Nature Immunology* **6,** 472–480 (2005).

201. Hui, K. L., Balagopalan, L., Samelson, L. E. & Upadhyaya, A. Cytoskeletal forces during signaling activation in Jurkat T-cells. *Molecular Biology of the Cell* **26,** 685–695 (2015).

202. Trickett, A. & Kwan, Y. L. T cell stimulation and expansion using anti-CD3/CD28 beads. *Journal of Immunological Methods* **275,** 251–255 (2003).

203. Fung-Leung, W.-P. *et al.* T cell subset and stimulation strength-dependent modulation of T cell activation by Kv1. 3 blockers. *PLoS One* **12,** e0170102 (2017).

204. *xCELLigence RTCA for cancer immunotherapy* `https://www.agilent.com/en/solutions/cell-analysis/immunotherapy/cancer-immunotherapy-rtca-flow`. Accessed: 2020-12-17.

205. Dang, N. H., Torimoto, Y., Schlossman, S. F. & Morimoto, C. Human CD4 helper T cell activation: functional involvement of two distinct collagen receptors, 1F7 and VLA integrin family. *The Journal of Experimental Medicine* **172,** 649–652 (1990).

206. Nojima, Y. *et al.* VLA-4 mediates CD3-dependent CD4+ T cell activation via the CS1 alternatively spliced domain of fibronectin. *The Journal of Experimental Medicine* **172,** 1185–1192 (1990).

207. Shimizu, Y., Van Seventer, G. A., Horgan, K. J. & Shaw, S. Costimulation of proliferative responses of resting CD4+ T cells by the interaction of VLA-4 and VLA-5 with fibronectin or VLA-6 with laminin. *The Journal of Immunology* **145,** 59–67 (1990).

208. Kühn, B. *et al.* Periostin induces proliferation of differentiated cardiomyocytes and promotes cardiac repair. *Nature Medicine* **13,** 962–969 (2007).

209. Taniguchi, K. *et al.* Periostin controls keratinocyte proliferation and differentiation by interacting with the paracrine IL-1α/IL-6 loop. *Journal of Investigative Dermatology* **134,** 1295–1304 (2014).

210. González-González, L. & Alonso, J. Periostin: a matricellular protein with multiple functions in cancer development and progression. *Frontiers in Oncology* **8,** 225 (2018).

211. Malanchi, I. *et al.* Interactions between cancer stem cells and their niche govern metastatic colonization. *Nature* **481,** 85–89 (2012).

212. Luke, J. J., Bao, R., Sweis, R. F., Spranger, S. & Gajewski, T. F. WNT/β-catenin pathway activation correlates with immune exclusion across human cancers. *Clinical Cancer Research* **25,** 3074–3083 (2019).

213. Spranger, S., Bao, R. & Gajewski, T. F. Melanoma-intrinsic β-catenin signalling prevents anti-tumour immunity. *Nature* **523,** 231–235 (2015).

214. Van Loosdregt, J. & Coffer, P. J. The role of WNT signaling in mature T cells: T cell factor is coming home. *The Journal of Immunology* **201,** 2193–2200 (2018).

215. Marusyk, A., Almendro, V. & Polyak, K. Intra-tumour heterogeneity: a looking glass for cancer? *Nature Reviews Cancer* **12,** 323–334 (2012).

216. Alizadeh, A. A. *et al.* Distinct types of diffuse large B-cell lymphoma identified by gene expression profiling. *Nature* **403,** 503–511 (2000).

217. Maruhashi, T., Kii, I., Saito, M. & Kudo, A. Interaction between periostin and BMP-1 promotes proteolytic activation of lysyl oxidase. *Journal of Biological Chemistry* **285,** 13294–13303 (2010).

218. Phillips, H. S. *et al.* Molecular subclasses of high-grade glioma predict prognosis, delineate a pattern of disease progression, and resemble stages in neurogenesis. *Cancer Cell* **9,** 157–173 (2006).

219. Sørlie, T. *et al.* Gene expression patterns of breast carcinomas distinguish tumor subclasses with clinical implications. *Proceedings of the National Academy of Sciences* **98,** 10869–10874 (2001).

220. Real, L. *et al.* Multiple mechanisms of immune evasion can coexist in melanoma tumor cell lines derived from the same patient. *Cancer Immunology, Immunotherapy* **49,** 621–628 (2001).

Appendix A

The extended $\triangle\triangle$Ct and Vandesompele methods for RT-qPCR data analysis

The Vandesompele method for RT-qPCR analysis[167,168] using multiple reference genes computes the fold gene expression as the ratio of the relative quantity

$$\mathrm{RQ} = E^{\,\Delta\mathrm{Ct}}$$

of the gene of interest (GOI) to the geometric mean of the relative quantities of the reference/housekeeping genes (HKGs). Here, E is primer efficiency converted to the base of exponential amplification and ΔCt is the difference in cycle threshold (Ct) values between the control and treated samples.

A much simpler method for calculation of fold gene expression of RT-qPCR data is the $\Delta\Delta$Ct or Livak method[166] which uses only one reference gene for normalization and assumes 100% primer efficiency. Using this method the fold change is obtained as 2 to the power of the difference in Ct values between treatment and control group after subtracting the Ct value of the housekeeping gene.

The $\Delta\Delta$Ct method can be extended to incorporate the use of multiple reference genes by using the average of the reference gene Ct values as reference. As is shown below, this is equivalent to the Vandesompele method if, additionally, 100% primer/amplification efficiency is assumed, that is $E = 2$.

$$\text{Fold-change} = \frac{E_{\mathrm{GOI}}^{\Delta\mathrm{Ct}_{\mathrm{GOI}}}}{\left(\prod_{i=1}^{m} E_{\mathrm{HKG},i}^{\Delta\mathrm{Ct}_{\mathrm{HKG},i}}\right)^{1/m}} = \frac{2^{\Delta\mathrm{Ct}_{\mathrm{GOI}}}}{\left(\prod_{i=1}^{m} 2^{\Delta\mathrm{Ct}_{\mathrm{HKG},i}}\right)^{1/m}} \tag{A.1}$$

$$= \frac{2^{\Delta\mathrm{Ct}_{\mathrm{GOI}}}}{\left(\{2^{\Delta\mathrm{Ct}_{\mathrm{HKG},1}} \cdot 2^{\Delta\mathrm{Ct}_{\mathrm{HKG},2}} \cdot \ldots \cdot 2^{\Delta\mathrm{Ct}_{\mathrm{HKG},m}}\}\right)^{1/m}} = \frac{2^{\Delta\mathrm{Ct}_{\mathrm{GOI}}}}{2^{\frac{\sum_{i=1}^{m}\Delta\mathrm{Ct}_i}{m}}} \tag{A.2}$$

$$= 2^{\left(\frac{\sum_{j=1}^{n}\mathrm{Ct}_{\mathrm{GOI},j}}{n} - \mathrm{Ct}_{\mathrm{GOI}}\right) - \left(\frac{\sum_{i=1}^{m}\left(\frac{\sum_{j=1}^{n}\mathrm{Ct}_{i,j}}{n}\right)}{m} - \frac{\sum_{i=1}^{m}\mathrm{Ct}_i}{m}\right)} \tag{A.3}$$

$$= 2^{\left(\frac{\sum_{j=1}^{n}\mathrm{Ct}_{\mathrm{GOI},j}}{n} - \mathrm{Ct}_{\mathrm{GOI}}\right) - \left(\frac{\sum_{j=1}^{n}\left(\frac{\sum_{i=1}^{m}\mathrm{Ct}_{i,j}}{m}\right)}{n} - \frac{\sum_{i=1}^{m}\mathrm{Ct}_i}{m}\right)} \tag{A.4}$$

$$= 2^{\left(\frac{\sum_{j=1}^{n}\left(\mathrm{Ct}_{\mathrm{GOI},j} - \frac{\sum_{i=1}^{m}\mathrm{Ct}_{i,j}}{m}\right)}{n}\right) - \left(\mathrm{Ct}_{\mathrm{GOI}} - \frac{\sum_{i=1}^{m}\mathrm{Ct}_i}{m}\right)} \tag{A.5}$$

$$= 2^{\frac{\sum_{j=1}^{n}\Delta\mathrm{Ct}_j}{n} - \Delta\mathrm{Ct}} = 2^{-\Delta\Delta\mathrm{Ct}} \tag{A.6}$$

where n is the number of samples in the control group and m is the number of housekeeping genes.

Appendix B

Supplementary tables

Table B.1: List of primers used for RT-qPCR and their oligonucleotide sequences.

Gene		Sequence
Actb	Forward	5'-CAC-TGT-CGA-GTC-GCG-TCC-3'
	Reverse	5'-TCA-TCC-ATG-GCG-AAC-TGG-TG-3'
Tubb5	Forward	5'-GTA-AAC-CGT-AGC-CAT-GAG-GGA-3'
	Reverse	5'-CCT-CCC-AGA-ACT-TAG-CAC-CG-3'
Ifng	Forward	5'-CGG-CAC-AGT-CAT-TGA-AAG-CC-3'
	Reverse	5'-TGT-CAC-CAT-CCT-TTT-GCC-AGT-3'
Tnfrsf9	Forward	5'-GTC-TGT-GCT-TAA-GAC-CGG-GA-3'
	Reverse	5'-GTC-TTC-TTA-AAT-GCT-GGT-CCT-CC-3'
Col1a1	Forward	5'-CCC-AAT-GGT-GAG-ACG-TGG-AA-3'
	Reverse	5'-TTG-GGT-CCC-TCG-ACT-CCT-AC-3'

Table B.2: List of proteins used for cytotoxicity assays and their product information. All proteins were ordered as carrier-free formulations from R&D Systems (Bio-Techne), except periostin which was also ordered from BioLegend (BL).

Gene	Recombinant protein name (alternative name)	Product number
AGRN	Agrin	6624-AG-050
BGN	Biglycan	2667-CM-050
COMP	Cartilage oligomeric matrix protein (Thrombospondin-5)	3134-CPB-050
IGFBP3	Insulin-like growth factor-binding protein-3	675-B3-025
MATN3	Matrillin-3	3017-MN-050
POSTN	Periostin (Osteoblast-specific factor-2)	R&D: 3548-F2-050
		BL: 770504
SPP1	Osteopontin (Secreted phosphoprotein 1, Bone sialoprotein-1)	1433-OP-050/CF
TGFBI	Transforming growth factor-β-induced protein (βIg-H3)	3409-BG-050
VCAN	Versican Isoform V3	3054-VN-050
WISP1	WNT1-inducible-signaling pathway protein-1 (CCN4)	1627-WS-050

Table B.3: List of upregulated tumor ECM genes identified by differential expression analysis of normal and cancer-associated fibroblasts from LUAD patients (adjusted p-value < 0.05 and $\log_2(\text{FC}) \geq 1$).

Gene	$\log_2$ FC	p-value	adjusted p-value
COL11A1	6.52	4.47E-05	7.99E-04
SPP1	6.27	2.24E-07	6.15E-06
COL10A1	5.93	4.40E-38	6.80E-36
LGI2	4.05	1.59E-04	2.54E-03
CTHRC1	3.90	4.14E-117	5.57E-114
POSTN	3.73	7.24E-38	1.11E-35
COMP	3.22	3.88E-09	1.34E-07
PODNL1	2.78	1.44E-17	1.00E-15
BGN	2.63	5.00E-180	2.12E-176
COL8A1	2.60	2.11E-90	1.49E-87
HAPLN3	2.59	5.04E-19	3.77E-17
WISP1	2.55	3.49E-03	3.91E-02
COL3A1	2.43	5.33E-85	3.10E-82
VCAN	2.28	5.00E-90	3.37E-87
TGFBI	2.16	3.20E-23	2.90E-21
MFAP2	2.08	6.49E-59	1.98E-56
COL6A3	2.07	2.00E-102	2.04E-99
ASPN	2.00	8.79E-32	1.13E-29
LTBP2	1.97	7.86E-74	3.64E-71
IGFBP3	1.90	3.73E-17	2.51E-15
COL4A1	1.86	9.73E-39	1.53E-36
COL4A2	1.82	1.40E-45	2.80E-43
EMILIN1	1.73	3.00E-84	1.71E-81
EMID1	1.69	6.82E-08	2.01E-06
COL5A2	1.58	1.77E-39	2.80E-37
MXRA5	1.54	9.98E-24	9.21E-22
COL5A1	1.46	1.08E-35	1.53E-33
COL8A2	1.45	1.33E-03	1.69E-02
AGRN	1.45	5.89E-04	8.29E-03
LAMB1	1.41	6.65E-32	8.57E-30
COL1A1	1.37	6.34E-29	7.09E-27
THBS2	1.37	1.40E-25	1.39E-23
EDIL3	1.17	1.68E-10	6.66E-09
IGFBP2	1.16	7.57E-13	3.75E-11
COL18A1	1.14	1.95E-22	1.70E-20
FNDC1	1.14	2.54E-03	2.98E-02
COL27A1	1.13	2.53E-05	4.86E-04
SPARC	1.02	9.18E-31	1.11E-28

Appendix C

Supplementary figures

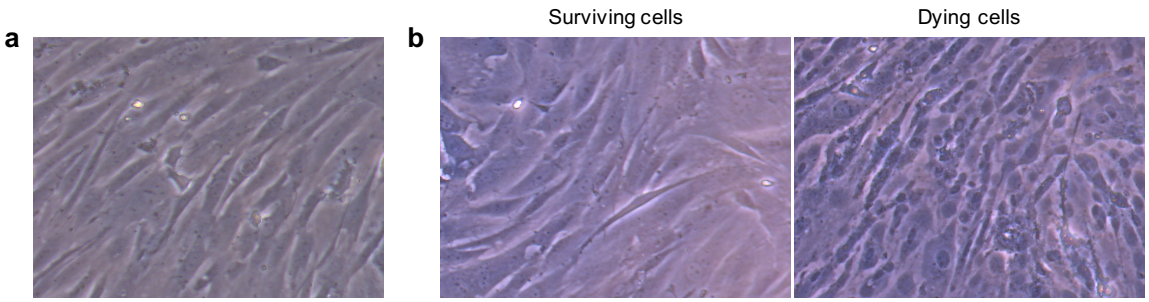

Figure C.1: Vacuole formation in ascorbic-acid treated fibroblasts. Fibroblasts from normal mammary gland tissue (**a**) before and (**b**) after treatment with ascorbic-acid containing fibroblast growth medium. Within minutes after addition of ascorbic-acid containing medium, extensive vacuolization could be observed in the fibroblasts that died (b, right). Figures are representative for fibroblasts from both normal mammary gland tissue and MMTV-PyMT tumors.

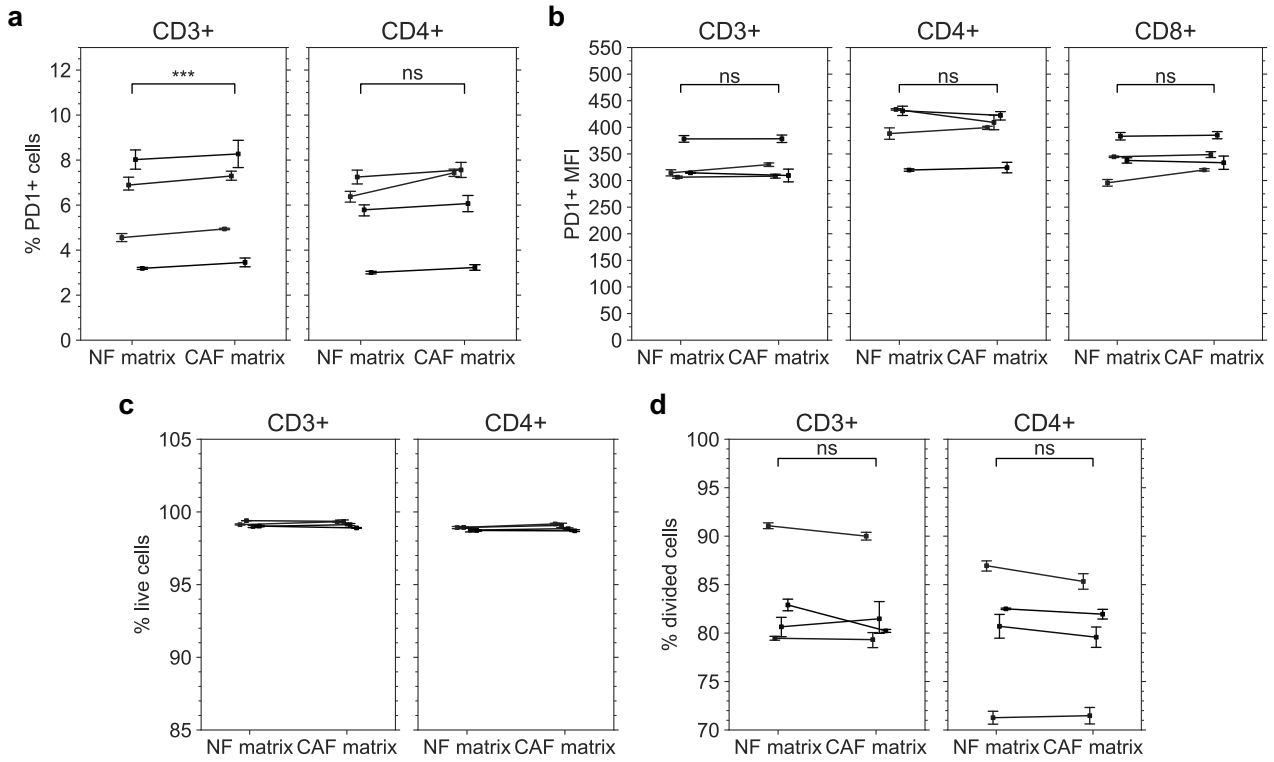

Figure C.2: T cells cultured on CAF CDMs upregulate PD1. Murine splenic $CD3^+$ T cells were labeled with Cell Trace Violet (CTV), stimulated with IL-2 and CD3/CD28 Dynabeads™ and cultured on NF- and CAF-derived CDMs. After 4 days, cells were harvested and stained for viability, CD3, CD4, CD8 and PD-1. (**a**) Fraction of PD-1 expressing live $CD3^+$ (left) and $CD4^+$ (right) T cells. (**b**) Level of PD-1 expression (mean fluorescence intensity, MFI) in live $CD3^+$ (left), $CD4^+$ (middle) and $CD8^+$ (right) T cells. (**c**) Viability of $CD3^+$ (left) and $CD4^+$ (right) T cells as determined from Zombie Aqua™ staining. (**d**) Proliferation of $CD3^+$ (left) and $CD4^+$ (right) T cells as determined from CTV labeling and proliferation modeling. Proliferation is quantified as the percentage of cells in the original culture that divided at least once (as defined in FlowJo). Figures show mean ± SEM of at least 4 technical replicates from 4 independent experiments.

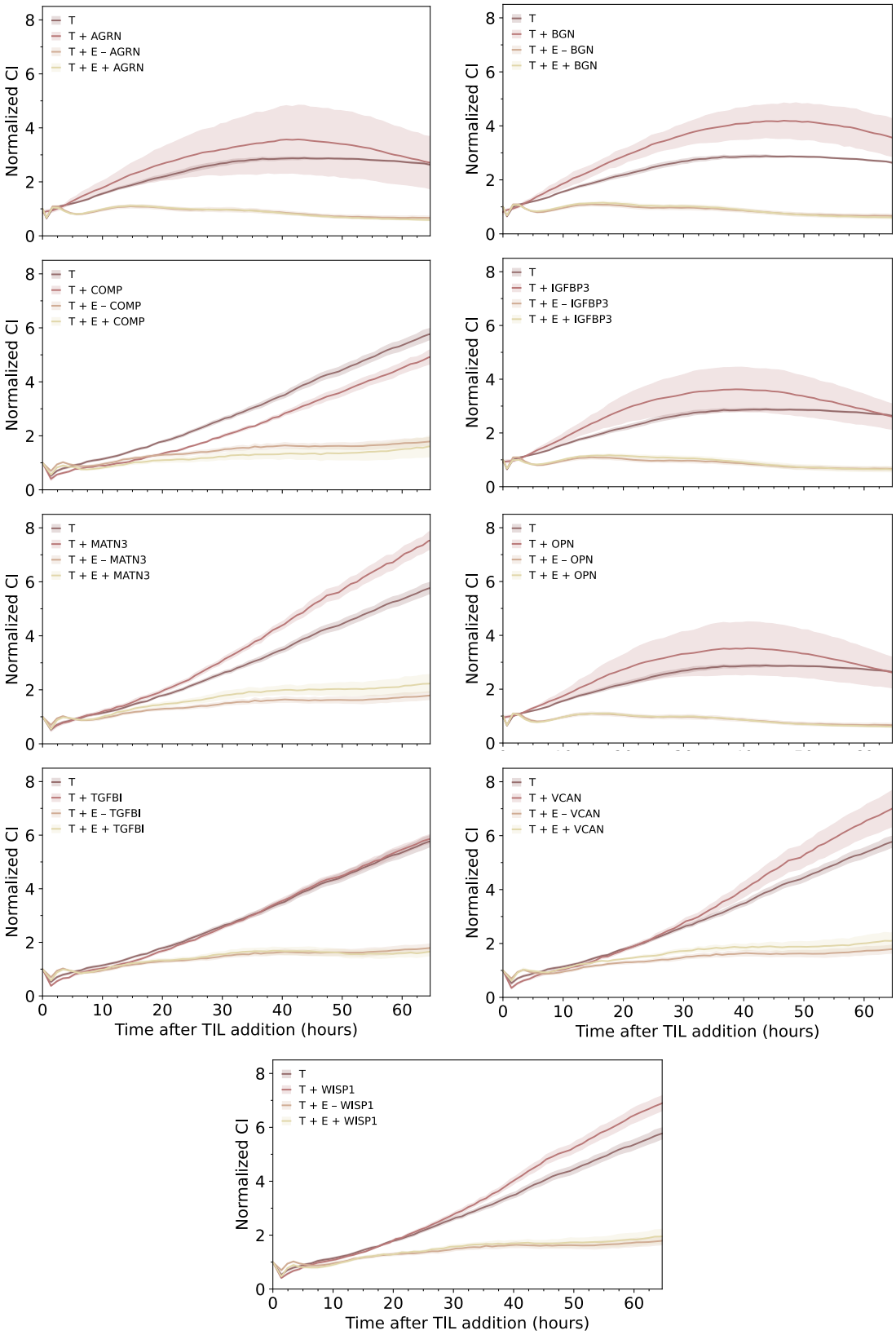

Figure C.3: Normalized CI traces for screened matrix proteins. Patient-derived melanoma cells were seeded and incubated overnight in an xCELLigence RTCA. After 24 hours, recombinant ECM protein at 5 µg/mL and/or autologous REP TILs that had been pre-incubated for 24 hours with the protein were added to the tumor cells. Figure shows example of normalized cell index (CI) traces for cells incubated with (+) and without (-) each type of protein at at E:T ratio 3:1. T = target/tumor cells, E = effector cells/TILs. Traces show the mean of 3-4 replicates and the shaded area corresponds to SEM.